Maastricht University

Fundamental studies to assess and restore vestibular function in patients with severe bilateral vestibular loss

Citation for published version (APA):

Pleshkov, M. (2022). *Fundamental studies to assess and restore vestibular function in patients with severe bilateral vestibular loss.* [Doctoral Thesis, Maastricht University]. Maastricht University. https://doi.org/10.26481/dis.20220906mp

Document status and date:
Published: 01/01/2022

DOI:
10.26481/dis.20220906mp

Document Version:
Publisher's PDF, also known as Version of record

Please check the document version of this publication:

• A submitted manuscript is the version of the article upon submission and before peer-review. There can be important differences between the submitted version and the official published version of record. People interested in the research are advised to contact the author for the final version of the publication, or visit the DOI to the publisher's website.
• The final author version and the galley proof are versions of the publication after peer review.
• The final published version features the final layout of the paper including the volume, issue and page numbers.

Link to publication

FUNDAMENTAL STUDIES TO ASSESS AND RESTORE VESTIBULAR FUNCTION IN PATIENTS WITH SEVERE BILATERAL VESTIBULAR LOSS

FUNDAMENTAL STUDIES TO ASSESS AND RESTORE VESTIBULAR FUNCTION IN PATIENTS WITH SEVERE BILATERAL VESTIBULAR LOSS

DISSERTATION

to obtain the degree of Doctor at the Maastricht University,
on the authority of the Rector Magnificus,
Prof.dr. Pamela Habibović
in accordance with the decision of the Board of Deans,
to be defended in public
on Tuesday 06 September 2022 at 10.00 hours

by
Maksim Olegovich Pleshkov
born on 20 July 1992 in Tomsk

Approved after corrections
Prof.dr. Pamela Habibović
Rector Magnificus

Supervisors:
Dr. R. van de Berg
Prof.dr. V.P. Demkin, Tomsk State University, Russia
Prof.dr. H. Kingma

Assessment Committee:
Prof.dr. R. Peeters (chair)
Prof.dr. P.P. van Benthem, LUMC, Leiden
Prof.dr. H.P.M. (Dirk) Kunst
Prof.dr. F. Wuyts, University of Antwerp, Belgium

Confirmation

Hereby I confirm that I have worked out the present doctoral thesis, which I submitted for consideration at Maastricht University and Tomsk State University for acquisition of a PhD degree. The present doctoral thesis is not submitted in other scientific institutions for acquisition of a scientific degree.

Name: Maksim Pleshkov
Date: 29.03.2022

Acknowledgments

I wish to thank Professor Demkin, Doctor Raymond van de Berg, and Professor Kingma for their outstanding supervision and support. I feel very privileged to be part of this cooperation between Tomsk State University and Maastricht University. Hopefully, many more fruitful cooperations between our universities will follow.

I also wish to thank all my fellow co-authors who made it possible to complete this PhD-thesis. Especially my colleagues and friends from Hall in Tirol (Simone D'Alessandro, Michael Handler, Rami Saba, and Daniel Baumgarten), Maastricht (Lisa van Stiphout and Joost Stultiens) and Tomsk (Dmitrii Starkov and Mikhail Svetlik).

And especially I would like to thank my wife Ekaterina who helped me to finalize the thesis and who supported me all the way.

Table of contents

Chapter 1 Introduction and outline of the thesis

INTRODUCTION

Anatomy of the vestibular system

The vestibular organs are located in the left and right temporal bones and, together with the hearing organ – cochlea, form the inner ear. The inner ear is also called: the labyrinth (Figure 1.1). Each vestibular system consists of five end organs: three semicircular canals that detect angular accelerations and two otolith organs that detect gravity, tilt, and linear accelerations. The inner space of the labyrinth is split into two compartments by the membranous labyrinth that follows the shape of the bony labyrinth. The labyrinth is filled with two types of liquid: endolymphatic fluid on the inside of the membranous labyrinth and perilymphatic fluid on the outside (Kingma & van de Berg, 2016).
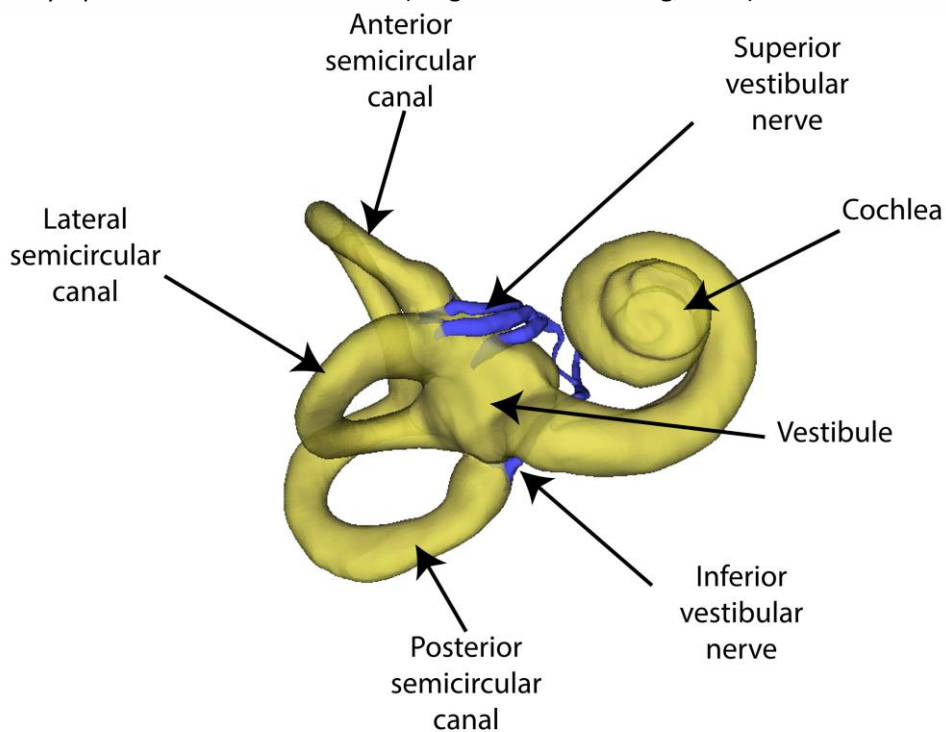
Figure 1.1 The human inner ear: bony labyrinth (yellow) and the vestibular nerve (blue) schematically.

Each semicircular canal has a wide part called the ampulla, where the sensor for angular accelerations is located. The mechanical sensor consists of the membranous body – cupula that bends under the action of liquid inertial displacement during head turns. The cupula includes hair cells that convert mechanical displacement into electrical action potentials (Kingma & van de Berg, 2016; Wilson & Jones, 1979). The hair cells are direction specific. Their alignment differs between canals and left and right vestibular organs. This results e.g., in the right semicircular canal being more sensitive for the rotations to the right, and the left semicircular canal being more sensitive for rotations to the left.

There are two otolith organs: the utricle and the saccule. These organs are arranged nearly orthogonal to each other, allowing three dimensional sensation of linear accelerations and gravity due to the different orientations of hair cells (Wilson & Jones, 1979). The mechanical sensor of otolith organs, called the macula, consists of three layers: the otoconia (calcium carbonate crystals) on top, a gelatinous membrane in the middle, and hair cells at the bottom.

The superior vestibular nerve innervates the utricle and the superior and lateral canals. The inferior vestibular nerve innervates the posterior canal and the saccule (Kudo & Nomura, 1996). The nerve fibers of both divisions merge and then enter the vestibular nuclei of the brainstem. From the brainstem, the vestibular nerve fibers project to the oculomotor nuclei, spinal cord, neck region, cerebellum, and cortex. The vestibular organs facilitate several reflexes. The main reflexes are the vestibulo-ocular, vestibulo-spinal, and vestibulo-collic reflex (Goetz, 2007).

Physiology of the vestibular system

The vestibular system facilitates three main functions: spatial orientation, gaze stabilization, and postural control. Regarding spatial orientation, the vestibular system has a high sensitivity for tilt (Janssen et al., 2011), angular (Grabherr et al., 2008), and linear accelerations (Kingma, 2005b).

Spatial orientation is facilitated by integrating signals originating from different sensory systems, including vestibular, visual, proprioceptive, and others. The contribution of the vestibular system is significant (Anson et al., 2021; Pfeiffer et al., 2014). However, it is challenging to study spatial orientation.

Gaze stabilization is facilitated by the vestibulo-ocular reflex (VOR) that turns the eyes opposite to the head movement direction, resulting in image stabilization on the retina (Fetter, 2007). The VOR has a short latency between 6 and 15 ms in humans (Collewijn & Smeets, 2000). The VOR serves as a basis for diagnosing the semicircular canal function by comparing eye movements with head movements.

Postural control is facilitated through vestibulo-spinal and vestibulo-collic reflexes (VSR and VCR, respectively) and the somatosensory and visual systems (Manzoni, 2009). Unlike the VOR, the VSR has longer latencies that vary between 40 and 160 ms (Britton et al., 1993; Fitzpatrick et al., 1994).

The information received by the vestibular end organ is encoded in the nerves by modulation of the baseline (~100 spikes/sec) firing rate (Brontë-Stewart & Lisberger, 1994). If the end organ is excited, the firing rate increases up to 400 Hz, and vice versa: during the inhibition phase the firing rate can decrease to 0 Hz (DiGiovanna et al., 2016).

DEFINING THE PROBLEM

Bilateral vestibulopathy

Bilateral vestibulopathy (BVP) is a disease characterized by deficits in the vestibular organs and/or vestibular nerves (Strupp et al., 2016). One of the most common causes of BVP is ototoxicity due to use of aminoglycosides such as gentamicin sulfate (Sun et al., 2014). Among other causes, there are genetic abnormalities, Menière's disease,

labyrinthitis, meningitis, ischemia, autoimmune disease, and head trauma (Lucieer et al., 2016). The typical symptoms include imbalance and oscillopsia (Hain et al., 2013; Lucieer et al., 2016, 2018; Strupp et al., 2017). Oscillopsia is an illusion of a moving (oscillating) world in the visual field during head movements. BVP significantly impairs quality of life and therefore leads to an extra social and economic burden for the society (Guinand et al., 2012; Sun et al., 2014). The prevalence of vestibular disorders is estimated at 1.1% in the whole population (Grill et al., 2018), 35% in the population over 40 years old (Agrawal et al., 2009), and the prevalence of BVP is about 0.03% (Ward et al., 2013). Therefore, timely diagnostics and treatment of vestibular disorders are very relevant.

Diagnostics

The most commonly used vestibular diagnostic tests are based on the assessment of the vestibular reflexes, especially the VOR (e.g., caloric test, torsion swing test, and head impulse test (HIT) (Lang & McConn Walsh, 2010; van de Berg et al., 2018; Wuyts et al., 2007). The development of oculography techniques allowed the quantitative analysis of the VOR by using a video camera (video-oculography, VOG) or recording of the electrical potential of an eye (electro-oculography, EOG), or scleral coil lens in a magnetic field (scleral coil technique, SCT) (Eggert, 2007)(Alhabib & Saliba, 2017; Halmagyi et al., 2017; Welgampola et al., 2019). Each oculography method has its advantages and disadvantages and should be applied in the appropriate case. For instance, the VOG relies on the visibility of the eye pupil, which can be limited in the case of vertical HIT or semi-closed eyelids. In contrast, the EOG can track the eye position even when eyes are closed, but it is a much more time-consuming technique. Eventually, the feasibility of the EOG application to perform HIT remains unknown.

Apart from vestibular reflexes, the vestibular system contributes to self-motion perception. Self-motion perception thresholds can be estimated by determining the slowest motion, which is still detectable, almost similar to an audiogram in patients with hearing difficulties (Bermúdez Rey et al., 2016; Grabherr et al., 2008; Kingma, 2005a; Merfeld, 2011). Self-motion perception thresholds have been investigated in recent years as a potential diagnostic tool, next to reflex testing. This required the development of a clinically applicable procedure to test BVP patients and assess the influence of the VI on motion perception.

Restoring vestibular function

Since the treatment options regarding (nearly) absent vestibular function are limited (Zingler et al., 2007), a novel treatment option was previously suggested: a neural prosthesis (vestibular implant, VI) that directly stimulates the vestibular afferents by the electrical current, which bypasses the damaged vestibular organ (Guinand et al., 2011). Several extensive studies in animals and humans demonstrated the feasibility of this VI (Guyot & Perez Fornos, 2019). After all, the VI can (partially) restore the VOR (Fornos et al., 2014), dynamic visual acuity (Starkov, Guinand, et al., 2020; Starkov, Snelders, et al., 2020), and influence postural control (Boutabla et al., 2020).

In silico experiments using simplified or detailed 3D geometry of the inner ear were used to visualize and predict the response of the neural afferents to the electrical stimuli

in humans and animals (Handler et al., 2017; Hayden et al., 2011; Marianelli et al., 2015; Schier et al., 2018). Ultimately, the electrical impedances of the tissues serve as a basis for the models and define the feasibility and quality of electrical stimulation. For example, electroconductive properties of biological tissues determine which structures will be stimulated in the inner ear. In addition, the process of fibrosis formation that occurs after vestibular implantation, may prevent any electric current the inner ear. Therefore, studying the inner ear electrical impedances is crucial to develop electroconductivity models used for optimizing electrical stimulation by the VI.

THE AIM OF THIS THESIS

This thesis aims to improve the diagnostics of the vestibular system and optimize electrical stimulation of the vestibular end organs using an artificial vestibular organ (the vestibular implant: VI) based on underlying physical principles. In particular, this thesis explored: the vestibular-ocular reflex testing using electro-oculography and video-oculography; self-motion perception using a motion platform; anatomy of the guinea pig inner ear and its electrical properties regarding electrical stimulation of the vestibular afferents.

OBJECTIVES

- to investigate the patterns of vestibular impairment in BVP in general and subsequently the implications regarding patient eligibility for vestibular implantation, and investigate whether the pattern and severity of vestibular impairment depends on the etiology (Chapter 2);
- to check the feasibility of applying EOG in the horizontal HIT by comparing eye velocity traces simultaneously recorded by EOG and VOG during the horizontal HIT (Chapter 3);
- to investigate the application of a simplified and shorter paradigm for testing vestibular perception (Chapter 4);
- to compare two paradigms for determining thresholds of self-motion perception (twelve-option versus two-option paradigm), in order to investigate whether reducing the choice options significantly influences the reported thresholds of healthy subjects, obtained with a more clinically oriented test (Chapter 5);
- to determine electrical impedances between each pair of stimulating electrodes, with contacts located close to the center of each ampulla of each semicircular canal and adjacent to the vestibular nerve in the guinea pig inner ear (Chapter 6 and Chapter 7);
- to construct the 3D electroconductivity model reflecting the measured electrical impedance in the guinea pig inner ear incorporating the electrical double layer present on electrode contact spot and to investigate the significance of the surrounding temporal bone (Chapter 6 and Chapter 8).

THESIS OUTLINE

Chapter two: Bilateral vestibular loss: underlying diseases and diagnostic criteria to define severe loss

The function of all five vestibular end organs was investigated in a large cohort of BVP-patients from three tertiary centers. The different patterns of vestibular disfunction were described to demonstrate the heterogeneity of the population and to identify the subgroup suited for vestibular implantation.

Chapter three: EOG vs. VOG: is EOG a reliable alternative for VOG to assess HIT?

Head and eye velocities were simultaneously recorded during the horizontal head impulse test (HIT) in a group of healthy volunteers. Two oculography methods were used: video-oculography (VOG) and electro-oculography (EOG). The recorded eye velocities were processed and compared between both methods. It was hypothesized that the EOG method could replace the VOG to perform HIT, especially when the latter method is challenging to use: in vertical head impulse test, in infants, and in cases when VOG goggles do not fit on the tested subject head.

Chapter four: A new and faster test to assess the vestibular perception

A six degrees of freedom motion platform was used in a group of healthy volunteers to investigate self-motion perception thresholds and the influence of age on these thresholds. For this, each subject was seated on the platform in complete darkness, while the platform performed one of twelve possible movement types: translation up or down, left or right, forward or backward, roll left or right, pitch forward or backward, yaw left or right with different acceleration. The subject had to indicate what type and direction of movement were felt. The lowest acceleration was considered to be the threshold. Threshold testing might ultimately complement vestibular reflex testing and might contribute to the diagnostic and/or rehabilitation.

Chapter five: Comparing the paradigms of motion perception measurement: 2-option vs. 12-option

The motion platform described in Chapter Four was used in a group of healthy volunteers to investigate the influence of the testing paradigm on self-motion perception thresholds. Two testing paradigms were compared: subjects had to choose between 1) two options or 2) twelve options of type and direction of movement. Since the chance of guessing might affect the measured outcome of the self-motion perception thresholds, normative values are required for each testing paradigm separately.

Chapter six: How to optimize the electrical stimulation for the VI: Geometry of the labyrinth

Three dimensional geometrical models of the guinea pig and rat bony labyrinths were constructed based on micro-CT scans. The key morphological parameters of the semicircular canals were measured and compared to each other.

Chapter seven: How to optimize the electrical stimulation for VI: Electrical properties

Electrical impedances were measured in the guinea pig inner ear *in vitro* using platinum electrodes located in three semicircular canal ampullae and the vestibular nerve. An equivalent circuit model was fitted to the measured impedances to evaluate physical phenomena affecting the impedance values: the electrical double layer and tissue polarization.

Chapter eight: How to optimize the electrical stimulation for VI: Modeling of electrical conductivity

The 3D geometrical model of the guinea pig inner ear (described in Chapter Six) was combined with electroconductivity laws and was fitted to the measured impedances described in Chapter Seven. The influence of the surrounding temporal bone on the electrical current propagation inside the bony labyrinth was investigated. In addition, based on the impedance measurements, the values of conductivity and permittivity of the electrical double layer and electrolytic liquid inside the inner ear were identified using the grid search algorithm.

REFERENCES

Agrawal, Y., Carey, J. P., Della Santina, C. C., Schubert, M. C., & Minor, L. B. (2009). Disorders of balance and vestibular function in US adults: data from the National Health and Nutrition Examination Survey, 2001-2004. *Archives of Internal Medicine*, *169*(10), 938–944. https://doi.org/10.1001/archinternmed.2009.66

Alhabib, S. F., & Saliba, I. (2017). Video head impulse test: a review of the literature. *European Archives of Oto-Rhino-Laryngology*, *274*(3), 1215–1222. https://doi.org/10.1007/s00405-016-4157-4

Anson, E., Ehrenburg, M. R., Simonsick, E. M., & Agrawal, Y. (2021). Association between vestibular function and rotational spatial orientation perception in older adults. *Journal of Vestibular Research : Equilibrium & Orientation*, *31*(6), 469–478. https://doi.org/10.3233/VES-201582

Bermúdez Rey, M. C., Clark, T. K., Wang, W., Leeder, T., Bian, Y., Merfeld, D. M., Rey, M. C. B., Clark, T. K., Wang, W., Leeder, T., Bian, Y., & Merfeld, D. M. (2016). Vestibular perceptual thresholds increase above the age of 40. *Frontiers in Neurology*, *7*(OCT), 1–17. https://doi.org/10.3389/fneur.2016.00162

Boutabla, A., Cavuscens, S., Ranieri, M., Crétallaz, C., Kingma, H., van de Berg, R., Guinand, N., & Pérez Fornos, A. (2020). Simultaneous activation of multiple vestibular pathways upon electrical stimulation of semicircular canal afferents. *Journal of Neurology*, *267*(Suppl 1), 273–284. https://doi.org/10.1007/S00415-020-10120-1

Britton, T. C., Day, B. L., Brown, P., Rothwell, J. C., Thompson, P. D., & Marsden, C. D. (1993). Postural electromyographic responses in the arm and leg following galvanic vestibular stimulation in man. *Experimental Brain Research*, *94*(1), 143–151. https://doi.org/10.1007/BF00230477

Brontë-Stewart, H. M., & Lisberger, S. G. (1994). Physiological properties of vestibular primary afferents that mediate motor learning and normal performance of the

vestibulo-ocular reflex in monkeys. *Journal of Neuroscience*, *14*(3 I), 1290–1308. https://doi.org/10.1523/jneurosci.14-03-01290.1994

Collewijn, H., & Smeets, J. B. J. (2000). Early components of the human vestibulo-ocular response to head rotation: latency and gain. *Journal of Neurophysiology*, *84*(1), 376–389. https://doi.org/10.1152/JN.2000.84.1.376

DiGiovanna, J., Nguyen, T. A. K., Guinand, N., Pérez-Fornos, A., & Micera, S. (2016). Neural network model of vestibular nuclei reaction to onset of vestibular prosthetic stimulation. *Frontiers in Bioengineering and Biotechnology*, *4*(APR). https://doi.org/10.3389/fbioe.2016.00034

Eggert, T. (2007). Eye movement recordings: Methods. In *Developments in Ophthalmology* (Vol. 40, pp. 15–34). Dev Ophthalmol. https://doi.org/10.1159/000100347

Fetter, M. (2007). Vestibulo-ocular reflex. *Developments in Ophthalmology*, *40*, 35–51. https://doi.org/10.1159/000100348

Fitzpatrick, R., Burke, D., & Gandevia, S. C. (1994). Task-dependent reflex responses and movement illusions evoked by galvanic vestibular stimulation in standing humans. *The Journal of Physiology*, *478*(Pt 2), 363. https://doi.org/10.1113/JPHYSIOL.1994.SP020257

Fornos, A. P., Guinand, N., Van De Berg, R., Stokroos, R., Micera, S., Kingma, H., Pelizzone, M., & Guyot, J. P. (2014). Artificial balance: Restoration of the vestibulo-ocular reflex in humans with a prototype vestibular neuroprosthesis. *Frontiers in Neurology*, *5 APR*, 66. https://doi.org/10.3389/fneur.2014.00066

Goetz, C. G. (2007). *TEXTBOOK OF CLINICAL NEUROLOGY* (C. G. Goetz (ed.); Third edit). https://doi.org/https://doi.org/10.1016/B978-1-4160-3618-0.X1000-4

Grabherr, L., Nicoucar, K., Mast, F. W., & Merfeld, D. M. (2008). Vestibular thresholds for yaw rotation about an earth-vertical axis as a function of frequency. *Experimental Brain Research*, *186*(4), 677–681. https://doi.org/10.1007/s00221-008-1350-8

Grill, E., Heuberger, M., Strobl, R., Saglam, M., Holle, R., Linkohr, B., Ladwig, K.-H., Peters, A., Schneider, E., Jahn, K., & Lehnen, N. (2018). Prevalence, Determinants, and Consequences of Vestibular Hypofunction. Results From the KORA-FF4 Survey. *Frontiers in Neurology*, *9*, 1076. https://doi.org/10.3389/fneur.2018.01076

Guinand, N., Boselie, F., Guyot, J.-P. P., & Kingma, H. (2012). Quality of life of patients with bilateral vestibulopathy. *Annals of Otology, Rhinology and Laryngology*, *121*(7), 471–477. https://doi.org/10.1177/000348941212100708

Guinand, N., Guyot, J. P., Kingma, H., Kos, I., & Pelizzone, M. (2011). Vestibular implants: The first steps in humans. *2011 Annual International Conference of the IEEE Engineering in Medicine and Biology Society*, *2011*, 2262–2264. https://doi.org/10.1109/IEMBS.2011.6090569

Guyot, J.-P., & Perez Fornos, A. (2019). Milestones in the development of a vestibular implant. *Current Opinion in Neurology*, *32*(1), 145–153. https://doi.org/10.1097/WCO.0000000000000639

Hain, T. C., Cherchi, M., & Yacovino, D. A. (2013). Bilateral vestibular loss. *Seminars in Neurology*, *33*(3), 195–203. https://doi.org/10.1055/s-0033-1354597

Halmagyi, G. M., Chen, L., MacDougall, H. G., Weber, K. P., McGarvie, L. A., & Curthoys, I. S. (2017). The Video Head Impulse Test. *Frontiers in Neurology*, *8*, 258.

https://doi.org/10.3389/fneur.2017.00258

Handler, M., Schier, P. P., Fritscher, K. D., Raudaschl, P., Chacko, L. J., Glueckert, R., Saba, R., Schubert, R., Baumgarten, D., & Baumgartner, C. (2017). Model-based vestibular afferent stimulation: Modular workflow for analyzing stimulation scenarios in patient specific and statistical vestibular anatomy. *Frontiers in Neuroscience*, *11*(DEC), 713. https://doi.org/10.3389/fnins.2017.00713

Hayden, R., Sawyer, S., Frey, E., Mori, S., Migliaccio, A. A., & Della Santina, C. C. (2011). Virtual labyrinth model of vestibular afferent excitation via implanted electrodes: Validation and application to design of a multichannel vestibular prosthesis. *Experimental Brain Research*, *210*(3–4), 623–640. https://doi.org/10.1007/s00221-011-2599-x

Janssen, M., Lauvenberg, M., van der Ven, W., Bloebaum, T., & Kingma, H. (2011). Perception Threshold for Tilt. *Otology & Neurotology*, *32*(5), 818–825. https://doi.org/10.1097/MAO.0b013e31821c6c7b

Kingma, H. (2005a). Thresholds for perception of direction of linear acceleration as a possible evaluation of the otolith function. *BMC Ear, Nose and Throat Disorders*, *88*(1 B), 82–87. https://doi.org/10.1186/1472-6815-5-Received

Kingma, H. (2005b). Thresholds for perception of direction of linear acceleration as a possible evaluation of the otolith function. *BMC Ear, Nose, and Throat Disorders*, *5*(1), 5. https://doi.org/10.1186/1472-6815-5-5

Kingma, H., & van de Berg, R. (2016). Anatomy, physiology, and physics of the peripheral vestibular system. In J. M. Lempert & T. Furman (Eds.), *Handbook of Clinical Neurology* (Vol. 137, pp. 1–16). Elsevier B.V. https://doi.org/10.1016/B978-0-444-63437-5.00001-7

Kudo, Y., & Nomura, Y. (1996). The vestibular nerve: Its course to the anterior and lateral ampullae. *Orl*, *58*(4), 208–212. https://doi.org/10.1159/000276838

Lang, E. E., & McConn Walsh, R. (2010). Vestibular function testing. *Irish Journal of Medical Science*, *179*(2), 173–178. https://doi.org/10.1007/S11845-010-0465-7

Lucieer, F., Duijn, S., Van Rompaey, V. V., Fornos, A. P., Guinand, N., Guyot, J. P., Kingma, H., & van de Berg, R. (2018). Full spectrum of reported symptoms of bilateral vestibulopathy needs further investigation-A systematic review. In *Frontiers in Neurology* (Vol. 9, Issue JUN). Frontiers Media S.A. https://doi.org/10.3389/fneur.2018.00352

Lucieer, F., Vonk, P., Guinand, N., Stokroos, R., Kingma, H., & van de Berg, R. (2016). Bilateral vestibular hypofunction: Insights in etiologies, clinical subtypes, and diagnostics. *Frontiers in Neurology*, *7*(MAR), 26. https://doi.org/10.3389/fneur.2016.00026

Manzoni, D. (2009). Vestibulo-spinal Reflexes. *Encyclopedia of Neuroscience*, 4245–4250. https://doi.org/10.1007/978-3-540-29678-2_6315

Marianelli, P., Capogrosso, M., Luciani, L. B., Panarese, A., Bassi Luciani, L., Panarese, A., & Micera, S. (2015). A Computational Framework for Electrical Stimulation of Vestibular Nerve. *IEEE Transactions on Neural Systems and Rehabilitation Engineering*, *23*(5), 897–909. https://doi.org/10.1109/TNSRE.2015.2407861

Merfeld, D. M. (2011). Signal detection theory and vestibular thresholds: I. Basic theory and

practical considerations. *Experimental Brain Research*, *210*(3–4), 389–405. https://doi.org/10.1007/s00221-011-2557-7

Pfeiffer, C., Serino, A., & Blanke, O. (2014). The vestibular system: A spatial reference for bodily self-consciousness. *Frontiers in Integrative Neuroscience*, *8*(APR), 31. https://doi.org/10.3389/FNINT.2014.00031/BIBTEX

Schier, P., Handler, M., Chacko, L. J., Schrott-Fischer, A., Fritscher, K., Saba, R., Baumgartner, C., & Baumgarten, D. (2018). Model-based vestibular afferent stimulation: Evaluating selective electrode locations and stimulation waveform shapes. *Frontiers in Neuroscience*, *12*, 1–15. https://doi.org/10.3389/fnins.2018.00588

Starkov, D., Guinand, N., Lucieer, F., Ranieri, M., Cavuscens, S., Pleshkov, M., Guyot, J. P., Kingma, H., Ramat, S., Perez-Fornos, A., & Van De Berg, R. (2020). Restoring the high-frequency dynamic visual acuity with a vestibular implant prototype in humans. *Audiology and Neurotology*, *25*(1–2), 91–95. https://doi.org/10.1159/000503677

Starkov, D., Snelders, M., Lucieer, F., Janssen, A. M. L., Pleshkov, M., Kingma, H., van Rompaey, V., Herssens, N., Hallemans, A., Vereeck, L., McCrum, C., Meijer, K., Guinand, N., Perez-Fornos, A., & van de Berg, R. (2020). Bilateral vestibulopathy and age: experimental considerations for testing dynamic visual acuity on a treadmill. *Journal of Neurology*, *267*(0123456789), 265–272. https://doi.org/10.1007/s00415-020-10249-z

Strupp, M., Feil, K., Dieterich, M., & Brandt, T. (2016). Bilateral vestibulopathy. *Handbook of Clinical Neurology*, *137*, 235–240. https://doi.org/10.1016/B978-0-444-63437-5.00017-0

Strupp, M., Kim, J. S., Murofushi, T., Straumann, D., Jen, J. C., Rosengren, S. M., Della Santina, C. C., & Kingma, H. (2017). Bilateral vestibulopathy: Diagnostic criteria consensus document of the classification committee of the barany society. *Journal of Vestibular Research: Equilibrium and Orientation*, *27*(4), 177–189. https://doi.org/10.3233/VES-170619

Sun, D. Q., Ward, B. K., Semenov, Y. R., Carey, J. P., & Della Santina, C. C. (2014). Bilateral Vestibular Deficiency: Quality of Life and Economic Implications. *JAMA Otolaryngology-- Head & Neck Surgery*, *140*(6), 527–534. https://doi.org/10.1001/jamaoto.2014.490

van de Berg, R., Rosengren, S., & Kingma, H. (2018). Laboratory examinations for the vestibular system. *Current Opinion in Neurology*, *31*(1), 111–116. https://doi.org/10.1097/WCO.0000000000000526

Ward, B. K., Agrawal, Y., Hoffman, H. J., Carey, J. P., & Della Santina, C. C. (2013). Prevalence and impact of bilateral vestibular hypofunction: Results from the 2008 US national health interview survey. *JAMA Otolaryngology - Head and Neck Surgery*, *139*(8), 803–810. https://doi.org/10.1001/jamaoto.2013.3913

Welgampola, M. S., Taylor, R. L., & Halmagyi, G. M. (2019). Video head impulse testing. *Advances in Oto-Rhino-Laryngology*, *82*, 56–66. https://doi.org/10.1159/000490272

Wilson, V. J., & Jones, G. M. (1979). Mammalian Vestibular Physiology. In *Mammalian Vestibular Physiology*. Springer US. https://doi.org/10.1007/978-1-4757-5702-6

Wuyts, F. L., Furman, J., Vanspauwen, R., & Van De Heyning, P. (2007). Vestibular function

testing. *Current Opinion in Neurology*, *20*(1), 19–24. https://doi.org/10.1097/WCO.0B013E3280140808

Zingler, V. C., Cnyrim, C., Jahn, K., Weintz, E., Fernbacher, J., Frenzel, C., Brandt, T., & Strupp, M. (2007). Causative factors and epidemiology of bilateral vestibulopathy in 255 patients. *Annals of Neurology*, *61*(6), 524–532. https://doi.org/10.1002/ana.21105

Chapter 2 Bilateral vestibular loss: underlying diseases and diagnostic criteria to define severe loss

ABSTRACT

Objective

This study aimed to 1) investigate the patterns of vestibular impairment in bilateral vestibulopathy (BVP) in general and subsequently the implications regarding patient eligibility for vestibular implantation, and 2) investigate whether the pattern and severity of vestibular impairment is etiology dependent.

Methods

One hundred and seventy-three subjects from three tertiary referral centers in The Netherlands, Belgium and Germany were diagnosed with BVP according to the Bárány Society diagnostic criteria. Subjects underwent different vestibular testing such as the caloric test, torsion swing test, three-dimensional or horizontal video Head Impulse Test (vHIT), and cervical and/or ocular vestibular evoked myogenic potentials (c- and oVEMPs). The underlying etiologies were split into: idiopathic, genetic, ototoxicity, infectious, Menière's Disease, (head)trauma, auto-immune, neurodegenerative, congenital, and mixed etiology.

Results

Fifty-four percent of the patients diagnosed with BVP who underwent caloric test, torsion swing test, and horizontal vHIT met all three Bárány Society diagnostic test criteria, whereas 76% of the patients were eligible for implantation according to the vestibular implantation criteria. Overall, the caloric test and horizontal vHIT more often indicated horizontal semicircular canal impairment than torsion swing test. Three-dimensional vHIT results showed significantly higher gains for both anterior canals compared with horizontal and posterior canals (p<0.001). Rates of bilaterally absent oVEMP responses were higher compared to bilaterally absent cVEMP responses (p=0.010). Regarding the relationship between vestibular test results and etiology, only horizontal vHIT results were significantly lower for trauma, neurodegenerative and genetic disorders, whereas horizontal vHIT results were significantly higher for Menière's Disease and infectious disorders. Exploration with hierarchical cluster analysis showed no significant association between etiology and patterns of vestibular impairment.

Conclusion

This study showed differences in the degree of vestibular impairment measured with different vestibular tests. More specific, caloric testing and vHIT seem to be more sensitive for measuring vestibular impairment, whereas torsion swing test is more suited for measuring residual vestibular function. In addition, no striking patterns of vestibular impairment in relation to etiology were found. Nevertheless, when comparing the Bárány Society diagnostic criteria and vestibular implantation criteria, it was demonstrated that although the implantation criteria are more strict, still 76% of BVP patients were eligible for implantation based on vestibular test criteria. It is advised to carefully examine every patient for their overall pattern of vestibular impairment, in order to make well informed and personalized therapeutic decisions.

INTRODUCTION

Bilateral vestibulopathy (BVP) is a chronic disease which is characterized by bilaterally reduced or absent vestibular function due to deficits of the vestibular organs, the vestibular nerves, and/or the brain (Hain et al., 2013; Lucieer et al., 2016; Strupp et al., 2017). Patients typically suffer from imbalance, worsening in the dark and/or on uneven ground and movement-induced blurred vision (oscillopsia) (Lucieer et al., 2018). BVP also leads to additional symptoms such as an increased risk of falling, cognitive deficits, impairment of navigation and spatial memory, autonomic dysfunction, anxiety and depression (Brandt et al., 2005; Kremmyda et al., 2016; Lucieer et al., 2018; Dobbels et al., 2019a; Dobbels et al., 2019b; Dobbels et al., 2020; Lucieer et al., 2020; Paredis et al., 2021). Consequently, BVP leads to reduced quality of life and imposes significant socioeconomic burden on Society (Guinand et al., 2012; Sun et al., 2014; Kovacs et al., 2019). BVP appears to be a heterogeneous disorder with various clinical characteristics and multiple identified etiologies, such as ototoxicity (e.g. gentamicin exposure), genetic disorders (e.g. DFNA9), Menière's Disease, infectious causes (e.g. meningitis), neurodegenerative and inherited syndromes (e.g. CANVAS), autoimmunity (e.g. Cogan's syndrome) or trauma (Rinne et al., 1998; Ishiyama et al., 2006; Cushing et al., 2009; Zingler et al., 2009; Bovo et al., 2010; Clemmens and Ruckenstein, 2012; Greco et al., 2013; de Varebeke et al., 2014; Szmulewicz et al., 2014; Lucieer et al., 2016). Nonetheless, the reported percentages of idiopathic BVP vary between 20-75%, indicating that identifying the etiology can be challenging (Rinne et al., 1998; Zingler et al., 2009; Sun et al., 2014; Lucieer et al., 2016).

To date, the prognosis for recovery of vestibular function is poor and an effective treatment for BVP is missing (Zingler et al., 2009; Porciuncula et al., 2012; Ward et al., 2013; Kingma et al., 2019). However, different research groups are in the process of developing a clinically applicable vestibular implant that might be able to address at least the major symptoms of BVP (Della Santina et al., 2007; Golub et al., 2014; Perez Fornos et al., 2014; Guinand et al., 2016; Perez Fornos et al., 2017; Ramos de Miguel et al., 2017; Guyot and Perez Fornos, 2019; Chow et al., 2021). Despite reaching important milestones in the development of the vestibular implant, many questions remain, and in order to develop a clinically useful device, it is crucial to gain a better understanding of the underlying disease BVP.

So far, it remains unclear which factors contribute to the severity of the vestibular impairment. The current diagnostic criteria for BVP are primarily based on the function of the horizontal semicircular canals (e.g. caloric test, video Head Impulse Test (vHIT), and torsion swing test) (Strupp et al., 2017). However, recent studies have highlighted the varying pattern of impairment of the other vestibular sensors in BVP patients (i.e. the otolith organs and the anterior and posterior semicircular canals) (Zingler et al., 2008; Fujimoto et al., 2009; Agrawal et al., 2013; Tarnutzer et al., 2016; Hermann et al., 2018; Tarnutzer et al., 2018; Fu et al., 2020; Lee and Kim, 2020). For example, anterior semicircular canal sparing was found in aminoglycoside-related BVP, in BVP due to bilateral Menière's Disease and in idiopathic BVP (Tarnutzer et al., 2016; Hermann et al., 2018; Lee and Kim, 2020). Ocular vestibular evoked myogenic potentials, most likely reflecting utricular function, showed to be the most impaired in aminoglycoside-related BVP and the

least impaired in BVP due to bilateral Menière's Disease (Agrawal et al., 2013). Another evidently rare subtype of idiopathic BVP was proposed in which the saccular function was impaired in the presence of normal functioning horizontal semicircular canals (Fujimoto et al., 2009). Another study showed that horizontal semicircular canal function was more often affected than saccular function in aminoglycoside-related BVP (Fu et al., 2020).

All studies mentioned above either included small patient groups, retrospectively analyzed the data, did not always include BVP patients according to the Bárány Society criteria, or investigated only one or two of the vestibular sensors. To date, no studies investigated the pattern of vestibular impairment of all vestibular sensors with relatively large patient groups, while recently published vestibular implantation criteria developed for research settings, take all vestibular sensors into consideration. According to these criteria, for instance, all vestibular tests (i.e. caloric test, three dimensional video head impulse test and torsion swing test) need to show a significantly impaired function in order to qualify as a vestibular implant candidate (Van De Berg et al., 2020).

This study provides a description of vestibular function, in a large cohort of BVP patients diagnosed according to the Bárány Society criteria. The objective was to 1) investigate the patterns of vestibular impairment in BVP in general and subsequently the implications regarding patient eligibility for vestibular implantation, and 2) investigate whether the pattern and severity of vestibular impairment depends on the etiology.

METHODS

Subjects

Study subjects were recruited from three tertiary referral centers in The Netherlands, Belgium and Germany: The Department of Otorhinolaryngology and Head & Neck surgery from Maastricht University Medical Center (MUMC+, center 1) and Antwerp University Hospital (UZA, center 2), and the Department of Neurology and the German Center for Vertigo and Balance Disorders, Ludwig Maximilians University Munich (LMU, center 3). Enrolled subjects were diagnosed with BVP in accordance with the BVP diagnostic criteria, which included unsteadiness and/or oscillopsia during walking or head movements, and a reduced bithermal caloric response (sum of bithermal maximal peak slow phase velocity <6°/s bilaterally) and/or a bilaterally reduced horizontal vHIT gain of <0.6, and/or a VOR gain <0.1 during torsion swing test at 0.1 Hz (Strupp et al., 2017). Subjects below the age of 18 and subjects who were not able to stop vestibulosuppressive medication were excluded from participation in this study.

Vestibular testing

All centers performed vestibular testing to confirm a BVP diagnosis, although the number of tests performed, differed between centers. In center 1, vestibular testing included electronystagmography with caloric and rotatory chair testing, as well as three dimensional (3D-)vHIT and cervical and ocular vestibular evoked myogenic potential testing (c- and oVEMPs). In center 2, subjects underwent electronystagmography with caloric and rotatory chair testing, a 3D-vHIT and cVEMPs. In center 3, videonystagmography with

caloric testing was performed, together with a horizontal vHIT. An overview of different tests performed in each center is shown in table 1 of the supplementary materials (see appendix 1).

The caloric test

An extensive description of caloric testing was described previously (van Stiphout et al., 2021). To summarize, in all centers bithermal caloric testing was performed in both ears whilst patients were in supine position with a forward head inclination of 30°. Each irrigation lasted 30 seconds with a volume of at least 250 ml water in center 1 and 2 and at least 100 ml water in center 3, for both cold (30°C) and warm (44°C) irrigations with a 5-minute stimulus interval between irrigations (Variotherm Plus device, Atmos Medizin Technik GmbH, Lenzkirch, Germany for all three centers). Eye movements were recorded using electronystagmography with self-adhesive electrodes at center 1 and 2 (Blue sensor, Ambu, Denmark) and with videonystagmography at center 3 (Interacoustics, Munich, Germany). The maximum peak slow phase eye velocity at the culmination phase (°/s) was measured (KingsLab 1.8.1, Maastricht University, Maastricht, The Netherlands at center 1; Nystagliner, Toennies, Germany at center 2; Interacoustics, Munich, Germany at center 3).

Torsion swing test

During torsion swing test, patients were seated in a servo-controlled rotatory chair in complete darkness with their eyes open (Ekida GmbH, Buggingen, Germany at center 1 and ServoMed AB, Varberg, Sweden at center 2). Sinusoidal rotatory stimulation was performed at 0.1 Hz at MUMC+ and at 0.05 Hz at UZA with a peak velocity of 60°/s. Again, eye movements were recorded with electronystagmography with self-adhesive electrodes (Blue sensor, Ambu, Denmark in both center 1 and 2) and the VOR gain was calculated as the ratio between peak eye velocity and peak head velocity (KingsLab 1.8.1, Maastricht University, Maastricht, The Netherlands at center 1; Nystagliner, Toennies, Germany at center 2).

Video Head Impulse Test

The horizontal vHIT and the vHIT in the Right-Anterior-Left-Posterior (RALP) and Left-Anterior-Right-Posterior (LARP) canal planes (3D-vHIT) were performed using the Video-Head Impulse Test device from Otometrics at center 1 and 2 (Otometrics, Taastrup, Denmark). At center 3 horizontal vHIT was performed using the Eye-SeeCam (Interacoustics, Munich, Germany). The testing method was described previously (van Dooren et al., 2018; Van Dooren et al., 2020). In brief, the technician stood behind the subject (who was sitting on a static chair) and held their head firmly without touching the goggles. The subject was instructed to maintain visual fixation on an earth-fixed target at a distance of 2 meters at center 1 and 2 and 1.8 meters at center 3. Head impulses comprised fast unpredictable, low-amplitude (±20°) head movements in the horizontal plane (all three centers, peak head velocity >150°/s) and in the RALP and LARP planes (center 1 and 2, peak head velocity >100°/s). The Otometrics system defines the VOR gain as the ratio of the area under the eye velocity curve to the area under the head velocity curve from the impulse onset until the head velocity drops to zero again (Macdougall et al., 2013). The

interacoustics system divides the eye and head velocity at a certain point in time (around 60ms after impulse onset) (Van Dooren et al., 2020).

Vestibular Evoked Myogenic Potentials

Both center 1 and 2 used the Neuro-Audio system with electromyographic software (v2010, Neurosoft, Ivanovo, Russia) and self-adhesive electrodes (Blue sensor, Ambu, Denmark) to record ocular and/or cervical VEMPS. cVEMPs were measured over the sternocleidomastoid muscle after stimulating the ipsilateral vestibular organ with air-conducted tone bursts of 500Hz, provided via inserted earphones at a stimulation rate of 13Hz. oVEMPs were measured over the inferior oblique muscle after stimulating the contralateral vestibular organ with the same stimulation parameters as for cVEMPs. Details on the procedure have been published previously (Colebatch et al., 1994; Vanspauwen et al., 2011; van Stiphout et al., 2021). In brief, for cVEMPS, subjects were in a supine position with their back tilted in an angle of 30° from the horizontal plane and were instructed to turn their head away from the stimulus and to lift their head up slightly. Two hundred electromyography (EMG) traces with a minimum rectified voltage of 65 µV and a maximum rectified voltage of 205 µV were accepted. A visual feedback system (v2010, Neurosoft, Ivanovo, Russia) provided patient feedback to maintain correct muscle contraction. For oVEMPS, subjects were in a supine position and were instructed to keep their gaze fixed on a focus point 30 degrees behind the head to achieve superomedial gaze. A minimum of 300 EMG traces were accepted.

VEMPs were first recorded starting at maximum stimulus intensities of 130dB SPL (center 1) or 95dB HL (center 2). Then recordings were attempted again using stimulus amplitudes successively decreasing by 5dB at each step. Thresholds were determined in consensus between two independent technicians at the level where a biphasic wave response was present. When no typical biphasic wave was found at 130 dB SPL at center 1 or at 95 dB HL at center 2, a patient was considered to have an absent c- or oVEMP response.

Data collection, processing & analysis

The caloric test was performed in all three centers. The torsion swing test was performed in center 1 and 2, but at different frequencies (0.1Hz and 0.05Hz respectively). Since the frequency of sinusoidal rotatory stimulation at center 2 differed from the frequency stated in the BVP diagnostic criteria, patients from center 2 were not included in this analysis based on their VOR gain measured during torsion swing test alone. As described above, the horizontal vHIT was performed in all three centers, vertical vHIT and cVEMPs in center 1 and 2, and oVEMPs only in center 1. Therefore, the amount of data available for analysis, differed between tests.

IBM SPSS Statistics version 25 and R version 3.5.2 were used for data-analysis. Descriptive statistics were used to describe basic features of the data (e.g. percentages). Non-parametric methods were applied to determine significant differences between test results (e.g. Kruskal Wallis H test with post hoc Dunn's test and Mann-Whitney U test). P-values ≤ 0.05 were considered significant and were adjusted and reported with Benjamini-

Hochberg correction for multiple testing. Fisher's exact test and the Chi-squared test were used to compare proportions of categorical outcomes.

Before the data was analysed extensively, it was checked whether the data between centers could be pooled. Caloric test results differed between the three centers ($\chi2(2)$ = 40.8, p < 0.001), therefore data could not be pooled. Torsion swing test results from center 1 and center 2 could not be pooled since the frequency of sinusoidal rotatory stimulation at center 1 (0.1Hz) differed from center 2 (0.05Hz) and the results were significantly different (Mann-Whitney U = 1954.5, p = 0.002). No significant differences for 3D-vHIT results between centers for five out of six semicircular canals were found (Kruskal-Wallis H test, p > 0.05). The left horizontal canal showed a significant difference between centers ($\chi2(2)$= 7.2, p = 0.029), however the Levene's test for homogeneity of variance did not show a significant difference (F = 1.32, p = 0.192). Therefore, 3D-vHIT results of all centers were pooled per canal.

VEMP results were categorized in absent versus present responses (i.e. when no typical biphasic wave was found at 130 dB SPL at center 1 or at 95 dB HL at center 2, a patient was considered to have an absent c- or oVEMP response). cVEMPs were analysed for each center separately since 1) the decibel measurement level differed between center 1 (dB SPL) and center 2 (dB HL) and 2) the Chi-squared test showed that there was a significant association between centers and absent versus present cVEMP responses ($\chi(2)$ = 8.57, p = 0.014).

To investigate the patterns of vestibular impairment in BVP in general, the vestibular test results were first analysed using descriptive statistics to describe basic features of the data. Subsequently, the results were interpreted according to the Bárány diagnostic criteria for BVP, which included a reduced bithermal caloric response (sum of bithermal maximal peak slow phase velocity <6°/s bilaterally) and/or a VOR gain <0.1 during torsion swing test at 0.1 Hz and/or a bilaterally reduced horizontal vHIT gain of <0.6 (Strupp et al., 2017). To investigate patient eligibility for vestibular implantation regarding results from vestibular reflex testing, vestibular test results were interpreted according to the vestibular implantation criteria, which included a bilaterally reduced or absent angular VOR function documented by at least one of the major criteria and all minor criteria (i.e. in case only one or two major criteria were met, the remaining tests should comply the minor criteria). The major criteria included a reduced bithermal caloric response (sum of bithermal maximal peak slow phase velocity ≤6°/s bilaterally), a reduced horizontal VOR gain ≤0.1 during torsion swing test at 0.1 Hz and a pathological horizontal VOR gain ≤0.6 bilaterally with at least one vertical VOR gain <0.7 bilaterally, measured with vHIT. The minor criteria included a reduced bithermal caloric response (sum of bithermal maximal peak slow phase velocity <10°/s bilaterally), a reduced horizontal VOR gain <0.2 during torsion swing test at 0.1 Hz and pathological VOR gains of at least two semicircular canals <0.7 bilaterally, measured by vHIT (Van De Berg et al., 2020).

Hierarchical cluster analysis was applied to explore and visualize patterns of vestibular impairment with respect to etiology. Cluster analysis requires complete cases (i.e. no missing data), therefore only patients with complete data for caloric testing, torsion swing test, 3D-vHIT, cVEMPs and oVEMPS were included (i.e. 45 patients from center 1). Before clustering, the data were standardized in Z-scores (i.e. the individual scores minus the

mean, divided by the standard deviation), in order to have the variables weigh equally in the cluster analysis. Ward's method with the distance measure squared Euclidian distance was used, since Ward's method has the highest agglomerative coefficient compared with the other hierarchical clustering methods. The silhouette method was used to determine the optimum number of clusters (Rousseeuw, 1987). Hierarchical cluster analysis resulted in two dendrograms with etiology on the x-axis and vestibular tests results on the y-axis. A heatmap was created. Each column represented one subject and each row represented the output of a specific vestibular test. A "relatively bad (vestibular) score" was illustrated by lower Z scores in the colour red. A "relatively good (vestibular) score" was illustrated by higher Z scores in the colour blue. After performing the analysis, etiology and patient characteristics and vestibular test results were compared between clusters.

Ethical considerations

The study was approved by the local ethical committee of center 1 (protocol number NL52768.068.15 / METC 151027), the local ethical committee of center 2 (protocol number 16/42/426) and the local ethical committee of center 3 (project number 20-174). The study was registered on trialregister.nl (center 1, Trial NL5446 (NTR5573)) and ClinicalTrials.gov (center 2, (NCT03690817)). All study participants gave their written informed consent prior to inclusion in the study.

RESULTS

Patient characteristics

A total of 173 patients (50 from center 1, 58 from center 2 and 65 from center 3, 53% males) were included in this study with a mean age of 60 ± 15 years (range 19 – 91 years). A diagnosis of the underlying etiology of BVP could be identified in 112 out of the 173 patients. Genetic disorders (n=29, 17%), ototoxicity (n=28, 16%) and infectious disorders (n=21, 12%) were the most common etiologies. Less frequently, the cause of BVP was due to Menière's Disease (n=12, 7%), (head)trauma (n=6, 4%), auto-immune disease (n=5, 3%), neurodegenerative disorders (n=5, 3%) or congenital disorders (n=4, 2%). Two patients presented with a mixed etiology (vestibular schwannoma on one side and idiopathic etiology on the other side). In approximately one third of the cases (n=61, 35%), no underlying etiology could be identified. The distribution of etiology (Figure 2.1) was significantly different between centers (Fisher's Exact Test $p < 0.01$).

All 3 centers n=173
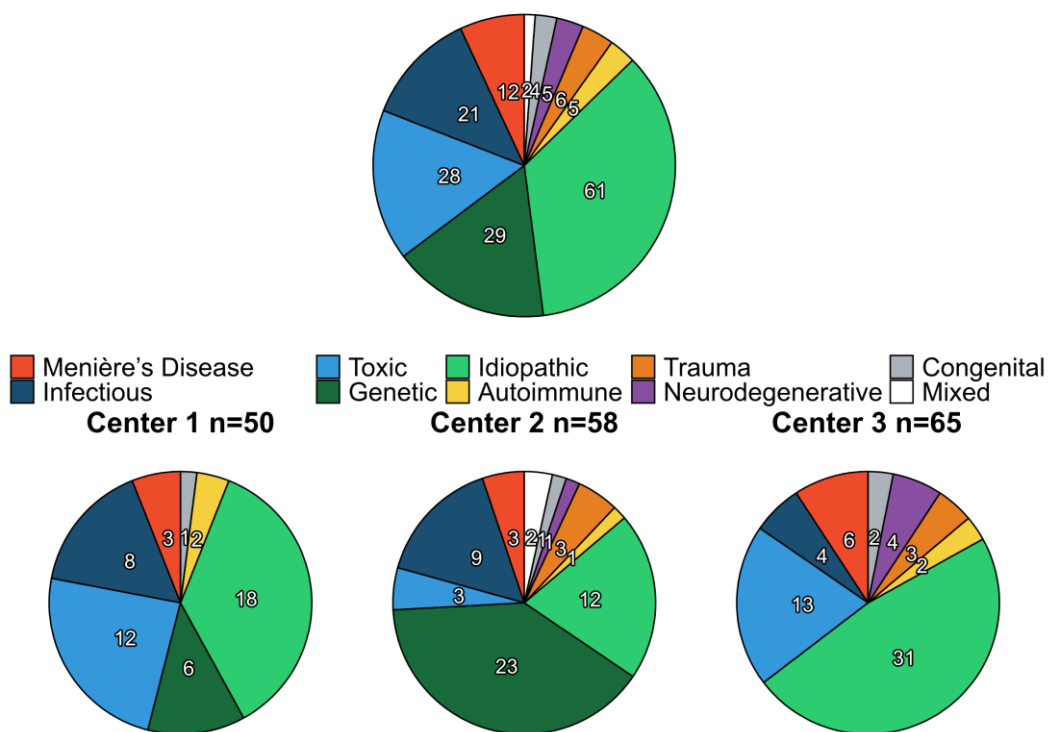
Figure 2.1 Distribution of etiology of bilateral vestibulopathy for all three centers combined and per center separately. Numbers shown in each pie chart represent the count (n) of each etiology.

Vestibular function

Vestibular test results

Median caloric test results were significantly higher for center 3 (6.2°/s) compared with center 1 and 2 (both 0°/s) ($\chi2(2)$ = 39.6, p < 0.001, Figure 2.2). No significant differences were found between median caloric test results for center 1 and 2. Torsion swing test results from center 1 (0.1Hz) were significantly higher compared with center 2 (0.05Hz) (Mann-Whitney U = 1954.5, p = 0.002, Figure 2.2).
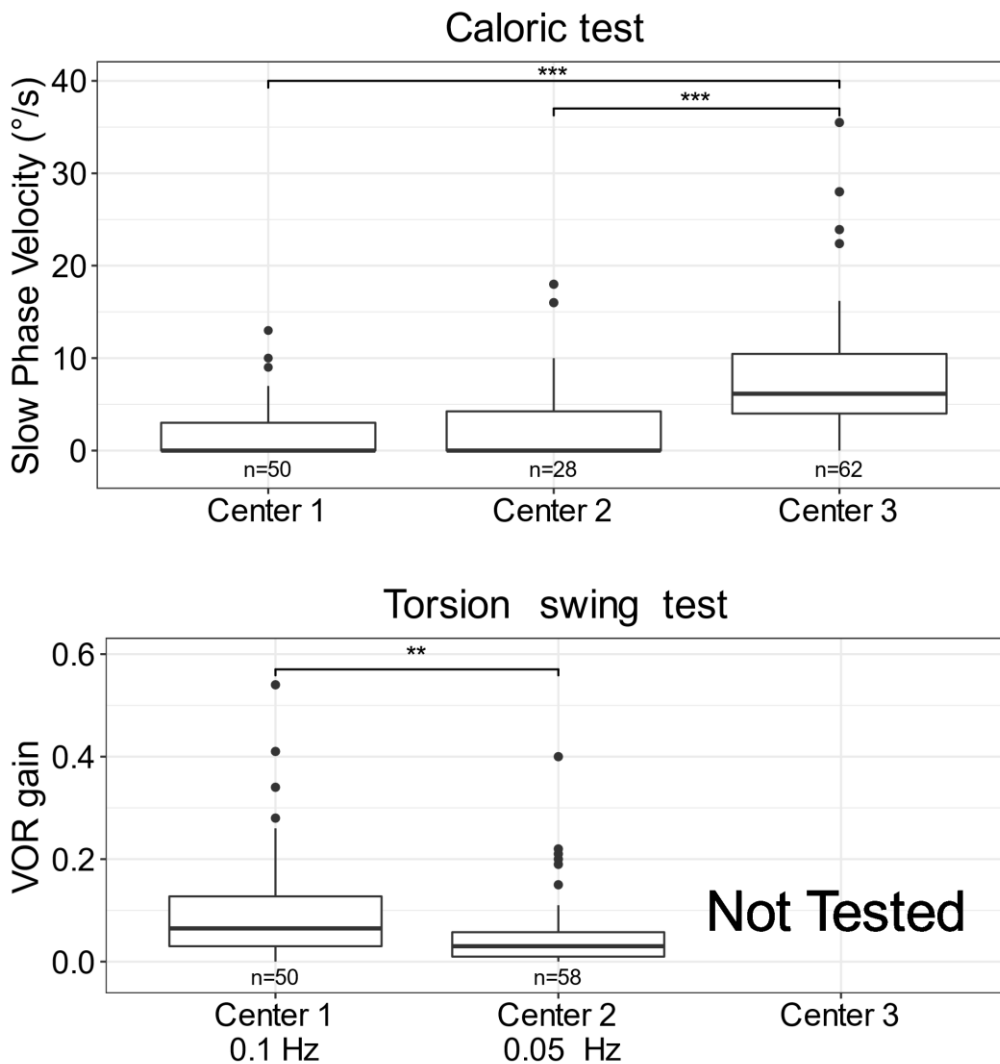
Figure 2.2 Vestibular test results for caloric test (sum of bithermal maximal peak slow phase velocity bilaterally) and torsion swing test (VOR gain) per center. Each box plot represents the 25 to 75 percentiles, bold black lines the median, dots the outliers and asterisks illustrate statistically significant differences.

Three dimensional vHIT results showed a median VOR gain below 0.5 for all semicircular canals, with the lowest VOR gain measured at the horizontal canals and the highest VOR gain measured at the anterior canals ($\chi2(5) = 35.5$, $p <0.001$, Figure 2.3). After analysing the data separately per center, this trend was detectable in both center 1 and 2

but only significant in center 2 after correction for multiple comparisons ($\chi 2(5)$ =35.7, $p <$ 0.001, Appendix 1 figure 1, figure 2 and table 2).
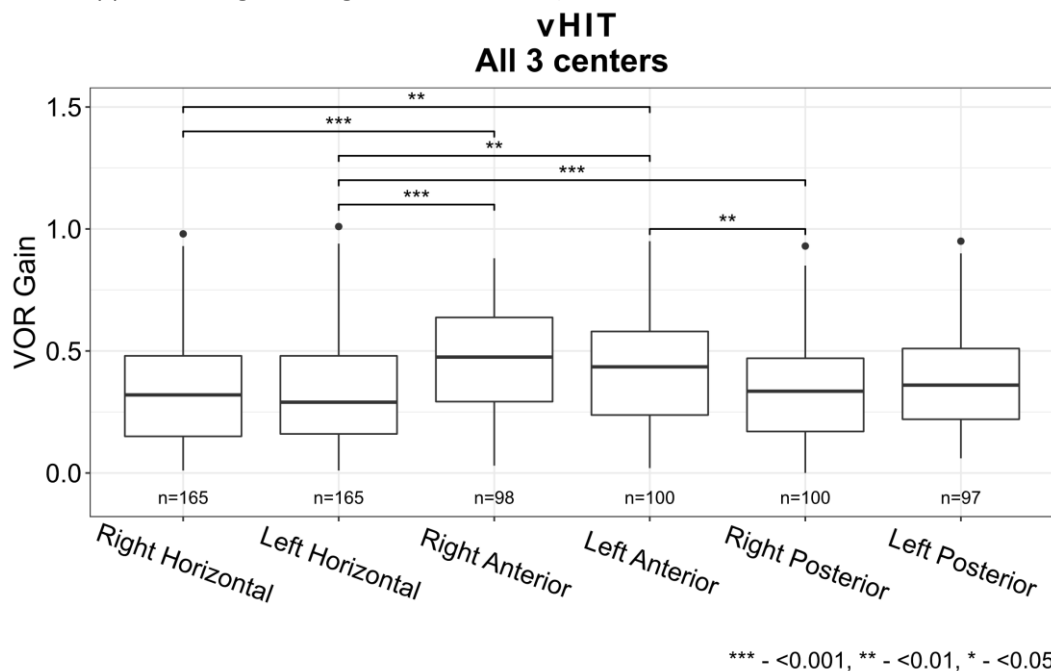
Figure 2.3 Vestibular Ocular Reflex (VOR) gain for all six semi-circular canals measured with video Head Impulse Test for all three centers combined (Horizontal canals: center 1, 2 and 3, Vertical canals: center 1 and 2). Each box plot represents the 25 to 75 percentiles, bold black lines the median, dots the outliers and asterisks (*) illustrate statistically significant differences.

The percentage of bilaterally absent cVEMP responses was higher in center 2 compared with center 1 (66% and 44% respectively, $\chi(2)$ = 8.57, p = 0.014). When looking at cVEMP and oVEMP responses at center 1, rates of bilaterally absent oVEMP responses were higher compared to bilaterally absent cVEMP responses (74% vs 44% respectively, $\chi(2)$ = 9.30, p = 0.010) (Figure 2.4).
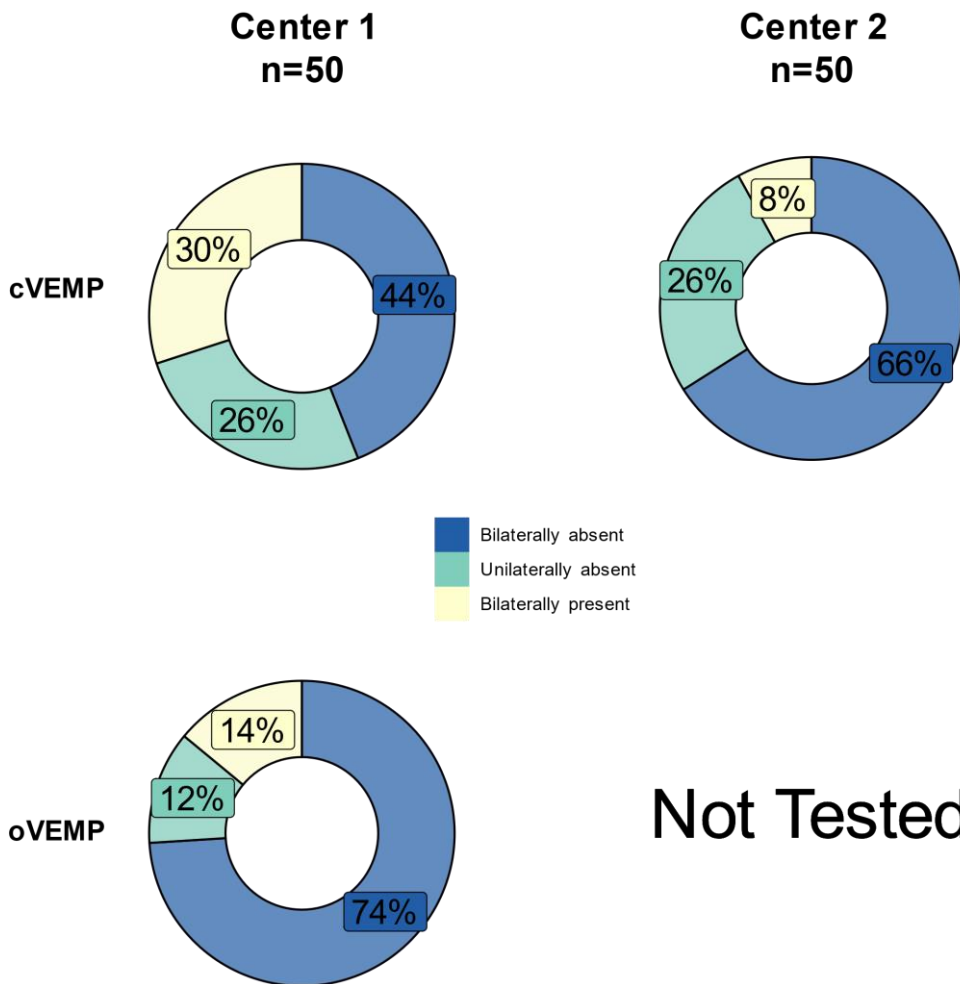
Figure 2.4 Percentages of bilaterally absent, unilaterally absent and bilaterally present cervical and ocular vestibular evoked myogenic potentials (cVEMPs, oVEMPs) of patients with bilateral vestibulopathy at center 1 and center 2.

Vestibular impairment according to the Bárány diagnostic criteria for BVP

Regarding the cases without missing data for caloric testing, torsion swing test and horizontal vHIT, the majority of the patients (54%) met three of the criteria of the Bárány Society described earlier, whereas 21% met two of the Bárány criteria and 25% only met one criterion. In the group of patients who met two out of three Bárány criteria, an impaired VOR gain measured with vHIT combined with a reduced caloric response was most prevalent (19%). In the group of patients who only met one of the Bárány criteria, a reduced caloric response was most prevalent (17%), followed by an impaired VOR gain measured with vHIT (6%) and torsion swing test (2%) (Figure 2.5).

When considering the total study population, the caloric test and horizontal vHIT more often indicated horizontal semicircular canal impairment than the torsion swing test (Figure 2.6). For example, in center 1 only one patient was diagnosed with BVP according to the Bárány criteria based on the torsion swing test alone, whereas the rest of the population was diagnosed using the caloric test or horizontal vHIT or both.
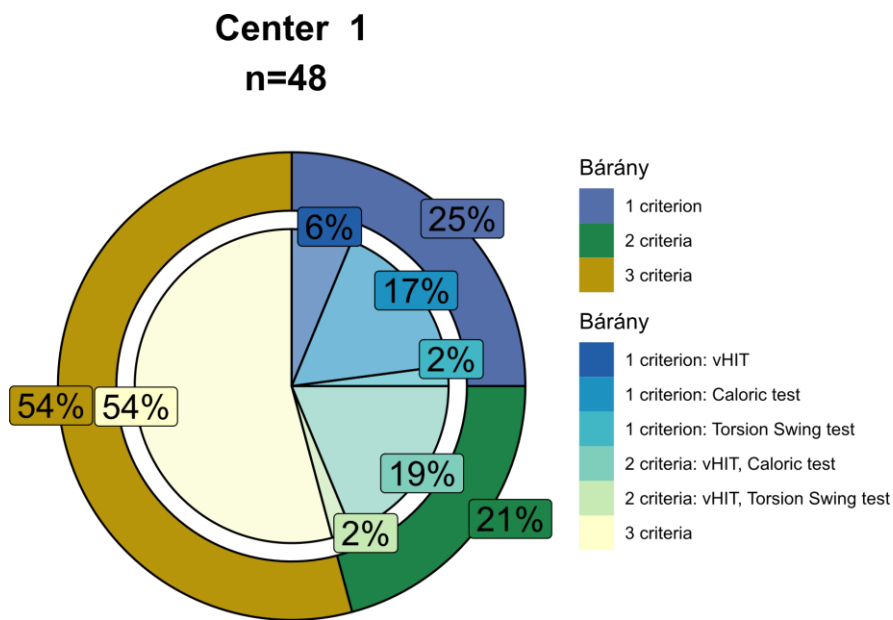
Figure 2.5 Percentages of patients with bilateral vestibulopathy meeting one, two or three of the diagnostic criteria of the Bárány Society (shown in the outer circle, i.e. a reduced bithermal caloric response with a sum of bithermal maximal peak slow phase velocity <6°/s bilaterally and/or a VOR gain <0.1 during torsion swing test at 0.1 Hz and/or a bilaterally reduced horizontal video Head Impulse Test gain of <0.6). The inner circle shows the percentages of which tests are met by patients meeting one or two of the diagnostic criteria. Only cases without missing data for caloric testing, torsion swing test and horizontal video Head Impulse Test were included (center 1, n=48).
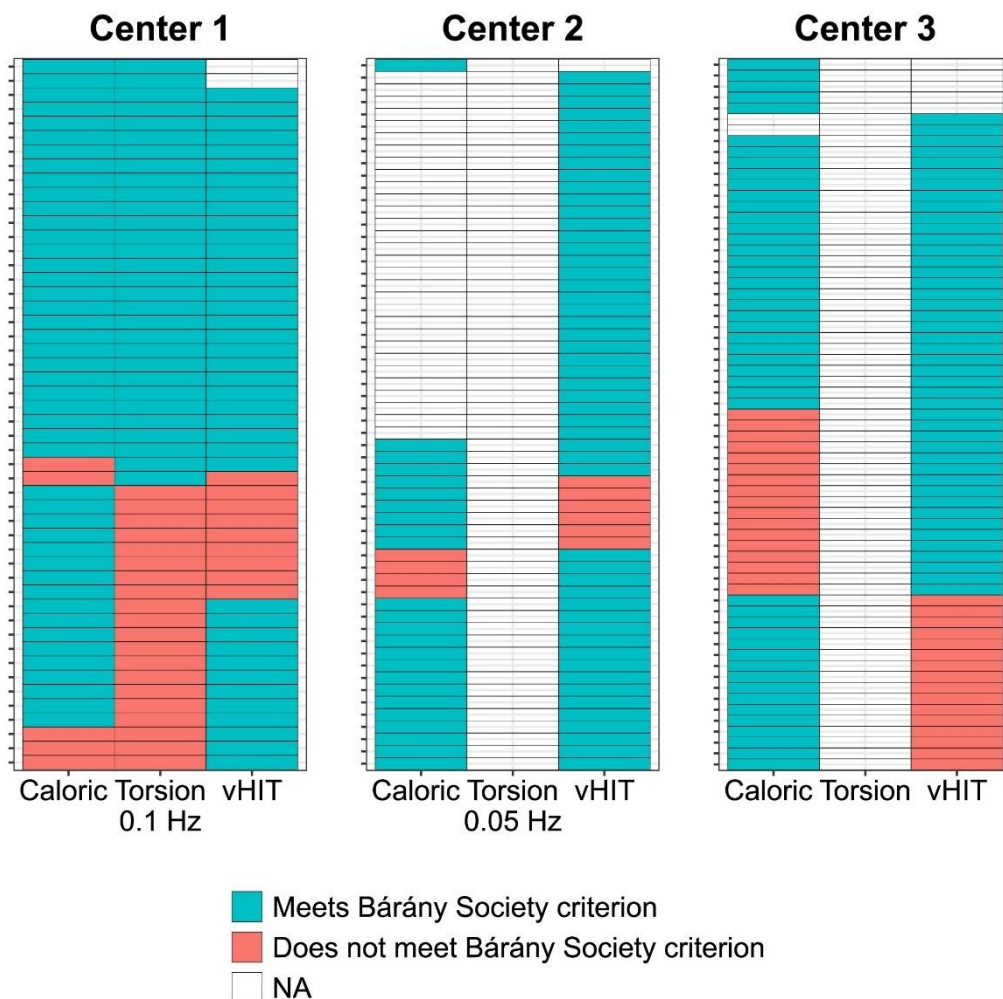
Figure 2.6 Distribution of patients with bilateral vestibulopathy meeting the diagnostic criteria of the Bárány Society, presented for each test separately in the colour blue (i.e. for the caloric test a reduced response with a sum of bithermal maximal peak slow phase velocity <6°/s bilaterally; for the torsion swing test (0.1 Hz) an impaired VOR gain <0.1; for horizontal video Head Impulse Test (vHIT) a bilaterally reduced VOR gain <0.6). Patients not meeting the diagnostic criteria for each test separately, are indicated with the colour red. Each column represents one of the diagnostic criteria per center; each row represents one subject per center.

Patient eligibility for vestibular implantation according to the Implantation criteria

Regarding the cases without missing data for caloric testing, torsion swing test and 3D-vHIT (n=45), the majority of the patients (n=34, 76%) met the implantation criteria. Seventy-one percent of this group met three of the major criteria, whereas 24% met two major criteria and 6% only met one major criterion. In the group of patients who met two

out of three major implantation criteria, an impaired VOR gain measured with vHIT combined with a reduced caloric response was most prevalent. In the group of patients who only met one of the major implantation criteria, a reduced caloric response and an impaired VOR gain measured with vHIT were equally common. None of the patients only met the major implantation criteria for torsion swing test (Figure 2.7).
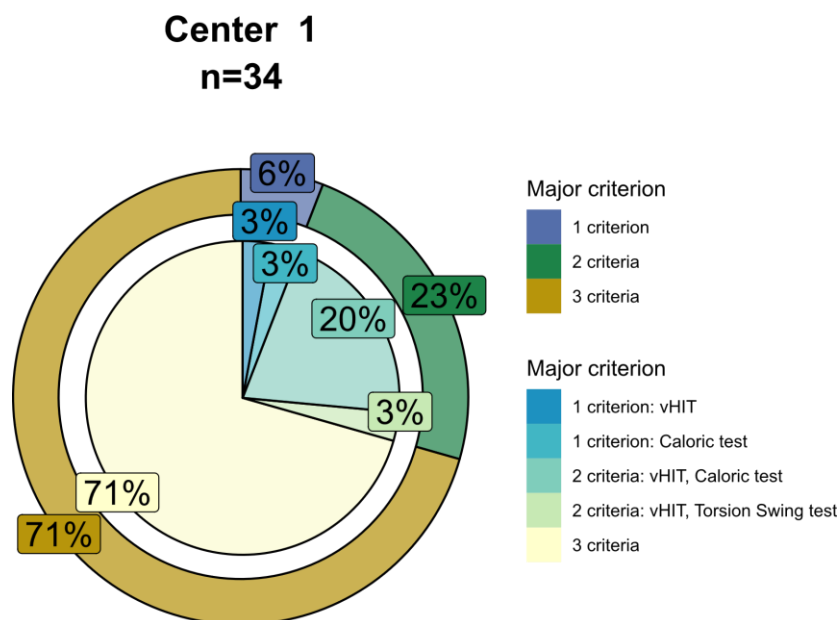
Figure 2.7 Seventy-six percent of the patients met the criteria for vestibular implantation (n=34). For this group, the outer circle shows the percentages of patients meeting one, two or three of the major implantation criteria (i.e. for caloric testing a bilateral impaired caloric responses with a sum of bithermal maximal peak slow phase velocity ≤6°/s, for torsion swing test a reduced VOR gain ≤0.1 and for three dimensional vHIT a bilaterally reduced horizontal VOR gain ≤0.6 combined with at least bilaterally one vertical VOR gain <0.7). The inner circle shows the percentages of which tests are met by patients meeting one or two of the major implantation criteria.

Vestibular function and possible relations to underlying BVP etiology

The median vestibular test results for caloric testing and torsion swing test did not differ between different etiologies (Kruskal-Wallis H test with post-hoc Dunn test and Benjamini Hochberg correction $p > 0.05$, Appendix 1 table 3 and 4). Three dimensional vHIT results did not differ between etiologies for the anterior and posterior canals in the total group (Kruskal Wallis H test, $p > 0.05$, table 3 Appendix 1). However, horizontal vHIT results were significantly lower in the total group for neurodegenerative disorders compared with the idiopathic group, infectious disorders, Menière's Disease and the mixed etiology group. Horizontal vHIT results were also significantly lower for genetic disorders compared with

the idiopathic group and Menière's Disease. Lastly, horizontal vHIT results were significantly lower for (head)trauma compared with the idiopathic group, Menière's Disease and mixed etiology (Kruskal-Wallis H test with post-hoc Dunn test and Benjamini Hochberg correction p <0.05, Figure 2.8 and Appendix 1 tables 3 and 4). After analysing the data separately per center, some trends were detectable per center (e.g. lower horizontal vHIT results for genetic disorders in center 1 and lower horizontal vHIT results for (head)trauma in center 2), however no significant differences were found except for lower horizontal vHIT results for neurodegenerative disorders compared with the idiopathic group and Menière's Disease in center 3 (Kruskal-Wallis H test with post-hoc Dunn test and Benjamini Hochberg correction, Appendix 1 table 4, Appendix 1 figure 3).
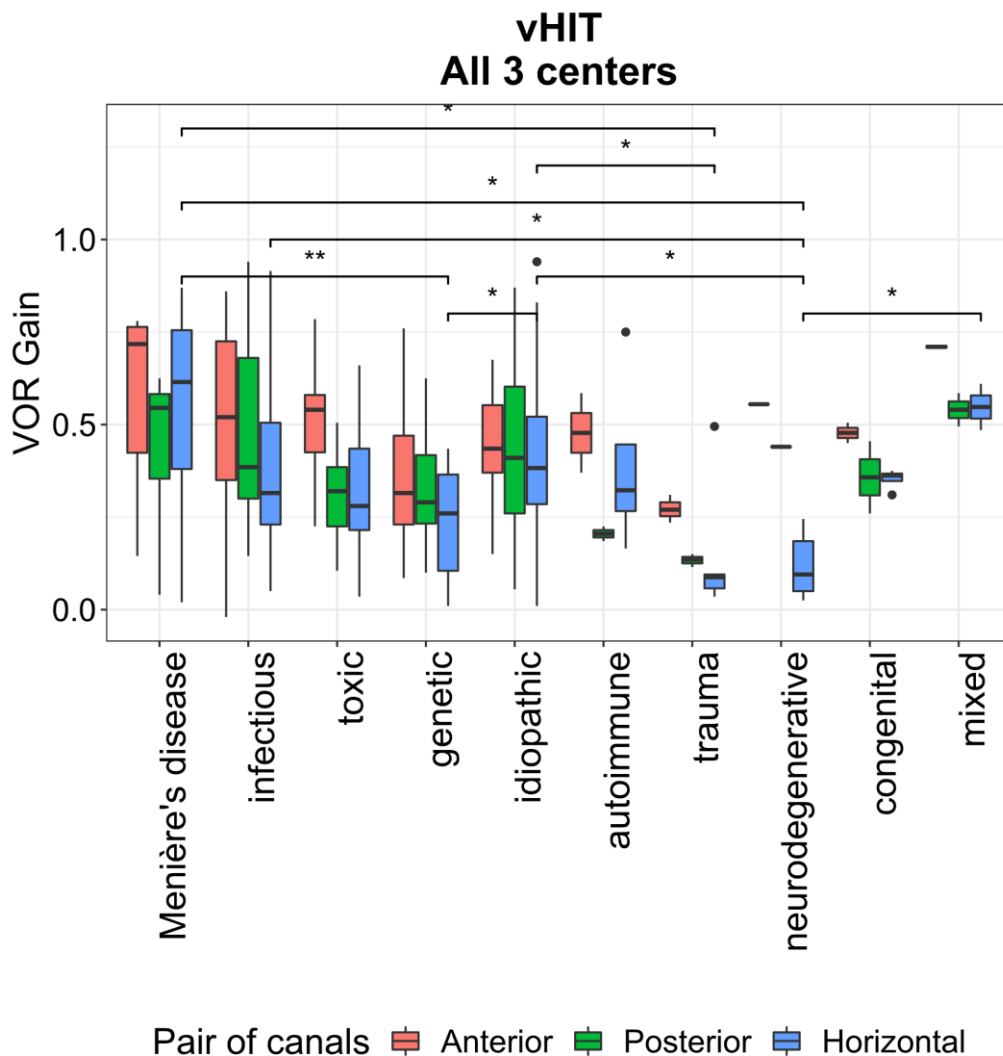
Figure 2.8 Vestibular Ocular Reflex (VOR) gain per etiology for all three pairs of semi-circular canals (i.e. horizontal, anterior and posterior canals) measured with video Head Impulse Test, presented for all three centers combined. Each box plot represents the 25 to 75 percentiles, bold black lines the median, and dots the outliers.

Regarding VEMPs, the highest fraction (≥50%) of bilaterally absent cVEMP responses in center 1 was found in patients with ototoxic, infectious, autoimmune and congenital etiologies, whereas in center 2 almost all etiologies showed high fractions (>60%) of bilaterally absent cVEMP responses (except neurodegenerative disorders). Next to this, all etiologies showed high fractions (≥50%) of bilaterally absent oVEMP responses (center 1) (Appendix 1 figure 4 and 5). No significant differences were seen between different etiologies and the proportion of patients with pathologic VEMP responses (Fisher's exact

test *p* = 0.52 and *p* = 0.99 for cVEMPs center 1 and 2 respectively and Fisher's exact test, *p* = 0.36 for oVEMPs center 1).

To investigate the pattern of vestibular impairment and its relation with etiology, hierarchical cluster analysis was performed, which resulted according to the silhouette method in two clusters (Figure 2.9). The first cluster (n=30; 47% female; mean age 58 years) showed overall lower median vestibular test results compared with the second cluster (n=15; 60% female; mean age 60 years). This was significant for the caloric test, torsion swing test, horizontal vHIT, vertical vHIT (Mann-Whitney U, p < 0.001) and cVEMP (Fisher's Exact Test *p* = 0.04). A detailed overview of all median test results and statistics can be found in Appendix 1table 5 and 6. Next to this, the distribution of the amount of Bárány criteria met, was significantly different among clusters: cluster 1 consisted of patients who predominantly met three criteria, whereas cluster 2 mainly included patients who only met one criterion (Appendix 1 figure 6).

Some etiologies were more prevalent in one of the two clusters. For example, genetic disorders were more prevalent in the first cluster, whereas Menière's Disease was more prevalent in the second cluster (Appendix 1 figure 7). However, no significant association between etiology and clusters was found (Fisher's Exact Test *p* = 0.854, Appendix 1 Table 7).

Next to this, some similarities in vestibular reflex tests were found in the cluster analysis (Figure 2.9, left dendrogram). It was observed that horizontal and anterior vHITs were arranged closely to each other and to caloric testing; posterior vHIT was located closely to the torsion swing test; and oVEMPs and cVEMPs formed a pair.
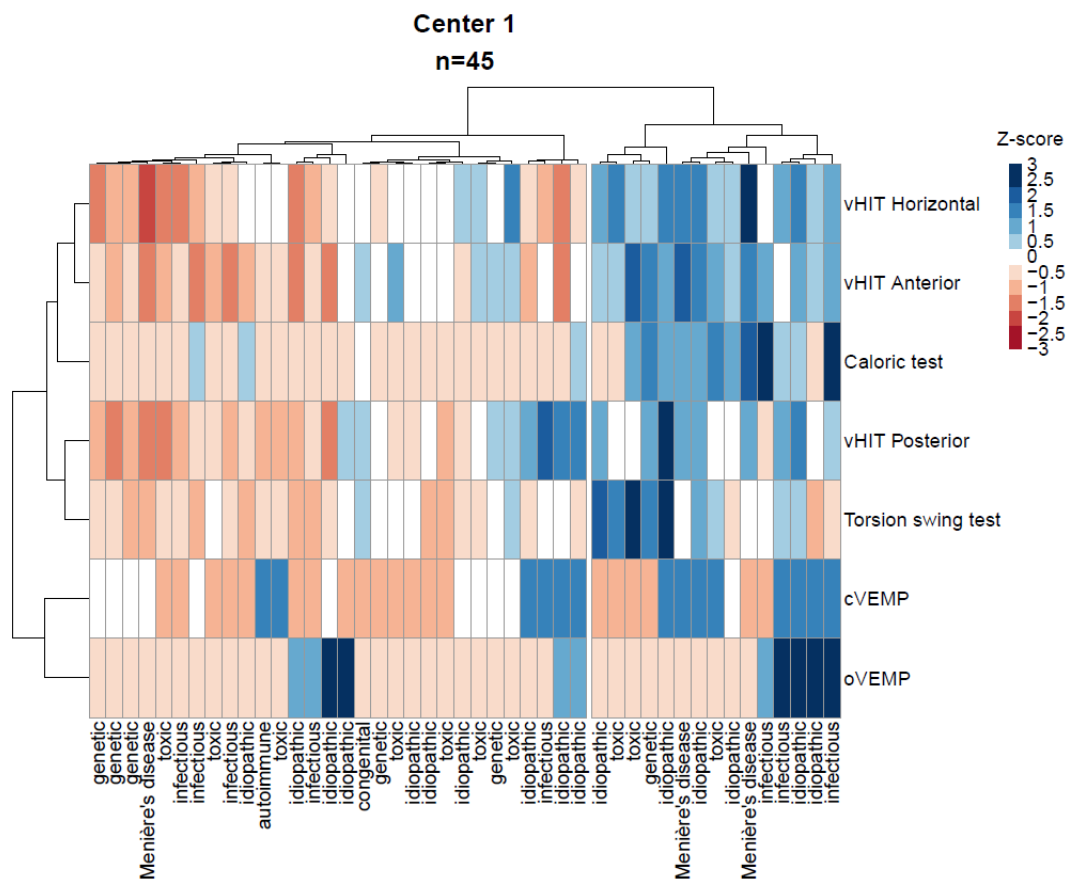
Figure 2.9 Heatmap as a result of hierarchical cluster analysis with 2 dendrograms; Each column represents one subject; each row represents the results of a specific vestibular test. A "bad (vestibular) score" (i.e. low scores on tests of vestibular reflexes) is illustrated by lower Z scores in the colour red. A "relatively good (vestibular) score" (i.e. relative high scores on tests of vestibular reflexes) is illustrated by higher Z scores in the colour blue. Curly brackets indicate the 2 clusters; "Cluster 1" and "Cluster 2". Only cases without missing data for caloric testing, torsion swing test and horizontal and vertical video Head Impulse Test and ocular and cervical Vestibular Evoked Myogenic Potentials were included (n=45). (vHIT: video Head Impulse Test, oVEMP: ocular Vestibular Evoked Myogenic Potential, cVEMP: cervical Vestibular Evoked Myogenic Potentials)

DISCUSSION

This study provided a description of patterns of vestibular impairment and its relation to BVP etiology in a cohort of 173 BVP patients from 3 centers, diagnosed according to the Bárány Society criteria. Vestibular function was measured using the caloric test, torsion swing test, 3D-vHIT, cVEMPs and/or oVEMPs. Etiologies were split into 10 separate groups (i.e. idiopathic, genetic disorders, ototoxicity, infectious disorders, Menière's Disease, (head)trauma, auto-immune disease, neurodegenerative disorders, congenital disorders,

and mixed etiology). The patterns of the vestibular impairment and their relation to BVP etiology are discussed below.

Patterns of vestibular impairment

Overall, this study demonstrated that more than half of patients diagnosed with bilateral vestibulopathy according to the Bárány Society diagnostic criteria, met all three criteria regarding vestibular testing. In patients who only met one or two of the criteria, the caloric test and horizontal vHIT criteria were most often met, in contrast to the torsion swing test criterion. The same trend was found when adhering to the vestibular implantation criteria. However, since the implantation criteria also include the vertical semicircular canals, the percentage of patients meeting the 3D-vHIT implantation criterion was lower compared with the percentage of patients meeting the horizontal vHIT diagnostic (Bárány Society) criterion. Despite the fact that the Bárány Society diagnostic criteria and vestibular implantation criteria seem to be, to some extent, similar to each other, they set different goals and have therefore several substantial differences. As stated above, the vestibular implantation criteria include all three semicircular canals. As a consequence, the vertical canal function should be considered next to the horizontal canal function. Additionally, although the major and especially the minor implantation criteria are less strict in terms of cut-off values for the caloric test, torsion swing test and horizontal vHIT compared with the diagnostic criteria, a potential implant candidate must meet all the implantation criteria (Figure 2.5 versus Figure 2.7). Furthermore, apart from vestibular reflex testing, the vestibular implantation criteria also include assessment of comorbidities and eligibility to undergo surgery (Van De Berg et al., 2020). Therefore, only a subgroup of the BVP population will be eligible for implantation.

When investigating vestibular test results per test and per center separately, it was observed that the slow phase eye velocities measured during caloric test were significantly higher in center 3 compared with center 1 and 2 (Figure 2.2). This can be explained by different factors, varying from differences in caloric testing methods used (namely electronystagmography at center 1 and 2 and videonystagmography at center 3) which can result in different phase velocities values due to different blink detection and image processing algorithms used (Pietkiewicz et al., 2012), to different patient populations included in each center (Lucieer et al., 2016). Next to this, torsion swing test results were significantly higher in center 1 compared with center 2, which can be explained by differences in used frequency (0.1Hz at center 1 and 0.05 Hz at center 2): the vestibular system is more sensitive for rotations at 0.1 Hz than 0.05 Hz, leading to a higher response (i.e. VOR gain) (Baloh et al., 1979; Kingma and van de Berg, 2016; Lucieer et al., 2016). This sensitivity might also account for the fact that the diagnostic torsion swing test criterion was less often met than the criteria of the caloric test. After all, since the vestibular system has its optimum sensitivity around frequencies tested by the torsion swing test at 0.1Hz (in contrast to the frequencies tested by the caloric), a uniform decrease in semicircular canal function across all frequencies might result in losing responses to caloric testing first. Although frequencies tested with vHIT are also within the optimum frequency range of the vestibular system, vHIT more often indicated horizontal semicircular canal impairment than

the torsion swing test. Therefore, it might be hypothesized that the vestibular system shows earlier an impairment for conditions which demand a relatively large vestibular output in response to high accelerations and velocities. This hypothesis needs further investigation.

Nevertheless, the results of this study showed that the response to torsion swing testing might be preserved the longest (Kingma and van de Berg, 2016). Therefore, the torsion swing test is least sensitive in detecting bilateral vestibulopathy, but most sensitive in measuring residual vestibular function, whereas caloric testing and vHIT seem to be more sensitive for measuring vestibular impairment (Lucieer et al., 2016).

The variability of VEMP responses in this study is in line with results from previous studies, which also demonstrated the wide range of otolith function (as measured with c- and oVEMPs) in patients with BVP (Zingler et al., 2008; Agrawal et al., 2013; Rosengren et al., 2018). This variability could be explained by the large range of VEMP responses present in normal subjects, the heterogenous nature of BVP and the nature of VEMP testing itself (e.g. it is still unknown how much residual otolith function needs to be present to produce a synchronous motor discharge) (Rosengren et al., 2018). Furthermore, because of the diagnostic inclusion criteria, all of the included patients have horizontal canal semicircular impairment, whereas the function of the other vestibular end organs can have variable degrees of (dys)function. Since the utricle (tested with oVEMPs) projects into the superior branch of the vestibular nerve together with the horizontal semicircular canal, it can be hypothesized that patients included based on horizontal canal impairment also show bilaterally absent oVEMP responses (Bordoni et al., 2019). This might explain why rates of bilaterally absent oVEMP responses were higher compared to bilaterally absent cVEMP responses in center 1 (Figure 2.4), since there is possibly an intact inferior vestibular nerve function on which the saccule projects. Currently, it is not known whether isolated bilateral dysfunction of both otolith organs also causes significant disability (Rosengren et al., 2018). Therefore, all vestibular end organs should be evaluated before and after vestibular implantation in order to create awareness about potential damage to intact vestibular structures.

Contribution of etiology to vestibular impairment

The distribution of etiologies (Figure 2.1) was significantly different among 3 centers, indicating inhomogeneity of the data. This can potentially be caused by differences in clinical settings, namely ENT clinics (center 1 and center 2) compared with a neurological clinic (center 3). This fact can explain the trend that among all 3 centers the biggest fraction of neurodegenerative and idiopathic patients was observed in center 3, whereas the biggest fraction of infectious and genetic disorders was observed in center 1 and 2.

The distribution of the 3D-vHIT VOR gains between different etiologies indicated several trends, although not every trend proved to be statistically significant (Figure 2.9). Overall, 3D-vHIT results showed significantly better gains for both anterior canals compared with the horizontal and posterior canals, which corresponds with previous literature (Tarnutzer et al., 2016). Three dimensional vHIT results did not differ significantly between etiologies for anterior and posterior canals although trends of anterior canal sparing were observed for Menière's Disease, infectious disorders, ototoxicity, trauma and

idiopathic BVP. This is congruent with previous literature (Tarnutzer et al., 2016). Next to this, horizontal vHIT results were significantly lower for neurodegenerative disorders, genetic disorders, and trauma whereas horizontal vHIT results were significantly higher for Menière's disease and infectious disorders.

Cluster analysis identified two separate clusters of BVP patients in center 1 (which was the center with most available vestibular test data) with significant differences in residual vestibular function according to vestibular testing. This was also reflected by the amount of diagnostic and vestibular implantation criteria met between clusters. Cluster 1 consisted of patients who predominantly met 3 criteria, whereas cluster 2 mainly included patients who met only 1 criterion (Appendix 1 figure 6). Although, no statistically significant differences were found in etiology distribution between clusters (Figure 2.9), a slightly higher prevalence of Menière's Disease was observed in cluster 2 that performed "better" in all vestibular tests, whereas the idiopathic and ototoxicity etiologies prevailed in cluster 1 and performed "worse" (Appendix 1 figure 4). This could imply that the contribution of etiology to specific patterns of vestibular impairment might be limited and would eventually result in an overall better or worse vestibular function. Despite some patterns were found for a few BVP etiologies, one should consider every case individually and investigate every part of the vestibular system separately to obtain full understanding of the vestibular impairment.

Order of vestibular test outcomes according to cluster analysis

Cluster analysis showed similarities in vestibular reflex tests used in center 1 (Figure 2.9, left dendrogram). For example, horizontal and anterior vHITs were arranged close to each other and to caloric testing; posterior vHIT was located close to torsion swing test; and oVEMPs and cVEMPs formed a pair. It is quite intuitive for VEMP results to be correlated to each other, since the two otolith organs are located next to each other. However, the opposite was found when testing the semicircular canal function. The caloric test, torsion swing test and horizontal vHIT are aimed to measure horizontal canal function and it could be hypothesized that they would closely correlate to each other. However, this was not observed in the cluster analysis, which showed close correlation of anterior and horizontal vHIT results together with the caloric test, and close correlation of posterior vHIT results with the torsion swing test. The proximity of the horizontal and anterior vHIT in the cluster analysis can be partly explained in terms of anatomy. The horizontal and anterior canals ampullae are located close to each other and project into the same superior vestibular nerve division, whereas the inferior vestibular nerve division receives input from the posterior canals (Khan and Chang, 2013). Next to this, as stated before, vHIT and the caloric test seem to be able to indicate vestibular impairment, whereas the torsion swing test is more sensitive to measure the residual vestibular function (Kingma and van de Berg, 2016). This could explain why the torsion swing test is not in close proximity to the horizontal vHIT and caloric test in the cluster analysis. The trends found in this cluster analysis differed from the trends described by a previous study (Tarnutzer et al., 2018). For example, differences in the arrangement of the variables after clustering (e.g. horizontal and posterior canals in close proximity to the utriculus according to the previous study

(Tarnutzer et al., 2018)). Furthermore, in contrast to the study presented here, no differences in vestibular impairment were found. This could be the result of different approaches used, namely: 1) Normalization of data using single test results across patient groups (this study) compared with using all vestibular test results within one single patient ((Tarnutzer et al., 2018)); and 2) scoring of vestibular function using results from separate vestibular reflex tests (this study) compared with considering separate vestibular organs (canals and otoliths, (Tarnutzer et al., 2018)). To sum up, the different study goals could result in a different distribution of patients among clusters and different interpretations regarding etiology, despite the implementation of the same analysis. Therefore, it is advised to investigate all vestibular end organs separately to appreciate the vestibular impairment as a whole.

Limitations

Most importantly, some etiology groups included small amounts of patients (n<5), which complicated statistical analysis. Next to this, the vestibular implantation criteria include a number of items that are not related to the vestibular reflex testing, which were not considered in this study (e.g. psychological or psychiatric disorders or an ability to undergo surgery). This could imply that the number of patients eligible for implantation in this study is an overestimation. Finally, the torsion swing test phase, being the 4th criterion according to Bárány criteria, was not used in this study, because either it was not measured or the automatic calculation algorithm was not reliable.

Future perspectives

In order to gather a much bigger dataset from different sources that can be pooled and analyzed together, an international standardized approach for vestibular testing will be crucial (Strupp et al., 2020). In particular, 1) different VEMP devices should be compared to each other in order to obtain the relation between stimuli and the threshold values; 2) the same torsion swing frequency and velocity should be used; and 3) raw traces of eye movements in both vHIT (obtained from different devices (Van Dooren et al., 2020)) and caloric testing (electronystagmography versus videonystagmography) should be analyzed, since different processing algorithms may lead to a significant difference in results of gain and SPV. In the case of a larger dataset, etiologies can be defined more specifically and at a more pathophysiological and morphological level (e.g. etiologies that lead to fibrosis). Next to this, future research between objective vestibular reflex test results and self-reported symptom severity could provide more insight into the effect of different patterns of vestibular impairment and degree of specific BVP symptoms (e.g. anterior canal sparing and self-reported oscillopsia severity).

CONCLUSION

This study provided a description of vestibular function in a large cohort of BVP patients diagnosed according to the Bárány Society criteria. Overall, this study showed differences in the degree of vestibular impairment measured with different vestibular tests such as caloric test, 3D-vHIT, torsion swing test, and VEMPs. More specific, some tests (i.e. caloric testing and vHIT) seem to be more sensitive for detecting vestibular impairment,

whereas other tests (e.g. torsion swing test) are more suited for measuring residual vestibular function. In addition, no striking patterns of vestibular impairment in relation to etiology were found. Nevertheless, when comparing the Bárány Society diagnostic and vestibular implantation criteria, it was shown that although the implantation criteria are more strict, still 76% of BVP patients were eligible for implantation based on vestibular test criteria. It is advised, especially in research setting, to carefully examine every patient for their overall pattern of vestibular impairment (i.e., all five vestibular end organs), in order to make well informed and personalized therapeutic decisions.

REFERENCES

Agrawal, Y., Bremova, T., Kremmyda, O., and Strupp, M. (2013). Semicircular canal, saccular and utricular function in patients with bilateral vestibulopathy: analysis based on etiology. *J Neurol* 260(3)**,** 876-883. doi: 10.1007/s00415-012-6724-y.

Baloh, R.W., Sills, A.W., and Honrubia, V. (1979). Impulsive and sinusoidal rotatory testing: a comparison with results of caloric testing. *Laryngoscope* 89(4)**,** 646-654. doi: 10.1288/00005537-197904000-00013.

Bordoni, B., Mankowski, N.L., and Daly, D.T. (2019). Neuroanatomy, cranial nerve 8 (vestibulocochlear).

Bovo, R., Ciorba, A., and Martini, A. (2010). Vertigo and autoimmunity. *Eur Arch Otorhinolaryngol* 267(1)**,** 13-19. doi: 10.1007/s00405-009-1122-5.

Brandt, T., Schautzer, F., Hamilton, D.A., Brüning, R., Markowitsch, H.J., Kalla, R., et al. (2005). Vestibular loss causes hippocampal atrophy and impaired spatial memory in humans. *Brain* 128(Pt 11)**,** 2732-2741. doi: 10.1093/brain/awh617.

Chow, M.R., Ayiotis, A.I., Schoo, D.P., Gimmon, Y., Lane, K.E., Morris, B.J., et al. (2021). Posture, Gait, Quality of Life, and Hearing with a Vestibular Implant. *New England Journal of Medicine* 384(6)**,** 521-532. doi: 10.1056/NEJMoa2020457.

Clemmens, C., and Ruckenstein, M. (2012). Characteristics of patients with unilateral and bilateral Ménière's disease. *Otol Neurotol* 33(7)**,** 1266-1269. doi: 10.1097/MAO.0b013e31826426b9.

Colebatch, J.G., Halmagyi, G.M., and Skuse, N.F. (1994). Myogenic potentials generated by a click-evoked vestibulocollic reflex. *J Neurol Neurosurg Psychiatry* 57(2)**,** 190-197.

Cushing, S.L., Papsin, B.C., Rutka, J.A., James, A.L., Blaser, S.L., and Gordon, K.A. (2009). Vestibular end-organ and balance deficits after meningitis and cochlear implantation in children correlate poorly with functional outcome. *Otol Neurotol* 30(4)**,** 488-495. doi: 10.1097/MAO.0b013e31819bd7c8.

de Varebeke, S.P., Termote, B., Van Camp, G., Govaerts, P.J., Schepers, S., Cox, T., et al. (2014). Focal sclerosis of semicircular canals with severe DFNA9 hearing impairment caused by a P51S COCH-mutation: is there a link? *Otol Neurotol* 35(6)**,** 1077-1086. doi: 10.1097/mao.0000000000000283.

Della Santina, C.C., Migliaccio, A.A., and Patel, A.H. (2007). A multichannel semicircular canal neural prosthesis using electrical stimulation to restore 3-d vestibular sensation. *IEEE Trans Biomed Eng* 54(6 Pt 1)**,** 1016-1030. doi: 10.1109/tbme.2007.894629.

Dobbels, B., Lucieer, F., Mertens, G., Gilles, A., Moyaert, J., van de Heyning, P., et al. (2020). Prospective cohort study on the predictors of fall risk in 119 patients with bilateral vestibulopathy. *PLoS One* 15(3)**,** e0228768. doi: 10.1371/journal.pone.0228768.

Dobbels, B., Mertens, G., Gilles, A., Claes, A., Moyaert, J., van de Berg, R., et al. (2019a). Cognitive Function in Acquired Bilateral Vestibulopathy: A Cross-Sectional Study on Cognition, Hearing, and Vestibular Loss. *Front Neurosci* 13**,** 340. doi: 10.3389/fnins.2019.00340.

Dobbels, B., Peetermans, O., Boon, B., Mertens, G., Van de Heyning, P., and Van Rompaey, V. (2019b). Impact of Bilateral Vestibulopathy on Spatial and Nonspatial Cognition: A Systematic Review. *Ear Hear* 40(4)**,** 757-765. doi: 10.1097/aud.0000000000000679.

Fu, T.S., Carr, S.D., Douglas-Jones, P., Dillon, W., Ilan, O., Syed, I.M., et al. (2020). Gentamicin Vestibulotoxicity: Further Insights From a Large Clinical Series. *Otol Neurotol*. doi: 10.1097/mao.0000000000002698.

Fujimoto, C., Murofushi, T., Chihara, Y., Suzuki, M., Yamasoba, T., and Iwasaki, S. (2009). Novel subtype of idiopathic bilateral vestibulopathy: bilateral absence of vestibular evoked myogenic potentials in the presence of normal caloric responses. *J Neurol* 256(9)**,** 1488-1492. doi: 10.1007/s00415-009-5147-x.

Golub, J.S., Ling, L., Nie, K., Nowack, A., Shepherd, S.J., Bierer, S.M., et al. (2014). Prosthetic implantation of the human vestibular system. *Otol Neurotol* 35(1)**,** 136-147. doi: 10.1097/mao.0000000000000003.

Greco, A., Gallo, A., Fusconi, M., Magliulo, G., Turchetta, R., Marinelli, C., et al. (2013). Cogan's syndrome: an autoimmune inner ear disease. *Autoimmun Rev* 12(3)**,** 396-400. doi: 10.1016/j.autrev.2012.07.012.

Guinand, N., Boselie, F., Guyot, J.P., and Kingma, H. (2012). Quality of life of patients with bilateral vestibulopathy. *Ann Otol Rhinol Laryngol* 121(7)**,** 471-477. doi: 10.1177/000348941212100708.

Guinand, N., Van de Berg, R., Cavuscens, S., Stokroos, R., Ranieri, M., Pelizzone, M., et al. (2016). Restoring Visual Acuity in Dynamic Conditions with a Vestibular Implant. *Frontiers in Neuroscience* 10(577). doi: 10.3389/fnins.2016.00577.

Guyot, J.P., and Perez Fornos, A. (2019). Milestones in the development of a vestibular implant. *Curr Opin Neurol* 32(1)**,** 145-153. doi: 10.1097/wco.0000000000000639.

Hain, T.C., Cherchi, M., and Yacovino, D.A. (2013). Bilateral vestibular loss. *Semin Neurol* 33(3)**,** 195-203. doi: 10.1055/s-0033-1354597.

Hermann, R., Ionescu, E.C., Dumas, O., Tringali, S., Truy, E., and Tilikete, C. (2018). Bilateral Vestibulopathy: Vestibular Function, Dynamic Visual Acuity and Functional Impact. *Frontiers in Neurology* 9**,** 555. doi: 10.3389/fneur.2018.00555.

Ishiyama, G., Ishiyama, A., Kerber, K., and Baloh, R.W. (2006). Gentamicin ototoxicity: clinical features and the effect on the human vestibulo-ocular reflex. *Acta Otolaryngol* 126(10)**,** 1057-1061. doi: 10.1080/00016480600606673.

Khan, S., and Chang, R. (2013). Anatomy of the vestibular system: a review. *NeuroRehabilitation* 32(3)**,** 437-443. doi: 10.3233/nre-130866.

Kingma, H., Felipe, L., Gerards, M.C., Gerits, P., Guinand, N., Perez-Fornos, A., et al. (2019). Vibrotactile feedback improves balance and mobility in patients with severe bilateral vestibular loss. *J Neurol* 266(Suppl 1)**,** 19-26. doi: 10.1007/s00415-018-9133-z.

Kingma, H., and van de Berg, R. (2016). Anatomy, physiology, and physics of the peripheral vestibular system. *Handbook of clinical neurology* 137**,** 1-16.

Kovacs, E., Wang, X., and Grill, E. (2019). Economic burden of vertigo: a systematic review. *Health Economics Review* 9(1)**,** 1-14.

Kremmyda, O., Hüfner, K., Flanagin, V.L., Hamilton, D.A., Linn, J., Strupp, M., et al. (2016). Beyond Dizziness: Virtual Navigation, Spatial Anxiety and Hippocampal Volume in Bilateral Vestibulopathy. *Frontiers in Human Neuroscience* 10(139). doi: 10.3389/fnhum.2016.00139.

Lee, J.Y., and Kim, M.B. (2020). Change of VOR gain and pure-tone threshold after single low-dose intratympanic gentamicin injection in Meniere's disease. *Acta Otolaryngol* 140(4)**,** 314-318. doi: 10.1080/00016489.2019.1708457.

Lucieer, F., Duijn, S., Van Rompaey, V., Perez Fornos, A., Guinand, N., Guyot, J.P., et al. (2018). Full Spectrum of Reported Symptoms of Bilateral Vestibulopathy Needs Further Investigation-A Systematic Review. *Frontiers in Neurology* 9**,** 352. doi: 10.3389/fneur.2018.00352.

Lucieer, F., Vonk, P., Guinand, N., Stokroos, R., Kingma, H., and van de Berg, R. (2016). Bilateral Vestibular Hypofunction: Insights in Etiologies, Clinical Subtypes, and Diagnostics. *Frontiers in Neurology* 7**,** 26. doi: 10.3389/fneur.2016.00026.

Lucieer, F.M.P., Van Hecke, R., van Stiphout, L., Duijn, S., Perez-Fornos, A., Guinand, N., et al. (2020). Bilateral vestibulopathy: beyond imbalance and oscillopsia. *Journal of Neurology* 267(1)**,** 241-255. doi: 10.1007/s00415-020-10243-5.

Macdougall, H.G., McGarvie, L.A., Halmagyi, G.M., Curthoys, I.S., and Weber, K.P. (2013). The video Head Impulse Test (vHIT) detects vertical semicircular canal dysfunction. *PLoS One* 8(4)**,** e61488. doi: 10.1371/journal.pone.0061488.

Paredis, S., van Stiphout, L., Remmen, E., Strupp, M., Gerards, M.-C., Kingma, H., et al. (2021). DISCOHAT: An Acronym to Describe the Spectrum of Symptoms Related to Bilateral Vestibulopathy. *Frontiers in Neurology* 12(1949). doi: 10.3389/fneur.2021.771650.

Perez Fornos, A., Cavuscens, S., Ranieri, M., van de Berg, R., Stokroos, R., Kingma, H., et al. (2017). The vestibular implant: A probe in orbit around the human balance system. *J Vestib Res* 27(1)**,** 51-61. doi: 10.3233/ves-170604.

Perez Fornos, A., Guinand, N., van de Berg, R., Stokroos, R., Micera, S., Kingma, H., et al. (2014). Artificial Balance: Restoration of the Vestibulo-Ocular Reflex in Humans with a Prototype Vestibular Neuroprosthesis. *Frontiers in Neurology* 5(66). doi: 10.3389/fneur.2014.00066.

Pietkiewicz, P., Pepaś, R., Sułkowski, W.J., Zielińska-Bliźniewska, H., and Olszewski, J. (2012). Electronystagmography versus videonystagmography in diagnosis of vertigo. *Int J Occup Med Environ Health* 25(1)**,** 59-65. doi: 10.2478/s13382-012-0002-1.

Porciuncula, F., Johnson, C.C., and Glickman, L.B. (2012). The effect of vestibular rehabilitation on adults with bilateral vestibular hypofunction: a systematic review. *J Vestib Res* 22(5-6)**,** 283-298. doi: 10.3233/ves-120464.

Ramos de Miguel, A., Falcon Gonzalez, J.C., and Ramos Macias, A. (2017). Vestibular Response to Electrical Stimulation of the Otolith Organs. Implications in the Development of A Vestibular Implant for the Improvement of the Sensation of Gravitoinertial Accelerations. *J Int Adv Otol* 13(2)**,** 154-161. doi: 10.5152/iao.2017.4216.

Rinne, T., Bronstein, A.M., Rudge, P., Gresty, M.A., and Luxon, L.M. (1998). Bilateral loss of vestibular function: clinical findings in 53 patients. *J Neurol* 245(6-7)**,** 314-321. doi: 10.1007/s004150050225.

Rosengren, S.M., Welgampola, M.S., and Taylor, R.L. (2018). Vestibular-Evoked Myogenic Potentials in Bilateral Vestibulopathy. *Front Neurol* 9**,** 252. doi: 10.3389/fneur.2018.00252.

Rousseeuw, P.J. (1987). Silhouettes: A graphical aid to the interpretation and validation of cluster analysis. *Journal of Computational and Applied Mathematics* 20**,** 53-65. doi: https://doi.org/10.1016/0377-0427(87)90125-7.

Strupp, M., Grimberg, J., Teufel, J., Laurell, G., Kingma, H., and Grill, E. (2020). Worldwide survey on laboratory testing of vestibular function. *Neurol Clin Pract* 10(5)**,** 379-387. doi: 10.1212/cpj.0000000000000744.

Strupp, M., Kim, J.S., Murofushi, T., Straumann, D., Jen, J.C., Rosengren, S.M., et al. (2017). Bilateral vestibulopathy: Diagnostic criteria Consensus document of the Classification Committee of the Barany Society. *J Vestib Res* 27(4)**,** 177-189. doi: 10.3233/VES-170619.

Sun, D.Q., Ward, B.K., Semenov, Y.R., Carey, J.P., and Della Santina, C.C. (2014). Bilateral Vestibular Deficiency: Quality of Life and Economic Implications. *JAMA Otolaryngology–Head & Neck Surgery* 140(6)**,** 527-534. doi: 10.1001/jamaoto.2014.490.

Szmulewicz, D.J., McLean, C.A., MacDougall, H.G., Roberts, L., Storey, E., and Halmagyi, G.M. (2014). CANVAS an update: clinical presentation, investigation and management. *J Vestib Res* 24(5-6)**,** 465-474. doi: 10.3233/ves-140536.

Tarnutzer, A.A., Bockisch, C.J., Buffone, E., and Weber, K.P. (2018). Hierarchical Cluster Analysis of Semicircular Canal and Otolith Deficits in Bilateral Vestibulopathy. *Front Neurol* 9**,** 244. doi: 10.3389/fneur.2018.00244.

Tarnutzer, A.A., Bockisch, C.J., Buffone, E., Weiler, S., Bachmann, L.M., and Weber, K.P. (2016). Disease-specific sparing of the anterior semicircular canals in bilateral vestibulopathy. *Clin Neurophysiol* 127(8)**,** 2791-2801. doi: 10.1016/j.clinph.2016.05.005.

Van De Berg, R., Ramos, A., Van Rompaey, V., Bisdorff, A., Perez-Fornos, A., Rubinstein, J.T., et al. (2020). The vestibular implant: Opinion statement on implantation criteria for research. *Journal of Vestibular Research***,** 1-11. doi: 10.3233/ves-200701.

van Dooren, T.S., Lucieer, F.M.P., Janssen, A.M.L., Kingma, H., and van de Berg, R. (2018). The Video Head Impulse Test and the Influence of Daily Use of Spectacles to Correct a Refractive Error. *Front Neurol* 9**,** 125. doi: 10.3389/fneur.2018.00125.

Van Dooren, T.S., Starkov, D., Lucieer, F.M.P., Vermorken, B., Janssen, A.M.L., Guinand, N., et al. (2020). Comparison of three video head impulse test systems for the diagnosis of bilateral vestibulopathy. *Journal of Neurology*. doi: 10.1007/s00415-020-10060-w.

van Stiphout, L., Lucieer, F., Pleshkov, M., Van Rompaey, V., Widdershoven, J., Guinand, N., et al. (2021). Bilateral vestibulopathy decreases self-motion perception. *J Neurol*. doi: 10.1007/s00415-021-10695-3.

Vanspauwen, R., Weerts, A., Hendrickx, M., Buytaert, K.I., Blaivie, C., Jorens, P.G., et al. (2011). No effects of anti-motion sickness drugs on vestibular evoked myogenic potentials outcome parameters. *Otol Neurotol* 32(3), 497-503. doi: 10.1097/MAO.0b013e31820d94d0.

Ward, B.K., Agrawal, Y., Hoffman, H.J., Carey, J.P., and Della Santina, C.C. (2013). Prevalence and impact of bilateral vestibular hypofunction: results from the 2008 US National Health Interview Survey. *JAMA Otolaryngol Head Neck Surg* 139(8), 803-810. doi: 10.1001/jamaoto.2013.3913.

Zingler, V.C., Weintz, E., Jahn, K., Botzel, K., Wagner, J., Huppert, D., et al. (2008). Saccular function less affected than canal function in bilateral vestibulopathy. *J Neurol* 255(9), 1332-1336. doi: 10.1007/s00415-008-0887-6.

Zingler, V.C., Weintz, E., Jahn, K., Huppert, D., Cnyrim, C., Brandt, T., et al. (2009). Causative factors, epidemiology, and follow-up of bilateral vestibulopathy. *Ann N Y Acad Sci* 1164, 505-508. doi: 10.1111/j.1749-6632.2009.03765.x.

Chapter 3 EOG vs VOG: is EOG a reliable and affordable alternative for VOG to assess HIT?

EMBARGO

Chapter 4 A new and faster test to assess vestibular perception

Chapter 4

ABSTRACT

Objective: Clinical vestibular testing mainly consists of testing reflexes, but does not routinely include testing for perceptual symptoms. The objective of this study was to investigate a new and faster test for vestibular perception, and to compare its results with previous studies.

Methods: Fifty-five healthy subjects with no prior vestibular complaints were included and divided into three age groups. Vestibular perceptual thresholds were measured using a hydraulic platform in the dark. The platform delivered 12 different movements: six translations (forward, backward, right, left, up, and down) and six rotations/tilt (yaw left, yaw right, pitch forward, pitch backward, roll left, and roll right). The subject had to report the correct type and direction of movements. Thresholds were determined by a double confirmation of the lowest threshold. General trends in thresholds like relative interrelationship and the influence of age were analyzed and compared with values reported previously.

Results: Mean thresholds of age groups ranged between 0.092 and 0.221 m/s^2 for translations, and between 0.188 and 2.255$\circ/s^2$ for rotations. The absolute values differed from previous reports, but the relative interrelationship of thresholds between type and direction of motion remained. An association between age and vestibular thresholds was found, similar to previous reports.

Conclusion: This new and faster test for vestibular perception showed comparable patterns in perceptual thresholds when compared to more research oriented, lengthy tests. This might pave the way for establishing vestibular perception testing protocols useful for the clinic.

INTRODUCTION

The vestibular organ consists of three semicircular canals (lateral, anterior, and posterior) and two otolith organs (saccule and utricle). Three major vestibular functions are gaze stabilization, spatial orientation, and balance. These essential functions also rely on the contribution of other multiple senses, such as the visual and somatosensory system (Bringoux et al., 2016). In case of vestibular failure, contributions of the visual and somatosensory system increase in order to maintain balance (sensory substitution). Concurrently, readjustments of brainstem vestibular processing and adaptation occur (Lucieer et al., 2016; Van De Berg et al., 2015).

Current diagnostics for the vestibular system mainly rely on the evaluation of reflexes, such as the vestibulo-ocular reflex (VOR) and the vestibulo-collic reflex. However, one third of patients with dizziness or imbalance have normal vestibular results on these tests (Merfeld et al., 2010). This illustrates that perceptual symptoms cannot always be addressed with current vestibular tests, and is probably related to the fact that vestibular perception utilizes other sensory pathways than vestibular reflexes (Grabherr et al., 2008). In general, perceptual thresholds have high sensitivity and specificity, since it is not easy to adapt to deficits caused by threshold-level stimuli. Therefore, there is a real clinical need to go "beyond reflexes" and measure vestibular perception, which could provide important additional information in the diagnostic process (Merfeld et al., 2010). Until now, vestibular thresholds have proven to be useful in identifying specific peripheral deficits and in diagnosing central disorders such as vestibular migraine (Bermúdez Rey et al., 2016; Lewis et al., 2011; Priesol et al., 2014). However, the clinical value of tests for vestibular perception is not yet fully determined. For example, they might develop into the equivalent of the "speech audiogram" for vestibular disorders (Bermúdez Rey et al., 2016; Van De Berg et al., 2015).

Vestibular perception has been tested previously with a platform capable of producing different motion profiles: yaw rotations, combined translational and rotational movements (Grabherr et al., 2008)(Nooij et al., 2016), roll tilt (Bermúdez Rey et al., 2016), and lacked pitch movements (Bringoux et al., 2016; Priesol et al., 2014). The tested subject had to perceive and identify the type and/or direction of the movements. Next to this, differences between vestibular and visual thresholds were measured, and the effect of combining both was also evaluated (Karmali et al., 2014; Mardirossian et al., 2014). However, these vestibular perception tests take considerable time: up to 3 h (Bermúdez Rey et al., 2016). This not only increases the burden for the patient, but might also decrease the attention of the patient during the test. These factors can significantly influence reliability and reproducibility of the results. Therefore, there is a need to develop a clinically oriented test for vestibular perception that is sensitive and specific, but less time-consuming.

The objective of this study was to investigate the application of a simplified and shorter paradigm for testing vestibular perception and to compare its results with those obtained in previous, research oriented studies. This new paradigm might be used in the future for multiple purposes, including clinical evaluation of the vestibular implant and diagnosis of vestibular perceptual deficits (Merfeld et al., 2010; van de Berg et al., 2017).

It should be noted that vestibular perceptual tests are not purely testing the vestibular system (peripheral and central), since other sensory systems like proprioception are also involved in detecting movements. The brain integrates all these different inputs. Therefore, the vestibular perceptual thresholds can be considered as a functional outcome of the whole system, in which the vestibular system plays a major role (Merfeld et al., 2010).

METHODS

Participants

Fifty-five healthy subjects with no prior vestibular complaints were included in this study. Ages ranged from 21 to 81 years old (median age 55 years, mean age 49 years). Twenty-four males and 31 females participated. Exclusion criteria comprised current vestibular disease, and inability to sit in the testing chair for at least 1 h. Patients with migraine or using vestibulosuppressants were also excluded because both these factors are known to influence vestibular function (Lewis et al., 2011). All included subjects were able to complete the whole experiment.

Perception Platform

Vestibular perceptual thresholds were measured using the hydraulic CAREN platform combined with the D-flow 3.22.0 software from Motek Medical BV (Amsterdam, The Netherlands). The platform delivered 12 different smooth, controlled movements: six translations (forward, backward, right, left, up, and down) and six rotations or tilt (yaw left, yaw right, pitch forward, pitch backward, roll left, and roll right). Each of the 12 thresholds was measured independently of others, which implies that no (major) effect should be expected from one movement on the thresholds of other movements.

Preparations

The subject was informed about the testing paradigm. All subjects were tested by the same technician (BD). The subject was seated in a chair mounted on the platform, and then fastened with a seatbelt for security purposes and to limit information provided by the body sliding on the chair. The test was performed in complete darkness and a blindfold was put on to avoid any visual cues. An infrared camera was used to monitor the subject during the experiments. Subjects wore a headset for communication with the technician and to mask the surrounding noise of the platform by playing a mix of previous sound recordings of the platform. First, a practice run was performed to verify understanding of the testing paradigm and subject compliance. Then, the testing paradigm was carried out. The technician continuously checked and maintained attention of the patient by communicating via the headset.

Testing Paradigm

The objective of the testing paradigm was to measure perceptual thresholds for angular and translational motions. Movements were applied in a random order and started at the highest possible accelerations. For each movement, the platform was first positioned and then the "test movement" was performed. After that, the platform returned to its

neutral position. Then, the subject had to immediately report the direction and type of movement to the technician using the headset. Both the direction and type of movement had to be correct, in order for the response to be validated by the technician (i.e., to lower the acceleration for that specific movement). Translation accelerations were lowered in steps of 0.1 m/s^2, rotation accelerations in steps of 10∘/s^2. In case of an incorrect or absent response, a step up of respectively, 0.05 m/s^2 or 5∘/s^2 was used. If the response remained incorrect, the accelerations were increased again by 0.02 m/s^2 and 2∘/s^2, respectively. The perceptual threshold for each movement was determined by a double confirmation of the lowest threshold, plus two times an absent response at the acceleration one step below the threshold.

Stimulus

A special motion stimulus profile was developed to quantify perceptual thresholds for translational (six directions) and rotational (six directions) accelerations. The motion profile for translational stimuli are illustrated in Figure 4.1. The rotational stimuli had the same profile. They were composed of a smoothly increasing acceleration phase (low jerk) until constant acceleration was obtained for a fixed duration (plateau phase). This was followed by a smooth decrease of the acceleration (low jerk) down to zero. After each stimulus the platform moved with a subthreshold acceleration and jerk to the starting position needed for the next chosen stimulus. By this procedure, patients did not feel any movement or tilt between the subsequent stimuli, by which it was not possible to anticipate on the type or direction of the next stimulus. A random sequence of all possible 12 stimuli was used. Due to the limitations of the platform, the range of translational movements was restricted up to 0.4m, and the range of rotational movements up to 30∘. This stimulus profile was chosen to provide a constant acceleration at a certain magnitude, for a given duration, defined by the investigator. All non-linear parts of the stimulus were sinusoidal to smoothly reach the plateau phases of the acceleration. The sine parameters (amplitude and frequency) depended on the magnitudes of acceleration (a) and jerk (j) and varied for each separate motion stimulus. Therefore, every stimulus was controlled by three parameters: maximum range, acceleration magnitude, and jerk magnitude. Minimum acceleration was 0.01 m/s^2 for translations and 0.1∘/s^2 for rotations. Maximum acceleration was 0.4 m/s^2 for translations and 40∘/s^2 for rotations.
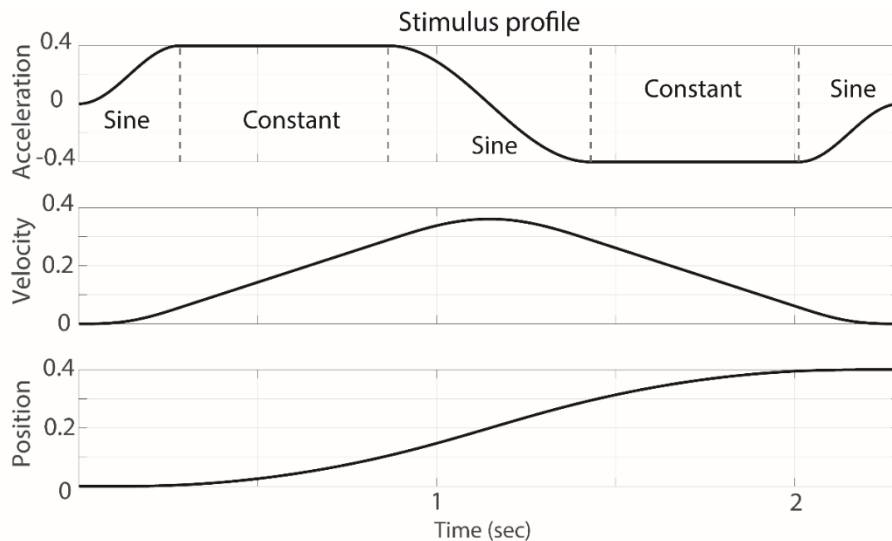
Figure 4.1 Schematic example of the stimulus shape of a translation.

Data-Analysis

IBM SPSS Statistics Version 24 was used for data-analysis. In order to compare the type of movements, results were grouped into the same type of movement (e.g., translations and rotations), same type of translation (translation left and right, forward and backward, up and down), and same type of rotation (yaw, pitch forward and backward, roll left and right). To be able to statistically evaluate the influence of age, age groups were made for ages 21–39, 40–59, and 60–81 years. Mean thresholds of movements were calculated for the whole population of tested subjects, as well as for each age group separately. Paired t-tests were performed between all types of translations and between all types of rotations, to evaluate possible significant differences between them. Scatterplots were made for every movement tested by the platform to visualize the relation between perceptual thresholds and age. To further investigate the influence of age and gender, multiple regression analyses were performed for mean perceptual thresholds. The mean threshold of all movements, the mean threshold of all translations and the mean threshold of all rotations were used as dependent variables. Age and gender were used as independent variables. P-values below 0.05 were considered significant. Regarding the multiple regression analysis, Cooks distances were determined and a multicollinearity test was performed, showing no multicollinearity. In order to compare thresholds from previous literature (Bermúdez Rey et al., 2016) presented in velocity units (v), with the thresholds in this study presented in acceleration units (a), peak velocities were converted into peak accelerations by $a_{peak} = v_{peak} * \pi * f$, where f was the motion frequency. Since both studies differed in terms of paradigm (determining thresholds differently, not all type of movements the same) and stimulus (different profile shape, duration, and frequencies), no statistics were applied to compare both datasets. However, general trends in thresholds like relative interrelationship and the influence of age were analyzed separately and compared between these studies.

Ethical Considerations

The procedures in this investigation were in accordance with the legislation and ethical standards on human experimentation in the Netherlands and in accordance with the Declaration of Helsinki (amended version 2013). Approval was obtained from the ethical committee of Maastricht University Medical Center (NL52768.068.15/METC). All procedures were performed at the Maastricht University Medical Center. All subjects provided written informed consent.

RESULTS

Perceptual Thresholds for Translations and Influence of Age and Gender

Thresholds for translations varied widely within and between age groups (Figure 4.2, Figure 4.4). Mean thresholds of age groups ranged between 0.092 and 0.221 m/s^2 (Table 4.1). Thresholds of the upward-downward plane were significantly higher than those of the forward-backward plane (p = 0.03; Table 4.1). No significant differences were found between the other translations. Mean thresholds increased with age group, except for leftward and rightward translations. A multiple regression was run to predict the mean perceptual threshold of all translations from age and gender [F(2, 52) = 12.48, p < 0.001, R^2 = 0.324]. Age added significantly to the prediction (p<0.001), not gender (p=0.24).

Figure 4.2 Normative thresholds for each direction of translation, obtained in 55 healthy subjects of different ages. Each dot represents the threshold of one subject for a specific translation. Each box plot represents the 25–75 percentiles of thresholds per decade, whiskers the 95 percentiles and bold black lines the median.

Perceptual Thresholds for Rotations and Influence of Age and Gender

Thresholds for rotations showed less variability within and between age groups than thresholds for translations (Figure 4.3, Figure 4.4). Mean thresholds of age groups varied between 0.188 and 2.255∘/s² (Table 4.1). Perceptual thresholds for yaw rotations were significantly higher than for pitches and rolls (p = 0.016; Table 4.1). No significant difference

was found between the pitches and rolls (p = 0.242). Mean thresholds increased with each age group for yaw and pitch rotations, but not for roll rotations. A multiple regression was run to predict the mean perceptual threshold of all rotations from age and gender [$F_{(2, 52)}$ = 8.644, $p < 0.005$, R^2 = 0.25]. Again, only age added significantly to the prediction ($p < 0.001$), not gender (p = 0.297).

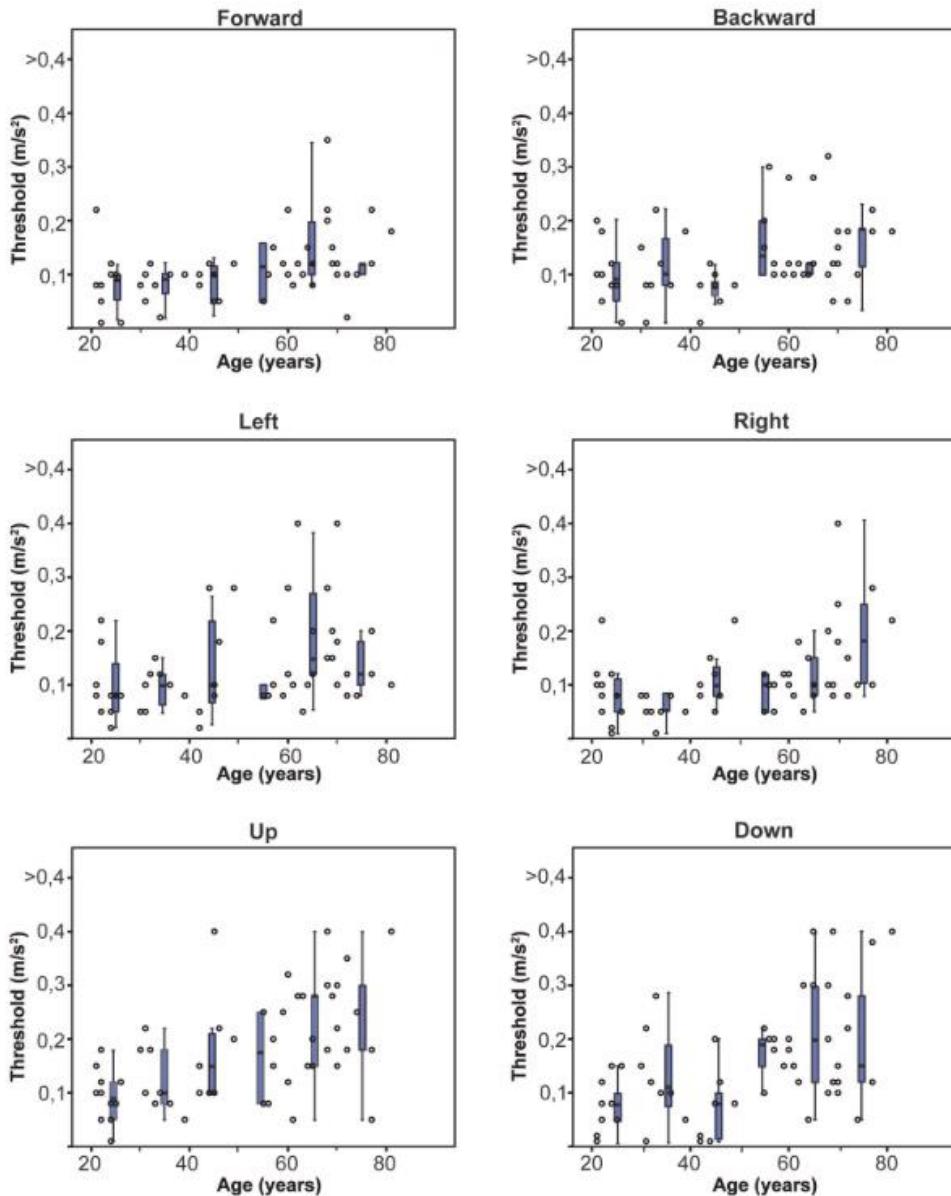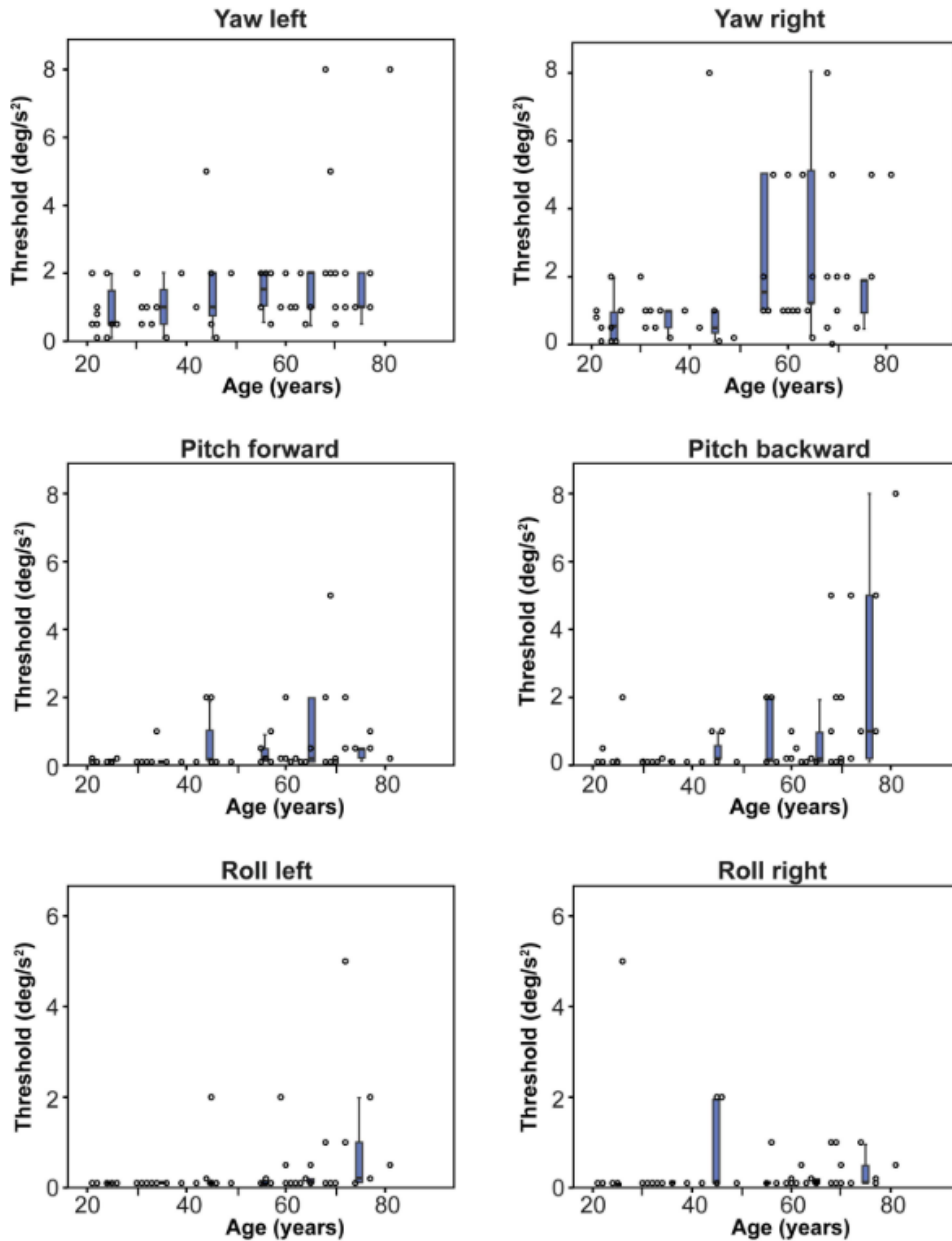*Figure 4.3 Normative thresholds for each direction of rotation, obtained in 55 healthy subjects of different ages. Each dot represents the threshold of one subject for a specific rotation. Each box plot represents the 25–75 percentiles of thresholds per decade, whiskers the 95 percentiles and bold black lines the median. Note that y-axes are optimized for each specific movement. Dots on the x-axis have a value of 0.01◦/s².*
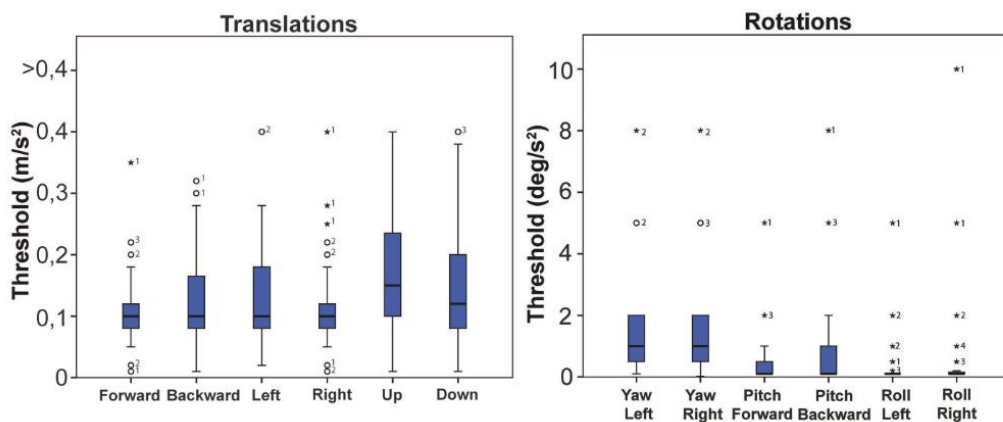
Figure 4.4 Normative values of all translations combined and all rotations combined. Bold black lines in the boxes represent medians, boxes the 25–75 percentiles, whiskers the 95 percentiles. Outliers are represented by an open circle, extreme outliers by an asterisk. Numbers next to a dot indicate the amount of dots with the same value.

Table 4.1 Mean thresholds for translations and rotations, presented for each age group, with standard deviation between brackets.

Age	No of subjects	Translations			Rotations		
		Forward / backward	Left / right	Up / down	Yaw	Pitch	Roll
All	55	0.12 (0.05)	0.14 (0.11)	0.16 (0.09)	1.62 (1.59)	0.61 (0.89)	0.44 (0.85)
20-39	20	0.09 (0.04)	0.12 (0.15)	0.10 (0.05)	0.82 (0.56)	0.19 (0.24)	0.2 (0.55)
40-59	13	0.11 (0.04)	0.11 (0.06)	0.15 (0.07)	1.79 (1.67)	0.52 (0.52)	0.81 (1.42)
60-81	22	0.14 (0.05)	0.16 (0.08)	0.22 (0.09)	2.26 (1.89)	1.04 (1.20)	0.42 (0.55)

Comparison of Perceptual Thresholds with Previous Literature

Figure 4.5 presents the perceptual thresholds for y- and z- translations and yaw and roll rotations in this study, compared to those in previous literature (Bermúdez Rey et al., 2016). Although the absolute thresholds varied between these studies, the relative interrelationship of thresholds between movements remained: y-translations and roll rotations showed lower mean thresholds than z-translations and yaw-rotations, respectively. Thresholds for roll rotations around 0.1Hz in this study were close to those previously measured at 0.2Hz. A significant age effect on thresholds was found in both studies (Bermúdez Rey et al., 2016).
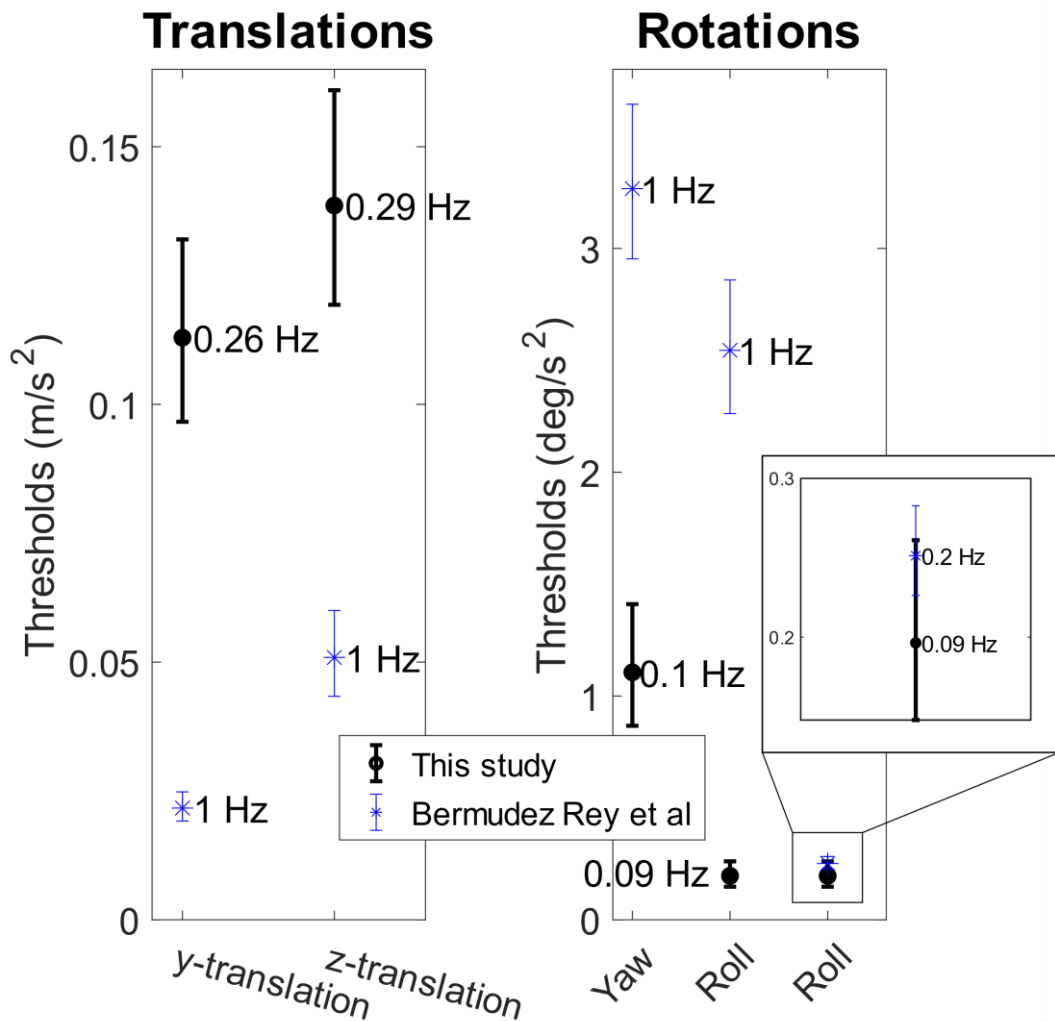
Figure 4.5 Mean and 95% confidence intervals of perceptual thresholds for translations and rotations in this study (n = 55), compared to those in previous literature (Bermúdez Rey et al., 2016) (n = 79). For each mean value, the frequency of the stimulus is given.

DISCUSSION

This study was the first step in evaluating a clinically oriented test for vestibular perception. Perceptual thresholds in a group of healthy subjects were obtained and thresholds significantly increased with increasing age. Gender did not have a significant effect. These findings were congruent with a previous study, despite of this study using a different testing paradigm and different type of stimulus, and including more directions (Bermúdez Rey et al., 2016).

This testing paradigm differed from more research oriented studies in several ways. Firstly, it was devised to be relatively fast and complete, in order to have a test more suited for clinical settings. Testing time was substantially reduced from ~3 h to less than 1 h (45–

60min). This reduced burden for the patient, costs of testing, and might have improved attention of the patient. The latter is particularly relevant, since after a long testing session attention is more likely to decrease, resulting in less reproducible and reliable results (van de Berg et al., 2015). Testing time was reduced by using fewer motions to determine the thresholds. Reliability of thresholds was therefore ensured by adding pitches forward and backward to the types of movement, and by randomly presenting all stimuli in the same session, without the subject being aware of the type of movement. This reduced the possibility of reporting the right threshold by chance. Secondly, this testing paradigm used different stimuli than previously reported. It was based on a stimulus with the longest possible duration of constant peak acceleration (plateau phase) and varying frequencies, instead of a fixed frequency with a sinusoidally shaped acceleration profile. This new profile was chosen to have a longer exposition of the subject to the main parameter of the stimulus of interest and the main stimulus for the vestibular system: acceleration. However, due to the limitations of the platform, the frequency of the stimulus had to differ for each acceleration. This is a potential limitation, since frequency-dependency of the system is more difficult to evaluate. Next to this, it prevented comparison of the absolute thresholds of this study with previously reported ones. After all, the frequency-dependency of the vestibular system implies that testing at difference frequencies might yield different results (Bermúdez Rey et al., 2016; Grabherr et al., 2008). Nevertheless, this could mainly explain the differences between the absolute values of thresholds between the studies. Thirdly, in this paradigm continuous interactive communication between the technician and the patient was added. In extensive preliminary trials, this strategy was found to be superior to using a joystick to indicate thresholds, without any significant communication. Communication also improved attention, reduced anxiety (since the patients sat in a dark room), and facilitated verification whether the reported thresholds were representative or not (e.g., a lack of attention at the moment of testing a certain threshold). If an unreliable threshold was suspected, the threshold was determined again. Fourthly, not all skin surfaces were covered to reduce somatosensory input as much as possible. Whether covering of all skin surfaces has any beneficial effects in this paradigm proposed, should still be determined.

More dispersion was observed in the thresholds for translations, than for rotations, pitches, and rolls. This was in accordance with previous literature (Bermúdez Rey et al., 2016) and could be attributed to a higher contribution of somatosensory input during these movements. Regarding the group of translations, thresholds of the vertical plane were significantly higher than those of the forward-backward plane. Regarding the group of rotations, thresholds for yaw rotations were significantly higher than those for pitches and rolls. It could be hypothesized that these two movements were less affected by somatosensory input, compared to the other movements in their group. For instance, a translation in the vertical plane will cause less activation of the somatosensory system, including neck proprioception (Pettorossi & Schieppati, 2014), than translations in other planes, since the body remains in line with gravity. Also, a rotation in yaw plane does not include any tilt with respect to gravity, in contrast to pitches and rolls. These two movements appear therefore to be those that most purely test the thresholds for

translations and rotations of the peripheral vestibular system, with the least interference of the somatosensory system.

The contribution of the somatosensory system implies that vestibular perceptual tests are not purely testing the vestibular system (peripheral and central), since somatosensory cues are also involved in detecting movements. The brain integrates all these different inputs. Therefore, the vestibular perceptual thresholds can be considered as a functional outcome of the whole system, in which the vestibular system plays a major role (Merfeld et al., 2010). This also implies that this test is not specifically designed to detect a peripheral or central vestibular deficit, but to demonstrate the vestibular perceptual functionality of a patient at a given time.

Limitations

Many subjects could still hear some movements of the platform (e.g., translations downward) in spite of the masking noise on the headphones. Platform sounds were almost the same for each movement. Therefore, the sounds might have indicated that the platform was moving, but could not help in distinguishing between direction and type of movements (e.g., translations vs. rotations, upwards vs. downwards). Since the thresholds of movements were defined by the right type and direction of movements, it was hypothesized that sounds might have not significantly influenced the thresholds. However, the platform sounds should be taken into consideration when refining this testing paradigm.

Perceptual thresholds significantly increased with increasing age. Since the vestibular function of the healthy controls was not measured but only screened with a questionnaire, it cannot be determined whether the increasing thresholds with age were mainly influenced by age, or other factors. For example, age- related decline in vestibular function (presbyvestibulopathy) as well as clinically asymptomatic vestibulopathies could account for the decline of vestibular perception. This needs to be determined in future studies.

Future

Next step is to investigate this testing paradigm in patients with unilateral and bilateral vestibulopathy. If this succeeds, it might pave the way for routinely measuring vestibular function "beyond reflexes." It might be used in clinic, in which it should be noted that this test is relatively expensive regarding time and equipment, compared to other vestibular tests. Therefore, it is hypothesized that it will probably first be suited for tertiary referral centers that have the resources and interest to investigate vestibular perceptual threshold deficits in patients (regardless of the etiology), or to use it to demonstrate perceptual changes after rehabilitation. It could also be used in research settings to e.g., evaluate the effect on perceptual thresholds of future therapies, for example the vestibular implant (Fornos et al., 2014; Guinand et al., 2015, 2016; van de Berg et al., 2015, 2017). For the latter, it should be noted again that vestibular perception is the end-result of detection and processing of movements by the whole vestibular system (see above): peripheral and central. This process is susceptible to multisensory integration and many other factors (e.g., adaptation, compensation, and cognition) (Ferrè et al., 2015). Therefore, vestibular

perception should be used in the future as an outcome measure by itself, and not purely as a marker of vestibulopathy.

CONCLUSION

This new and faster test for vestibular perception showed comparable patterns in perceptual thresholds when compared to more research oriented, lengthy tests. This might pave the way for establishing vestibular perception testing protocols useful for the clinic.

ETHICS STATEMENT

The procedures in this investigation were in accordance with the legislation and ethical standards on human experimentation in the Netherlands and in accordance with the Declaration of Helsinki (amended version 2013). Approval was obtained from the ethical committee of Maastricht University Medical Center (NL52768.068.15/METC). All procedures were performed at the Maastricht University Medical Center. All subjects provided written informed consent.

REFERENCES

Bermúdez Rey, M. C., Clark, T. K., Wang, W., Leeder, T., Bian, Y., Merfeld, D. M., Rey, M. C. B., Clark, T. K., Wang, W., Leeder, T., Bian, Y., & Merfeld, D. M. (2016). Vestibular perceptual thresholds increase above the age of 40. *Frontiers in Neurology*, *7*(OCT), 1–17. https://doi.org/10.3389/fneur.2016.00162

Bringoux, L., Di Cesare, C. S., Borel, L., Macaluso, T., & Sarlegna, F. R. (2016). Do visual and vestibular inputs compensate for somatosensory loss in the perception of spatial orientation? Insights from a deafferented patient. *Frontiers in Human Neuroscience*, *10*(APR2016), 1–10. https://doi.org/10.3389/fnhum.2016.00181

Ferrè, E. R., Walther, L. E., & Haggard, P. (2015). Multisensory interactions between vestibular, visual and somatosensory signals. *PLoS ONE*, *10*(4). https://doi.org/10.1371/journal.pone.0124573

Fornos, A. P., Guinand, N., Van De Berg, R., Stokroos, R., Micera, S., Kingma, H., Pelizzone, M., & Guyot, J. P. (2014). Artificial balance: Restoration of the vestibulo-ocular reflex in humans with a prototype vestibular neuroprosthesis. *Frontiers in Neurology*, *5 APR*, 66. https://doi.org/10.3389/fneur.2014.00066

Grabherr, L., Nicoucar, K., Mast, F. W., & Merfeld, D. M. (2008). Vestibular thresholds for yaw rotation about an earth-vertical axis as a function of frequency. *Experimental Brain Research*, *186*(4), 677–681. https://doi.org/10.1007/s00221-008-1350-8

Guinand, N., Van De Berg, R., Cavuscens, S., Stokroos, R. J., Ranieri, M., Pelizzone, M., Kingma, H., Guyot, J. P., & Perez-Fornos, A. (2015). Vestibular Implants: 8 Years of Experience with Electrical Stimulation of the Vestibular Nerve in 11 Patients with Bilateral Vestibular Loss. *ORL*, *77*(4), 227–240. https://doi.org/10.1159/000433554

Guinand, N., Van de Berg, R., Cavuscens, S., Stokroos, R., Ranieri, M., Pelizzone, M., Kingma, H., Guyot, J.-P., & Pérez Fornos, A. (2016). Restoring Visual Acuity in Dynamic Conditions with a Vestibular Implant. *Frontiers in Neuroscience*, *10*, 577. https://doi.org/10.3389/fnins.2016.00577

Karmali, F., Lim, K., & Merfeld, D. M. (2014). Visual and vestibular perceptual thresholds

each demonstrate better precision at specific frequencies and also exhibit optimal integration. *Journal of Neurophysiology*, *111*(12), 2393–2403. https://doi.org/10.1152/jn.00332.2013

Lewis, R. F., Priesol, A. J., Nicoucar, K., Lim, K., & Merfeld, D. M. (2011). Dynamic tilt thresholds are reduced in vestibular migraine. *Journal of Vestibular Research : Equilibrium & Orientation*, *21*(6), 323–330. https://doi.org/10.3233/VES-2011-0422

Lucieer, F., Vonk, P., Guinand, N., Stokroos, R., Kingma, H., & van de Berg, R. (2016). Bilateral vestibular hypofunction: Insights in etiologies, clinical subtypes, and diagnostics. *Frontiers in Neurology*, *7*(MAR), 26. https://doi.org/10.3389/fneur.2016.00026

Mardirossian, V., Karmali, F., & Merfeld, D. (2014). Thresholds for human perception of roll tilt motion: Patterns of variability based on visual, vestibular, and mixed cues. *Otology and Neurotology*, *35*(5), 857–860. https://doi.org/10.1097/MAO.0000000000000346

Merfeld, D. M., Priesol, A., Lee, D., & Lewis, R. F. (2010). Potential solutions to several vestibular challenges facing clinicians. *Journal of Vestibular Research : Equilibrium & Orientation*, *20*(1), 71–77. https://doi.org/10.3233/VES-2010-0347

Nooij, S. A. E., Nesti, A., Bülthoff, H. H., & Pretto, P. (2016). Perception of rotation, path, and heading in circular trajectories. *Experimental Brain Research*, *234*(8), 2323–2337. https://doi.org/10.1007/s00221-016-4638-0

Pettorossi, V. E., & Schieppati, M. (2014). Neck Proprioception Shapes Body Orientation and Perception of Motion. *Frontiers in Human Neuroscience*, *8*. https://doi.org/10.3389/fnhum.2014.00895

Priesol, A. J., Valko, Y., Merfeld, D. M., & Lewis, R. F. (2014). Motion perception in patients with idiopathic bilateral vestibular hypofunction. *Otolaryngology - Head and Neck Surgery (United States)*, *150*(6), 1040–1042. https://doi.org/10.1177/0194599814526557

van de Berg, R., Guinand, N., Khoa Nguyen, T. A., Ranieri, M., Cavuscens, S., Guyot, J. P., Stokroos, R., Kingma, H., & Perez-Fornos, A. (2015). The vestibular implant: Frequency-dependency of the electrically evoked vestibulo-ocular reflex in humans. *Frontiers in Systems Neuroscience*, *8*(JAN), 255. https://doi.org/10.3389/fnsys.2014.00255

van de Berg, R., Guinand, N., Ranieri, M., Cavuscens, S., Khoa Nguyen, T. A., Guyot, J.-P., Lucieer, F., Starkov, D., Kingma, H., van Hoof, M., & Perez-Fornos, A. (2017). The Vestibular Implant Input Interacts with Residual Natural Function. *Frontiers in Neurology*, *8*, 644. https://doi.org/10.3389/fneur.2017.00644

Van De Berg, R., Van Tilburg, M., & Kingma, H. (2015). Bilateral Vestibular Hypofunction: Challenges in Establishing the Diagnosis in Adults. In *ORL* (Vol. 77, Issue 4, pp. 197–218). ORL J Otorhinolaryngol Relat Spec. https://doi.org/10.1159/000433549

Chapter 5 Comparing the paradigms of motion perception measurement: 2-option vs 12-option

Chapter 5

ABSTRACT

Background/Objective: Different testing paradigms have been proposed to investigate perceptual self-motion thresholds. They can differ regarding the amount of possible motions that patients have to choose from. Objective of this study was to compare the two-option paradigm and twelve-option paradigm, in order to investigate whether reducing the choice options significantly influences the reported thresholds of self-motion perception of healthy subjects.

Methods: Thirty-three volunteers with no prior vestibular complaints were included and sequentially tested with both paradigms at a random sequence. Perceptual self-motion thresholds were measured using a hydraulic motion platform in the absence of external visual and auditory cues. The platform delivered twelve different movements: six translations and six rotations. Each subject had to report the correct type and direction of movements. Thresholds were determined by a double confirmation of the lowest threshold, in combination with a double rejection of the one-step lower stimulus. Perceptual self-motion thresholds of both paradigms were compared using the mixed model analysis.

Results: The twelve-option paradigm showed significantly higher reported thresholds for yaw rotations and translations left, right and down ($p < 0.001$), compared to the two-option paradigm. No statistical difference was found for rolls and translations up. No significant gender effect, learning effect and carry-over effect were present in any of the applied motion directions.

Conclusion: Reported thresholds of self-motion perception of healthy subjects are influenced by the testing paradigm. The twelve-option paradigm showed significantly higher thresholds than the two-option paradigm. Results obtained with each testing paradigm should therefore be compared to paradigm-specific normative data.

INTRODUCTION

The vestibular organ consists of three semi-circular canals and two otolith organs. The semi-circular canals detect angular accelerations, while the otolith organs mainly detect linear accelerations and head tilt. Besides these motion cues from the vestibular organ, the brain also receives visual, somatosensory and auditory information and combines these inputs to maintain posture, gaze stabilisation and spatial orientation (Mast et al., 2014; Okumura et al., 2015; Soyka et al., 2015).

The clinically mostly used vestibular function tests investigate the vestibulo-ocular reflex and the vestibulo-collic reflex. There is not one standard diagnostic test for analysing the vestibular function, as the clinically applied tests are complementary to each other, and one test cannot replace another. All tests need to be executed and interpreted by a well trained professional (Halmagyi et al., 2017; van de Berg et al., 2018). However, about one third of the patients with complaints of dizziness and/or imbalance have normal vestibular test results. This suggests that either some vestibular disorders may not involve the vestibulo-ocular reflex, and/or the standard diagnostic tests available are not applicable to all vestibular complaints. Therefore, there seems to be a need for a clinical test that measures beyond vestibular reflexes (Merfeld et al., 2010).

A relatively new method for assessing (part of) the vestibular function is determining perceptual self-motion thresholds (Dupuits et al., 2019). For this, the subject has to take place at a motion platform or sled that is able to move in different directions, with different accelerations. After every motion, it is checked whether the subject perceived the movement correctly. The perceptual thresholds can be determined by changing the acceleration and direction of the platform, according to the response of the subject. The threshold for each direction is determined by the lowest acceleration that can still be correctly perceived by the subject. Exclusion of the other somatosensory cues (vision, sense of hearing, sense of touch) is preferred, as they support the vestibular system in its spatial orientation. However, this is not totally possible, especially for somatosensory input (Dupuits et al., 2019; Grabherr et al., 2008). This therefore implies that mainly perceptual self-motion thresholds are tested, and not "pure" vestibular perceptual thresholds.

The advantage of testing perceptual self-motion thresholds could be that it does not depend on vestibular reflexes. Since different sensory mechanisms, other than reflex pathways, might be responsible for the perceptual responses (Merfeld et al., 2005; Nouri & Karmali, 2018; Tarnutzer et al., 2009), testing perceptual self-motion thresholds could be complementary to the other clinical tests (Kobel et al., 2021). Next to this, future development of a self-motion 'vestibulogram', might be a useful tool in the diagnostic work-up of vestibular disorders in clinic. This vestibulogram, adjusted to gender, age and current diseases, shows perceptual thresholds (in acceleration units) as a function of frequency, similar to the concept of an audiogram where the auditory thresholds (in decibel units) are shown as a function of frequency (Grabherr et al., 2008; Merfeld et al., 2010).

In literature, different methods are used to determine the perceptual self-motion thresholds. They mainly differ regarding 1) the type of platform or sled, 2) the type and amount of directions tested, 3) the stimulus profile, 4) testing time, and 5) paradigm for

determining the thresholds. Regarding this latter, subjects can have either a two- or plural-option paradigm. In other words, subjects are or are not informed about the possible motion directions before each test. The amount of possible motions can be either two or more. The effect of cognition, knowing the amount of available options beforehand, may influence the sensitivity of the perceptual thresholds (Bermúdez Rey et al., 2016; Grabherr et al., 2008; Janssen et al., 2011; Keywan et al., 2018; Kingma, 2005; Priesol et al., 2014). Next to this, the chance of guessing the correct movement might increase with fewer choice options.

Objective of this study was therefore to compare two previously described paradigms (Bermúdez Rey et al., 2016; Dupuits et al., 2019) for determining thresholds of self-motion perception (twelve-option versus two-option paradigm), in order to investigate whether reducing the choice options significantly influences the reported thresholds of healthy subjects, obtained with a more clinically oriented test (Dupuits et al., 2019).

METHODS

Study design

A more clinically oriented test for self-motion perception was used. This was previously described (Dupuits et al., 2019), and will be discussed more in detail below. Regarding testing paradigm, two different paradigms for determining perceptual self-motion thresholds were tested: 1) twelve-option paradigm, and 2) two-option paradigm. Each subject underwent two trials: one with the twelve-option paradigm and one with the two-option paradigm. In between the trials, a short break was scheduled of about 15 minutes. Randomization was applied (using https://www.randomizer.org) across and within the paradigms, i.e. subjects were randomized into two nearly equal groups that started with either the twelve or the two-option paradigm, and the sequence of motion types provided in each paradigm was randomized as well. All tests were conducted by the same technician (NR). Perceptual thresholds were measured in acceleration units (m/s^2 for translations, and deg/s^2 for rotations).

Setting

This study was conducted at Maastricht University Medical Center. Subjects were recruited at the university and hospital by addressing people personally and by distributing flyers.

Subjects

Thirty-three healthy individuals (14 males and 19 females, age 22 to 72 years) participated in this study. In order to be included, they had to be able to climb three stairs to the platform and sit on the platform for at least one hour and a half. Exclusion criteria comprised: vestibular and/or hearing complaints, headaches fitting the diagnostic criteria of migraine (Lempert et al., 2012; Lewis et al., 2011), the use of antidepressants for anxiety or depression, and the use of other vestibulosuppressants like sleeping pills. All subjects completed a short questionnaire on beforehand, that was used to collect personal data (age and gender) and to screen for exclusion criteria.

Perception platform

A hydraulic CAREN platform (Motek Medical BV, Amsterdam, The Netherlands) with D-flow 3.22.0 software was used for this study. The platform was programmed to move in twelve directions: six translations (up, down, left, right, forward, backward) and six rotations (yaw left, yaw right, roll left, roll right, pitch forward and pitch backward).

Preparations

Subjects had to take place on a chair on the platform and were strapped with two seatbelts. In order to exclude visual cues, testing was performed in a dark room and subjects were blindfolded. A headphone was used to mask the sounds of the moving platform by playing earlier recorded platform sounds. This headphone was also used by the examiner to communicate with the subjects, in order to keep their attention during the test. Next to this, an infrared camera made it possible to observe the subjects during the test. The head of the subject was intentionally not fixed during the test, since the chosen study design aimed at mimicking a relatively natural situation of whole-body motion, in which only visual and auditory feedback were prevented as much as possible.

TESTING PARADIGMS

Twelve-option paradigm

Seventeen subjects started with the twelve-option paradigm. Thresholds were determined during the same testing trial for all twelve motion directions possible (twelve-alternative). All subjects were informed about the total amount of motion types that were applied within this paradigm. The motion directions were randomly chosen by the examiner and started at the highest possible acceleration: 0.4 m/s^2 for translations and 40 deg/s^2 for rotations. After each motion the subject was asked to report both the type and direction of motion. In case of a correct answer, the stimulus was decreased with 0.03 m/s^2 or 3 deg/s^2. If the subject could not indicate the correct direction, the acceleration was increased by 0.03 m/s^2 or 3 deg/s^2.

Two-option paradigm

Sixteen subjects started with the two-option paradigm. This method was based on a two alternative choice paradigm. Before each motion subjects were informed about the type of motion including two options, for example "translation up or down" or "yaw left or right". Therefore, subjects only had to report the direction of motion, instead of reporting the type of motion as well. Thresholds of four types of motions were determined: translations left and right, translations up and down, yaw left and right, and roll left and right (Bermúdez Rey et al., 2016). All other elements of this paradigm were similar to the twelve-option paradigm.

Thresholds

Perceptual thresholds can be found by investigating a psychometric function, in which the relation between stimulus magnitude and level of correct answers are expressed. Thresholds are then often determined by finding the stimulus magnitude at which a

performance level (e.g. 50% correct answers) is reached (Klein, 2001). However, constructing the psychometric function was not the objective of this study. After all, investigating the psychometric function takes considerable time and this study involved a more clinically oriented test. It was therefore chosen to determine perceptual self-motion thresholds by a double confirmation of the lowest threshold in combination with an double incorrect response at the acceleration one step below the threshold (Dupuits et al., 2019). Furthermore, this study aimed at determining the reported self-motion perception thresholds as an "end result" of all variables involved (including sensitivity of the subject, contribution of the somatosensory system, amount of choice options etc.). Taking all these factors into account, the reported thresholds reflected the ability of self-motion perception as a result of all variables involved, not the vestibular perceptual threshold as a psychometric parameter.

Stimulus profile

The applied motion stimulus profile was previously described (Dupuits et al., 2019). For short, the platform motion profile was developed to provide the desired linear or rotational acceleration as long as possible. Every motion comprised an acceleration and deceleration of equal duration. The rise and decay of the acceleration followed a sinusoidal profile, in order to smoothly reach the selected magnitude (Figure 5.1). Due to platform limitations, frequency and duration of stimulus, but not displacement amplitude, varied for each separate motion stimulus. In between tested movements, the platform moved into its new position using subthreshold movements.
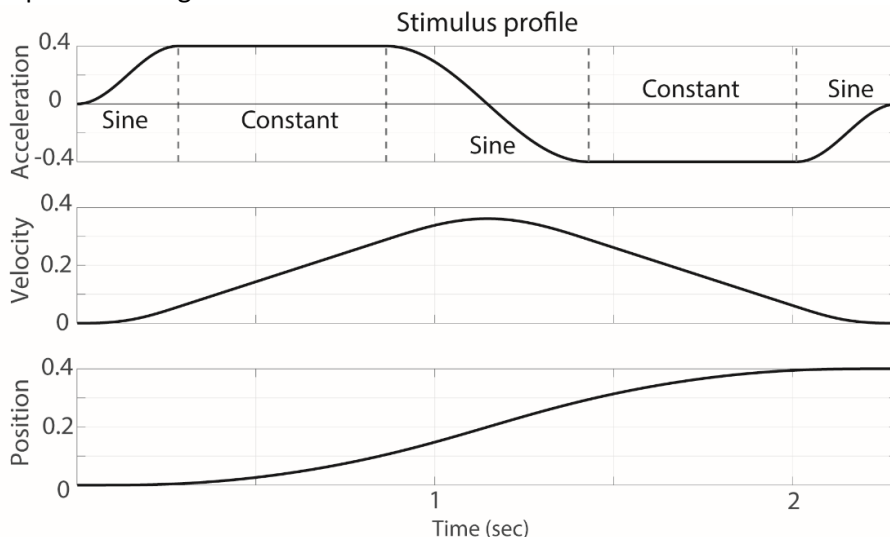
Figure 5.1 Motion profile used. The stimulus profile was composed of subsequent sine and constant functions. The units of measurement were either (m/s², m/s, m) or (deg/s², deg/s, deg) depending on the movement type: translational or rotational respectively.

Data analysis

R v.3.5.2 was used to compare both paradigms. A linear mixed model analysis was performed for each motion direction to investigate gender effect, learning effect, paradigm effect and carry-over effect. The learning effect was evaluated to check whether repeated measurements (first trial versus second trial) influenced the perceptual self-motion thresholds, independent of the paradigm used. The paradigm effect was investigated to check any influence of the tested paradigm (twelve-option versus two-option) on the perceptual self-motion thresholds. The carry-over effect was related to the influence of the variable "trial" on "paradigm" regarding the perceptual self-motion thresholds. Therefore, gender, trial number (first or second), paradigm (twelve- or two-option), and trial-paradigm interaction were applied as fixed factors, while the participant number was applied as a random factor. The threshold per motion direction was considered the dependent variable in the mixed model. Following the top-down procedure, the trial-paradigm interaction was tested first, followed by the factors gender and trial. They were not significant and therefore excluded from the mixed model. Since translations forwards-backwards and pitch forwards-backwards were not tested in the two-option paradigm (as in previous literature (Bermúdez Rey et al., 2016)), and thresholds of rolls could not reliably be determined due to physical limitations of the platform (see Results), outcomes of six directions were compared using the mixed model. These motions involved translations left and right, translations up and down, and yaw left and right. The significance of fixed effects was investigated using Type III tests ANOVA. The Bonferroni correction (n=6) for multiple comparisons was applied to the significance level *alpha=0.05*.

Ethical considerations

This study was in accordance with the legislation and ethical standards on human experimentation in the Netherlands as well as with the Declaration of Helsinki (2013). The study design was approved by the ethical committee of Maastricht University Medical Centre (NL52768.068.15/METC). All subjects provided written informed consent before starting the first test.

RESULTS

All measured perceptual self-motion thresholds are shown in the Table 5.1 as mean±SD. Figure 5.2 presents the comparison of perceptual self-motion thresholds between the twelve-option paradigm and the two-option paradigm. The twelve-option paradigm showed significantly higher perceptual self-motion thresholds than the two-option paradigm ($p<0.001$), except for translations up, and rolls left and right. Regarding translations up, thresholds of the twelve-option paradigm were higher, but not significant. During rolls left and right, the lowest measurable thresholds (0.1 deg/s^2) were obtained in nearly all subjects. Due to physical limitations of the platform, lower accelerations in these planes could not be provided for these types of movements and therefore these thresholds were considered as "not determined". Reported thresholds of self-motion perception did not differ significantly between male and female subjects and no significant learning effect and carry-over effect were present in any of the applied motion directions.
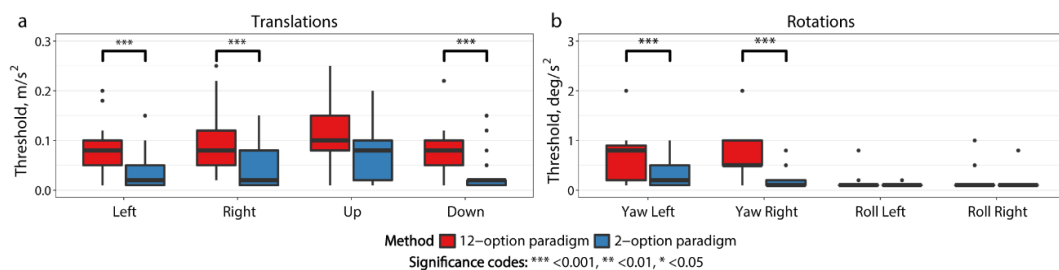
Figure 5.2 Reported thresholds of self-motion perception of translations (A) and rotations (B), tested with the twelve option-paradigm (red) and two-option paradigm (blue). Boxes represent the interquartile ranges, bold black horizontal lines the medians, and upper and lower whiskers the extreme lines. Outliers are represented by black dots.

Table 5.1 Mean reported thresholds of self-motion perception (±SD) presented for translations and rotations for both tested paradigms. ND – the threshold value could not be determined.

	Paradigm		Units
	12-option	2-option	
Translation Left	0.08 (0.05)	0.04 (0.04)	
Translation Right	0.10 (0.06)	0.04 (0.04)	
Translation Up	0.14 (0.10)	0.11 (0.14)	
Translation Down	0.11 (0.11)	0.03 (0.04)	m/s^2
Translation Forward	0.11 (0.06)	-	
Translation Backward	0.11 (0.07)	-	
Yaw Left	1.51 (1.75)	0.34 (0.30)	
Yaw Right	1.04 (1.20)	0.24 (0.24)	
Roll Left	ND	ND	
Roll Right	ND	ND	deg/s^2
Pitch Forward	0.31 (0.86)	-	
Pitch Backward	0.21 (0.36)	-	

DISCUSSION

This study investigated the reported self-motion perception thresholds of healthy volunteers, when using two different testing paradigms: the two-option and twelve-option paradigm. The reported self-motion perception thresholds were measured with a more clinically oriented test, in which only visual and auditory feedback were prevented as much

as possible, and in which thresholds were determined as a double confirmation of the lowest threshold in combination with an double incorrect response at the acceleration one step below the threshold. This implies that the obtained thresholds reflected the "end result" of many contributing factors (e.g. vestibular system, somatosensory system, etc.), and not the "pure vestibular threshold" as a psychophysical parameter.

The obtained values of the reported thresholds were compared among testing paradigms. The study showed that reported thresholds of healthy subjects are influenced by the testing paradigm. After all, reported thresholds of the twelve-option paradigm were (mostly) significantly higher than those determined by the two-option choice paradigm. No carry-over nor learning effect was present in any of the applied motion directions. This implies that results obtained with each testing paradigm should therefore be compared to paradigm-specific normative data.

The difference in reported thresholds might be explained by two factors. Firstly, the chance of guessing the correction motion direction was higher in the two-option paradigm than in the twelve-option paradigm. This could have decreased the thresholds in the two-option paradigm. No correction for guessing was applied in this study, since the amount of tested stimuli depended on the amount of correct answers, and therefore varied highly between subjects. Secondly, the pre-knowledge of the type of motion in the two-option paradigm could have positively influenced the subjects perception of motion (i.e. the subject was specifically focussed on a certain motion plane during the test). This might have also lowered the thresholds in the two-option paradigm. However, whether the sensitivity for motion stimuli of the healthy subjects truly differed between testing paradigms, can only be determined by constructing a psychometric function for both testing paradigms (see "Methods") (Merfeld, 2011). However, this was beyond the scope of this article. This study showed that paradigm-specific normative data should be used to interpret results obtained within a subject.

The roll left and roll right threshold values could not be determined due to physical limitations of the motion platform: the platform could not provide lower accelerations than already perceived by the subjects. These low magnitudes of roll thresholds could be explained by the fact that the somatosensory system might play a more prominent role in rolls, than in the other motions (Dupuits et al., 2019).

Regarding translations up, it was noted during testing that many subjects had difficulty in recognizing upward motions. This was reflected in the highest overall mean of perceptual self-motion thresholds. Whether this might have influenced the non-significant difference between testing paradigms, cannot be determined with certainty.

Implications for future research

Type of testing paradigm influences the reported thresholds of self-motion perception. Studies regarding this matter should therefore not be compared to each other, without taking these differences into account. Next to this, performance was variable between subjects. An association between increasing reported thresholds and age was already described using this clinically oriented test and a more research oriented test (Bermúdez Rey et al., 2016; Dupuits et al., 2019). This variability might lead to the question whether the vestibular organ is really that direction sensitive for perception, or whether it

mainly has a signaling function, whereas other sensory systems (e.g. visual, propriocepsis) are mainly used to determine the direction of motion. After all, divers under water in dark and subjects buried alive in an avalanche, have difficulties orienting themselves although gravity is still detected by the vestibular organs (Kingma & van de Berg, 2016). This signaling function at least implies that there will probably be another perceptual self-motion threshold: the threshold of perceiving motion itself, without being able to detect the right direction of motion. This might be explored in future research.

Implications for clinic

The more clinically oriented approach used in this paper, can pave the way for a relatively simple and faster way to assess perceptual self-motion thresholds in clinic, using normative data. Within this context, it should be noted that the twelve-option paradigm takes about 45-60 minutes, while the two-option paradigm takes about 30-45 minutes. This could be an important detail for clinical practice.

The motion platform used in this study is relatively expensive. This might hinder implementation in daily routine clinical practice. It could therefore be considered to use a less-expensive motorized rotatory chair (Seemungal et al., 2004). A rotatory chair might be able to provide a broader range of velocities, but it provides less movements: only yaw rotations. However, the clinical value of testing additional movement types is not yet fully determined.

Limitations of the study

Although all subjects wore headphones with a masking background sound, some subjects could still hear the sounds of the platform during the tests at high accelerations (Dupuits et al., 2019). However, the sounds did not provide any information about motion direction and were present only in the range of accelerations that were much higher than threshold values. Therefore, these audible sounds could not have influenced the measured outcome. Secondly, some subjects below 50 years old could still feel the subthreshold movements of the platform that were used to get the platform into a new testing position. For future testing, parameters of these subthreshold movements can be lowered to such an extent that subjects will less likely to be able to feel them. Thirdly, vestibular reflexes were not evaluated in the study population. Subjects were selected based on the absence of the vestibular complaints and vestibular deficits. This most likely would not have hindered the objective of the study, since patients served as their own controls.

CONCLUSION

Reported thresholds of self-motion perception of healthy subjects are influenced by the testing paradigm. The twelve-option paradigm showed significantly higher reported thresholds than the two-option paradigm. Results obtained with each testing paradigm should therefore be compared to paradigm-specific normative data.

Conflicts of interest All authors declare that they have no conflict of interest.

REFERENCES

Bermúdez Rey, M. C., Clark, T. K., Wang, W., Leeder, T., Bian, Y., & Merfeld, D. M. (2016). Vestibular Perceptual Thresholds Increase above the Age of 40. *Frontiers in Neurology*, *7*, 162. https://doi.org/10.3389/fneur.2016.00162

Dupuits, B., Pleshkov, M., Lucieer, F., Guinand, N., Pérez Fornos, A., Guyot, J. P., Kingma, H., & van de Berg, R. (2019). A New and Faster Test to Assess Vestibular Perception. *Frontiers in Neurology*, *10*, 707. https://doi.org/10.3389/fneur.2019.00707

Grabherr, L., Nicoucar, K., Mast, F. W., & Merfeld, D. M. (2008). Vestibular thresholds for yaw rotation about an earth-vertical axis as a function of frequency. *Experimental Brain Research*, *186*(4), 677–681. https://doi.org/10.1007/s00221-008-1350-8

Halmagyi, G. M., Chen, L., MacDougall, H. G., Weber, K. P., McGarvie, L. A., & Curthoys, I. S. (2017). The Video Head Impulse Test. *Frontiers in Neurology*, *8*, 258. https://doi.org/10.3389/fneur.2017.00258

Janssen, M., Lauvenberg, M., van der Ven, W., Bloebaum, T., & Kingma, H. (2011). Perception Threshold for Tilt. *Otology & Neurotology*, *32*(5), 818–825. https://doi.org/10.1097/MAO.0b013e31821c6c7b

Keywan, A., Wuehr, M., Pradhan, C., & Jahn, K. (2018). Noisy Galvanic Stimulation Improves Roll-Tilt Vestibular Perception in Healthy Subjects. *Frontiers in Neurology*, *9*, 83. https://doi.org/10.3389/fneur.2018.00083

Kingma, H. (2005). Thresholds for perception of direction of linear acceleration as a possible evaluation of the otolith function. *BMC Ear, Nose and Throat Disorders*, *88*(1 B), 82–87. https://doi.org/10.1186/1472-6815-5-Received

Kingma, H., & van de Berg, R. (2016). Anatomy, physiology, and physics of the peripheral vestibular system. In J. M. Lempert & T. Furman (Eds.), *Handbook of Clinical Neurology* (Vol. 137, pp. 1–16). Elsevier B.V. https://doi.org/10.1016/B978-0-444-63437-5.00001-7

Klein, S. A. (2001). Measuring, estimating, and understanding the psychometric function: A commentary. In *Perception and Psychophysics* (Vol. 63, Issue 8, pp. 1421–1455). Psychonomic Society Inc. https://doi.org/10.3758/BF03194552

Kobel, M. J., Wagner, A. R., Merfeld, D. M., & Mattingly, J. K. (2021). Vestibular Thresholds: A Review of Advances and Challenges in Clinical Applications. *Frontiers in Neurology*, *12*, 643634. https://doi.org/10.3389/fneur.2021.643634

Lempert, T., Olesen, J., Furman, J., Waterston, J., Seemungal, B., Carey, J., Bisdorff, A., Versino, M., Evers, S., & Newman-Toker, D. (2012). Vestibular migraine: diagnostic criteria. *Journal of Vestibular Research : Equilibrium & Orientation*, *22*(4), 167–172. https://doi.org/10.3233/VES-2012-0453

Lewis, R. F., Priesol, A. J., Nicoucar, K., Lim, K., & Merfeld, D. M. (2011). Dynamic tilt thresholds are reduced in vestibular migraine. *Journal of Vestibular Research : Equilibrium & Orientation*, *21*(6), 323–330. https://doi.org/10.3233/VES-2011-0422

Mast, F. W., Preuss, N., Hartmann, M., & Grabherr, L. (2014). Spatial cognition, body representation and affective processes: the role of vestibular information beyond ocular reflexes and control of posture. *Frontiers in Integrative Neuroscience*, *8*, 44. https://doi.org/10.3389/fnint.2014.00044

Merfeld, D. M. (2011). Signal detection theory and vestibular thresholds: I. Basic theory and practical considerations. *Experimental Brain Research*, *210*(3–4), 389–405. https://doi.org/10.1007/s00221-011-2557-7

Merfeld, D. M., Park, S., Gianna-Poulin, C., Black, F. O., & Wood, S. (2005). Vestibular Perception and Action Employ Qualitatively Different Mechanisms. I. Frequency Response of VOR and Perceptual Responses During *Translation* and *Tilt*. *Journal of Neurophysiology*, *94*(1), 186–198. https://doi.org/10.1152/jn.00904.2004

Merfeld, D. M., Priesol, A., Lee, D., & Lewis, R. F. (2010). Potential solutions to several vestibular challenges facing clinicians. *Journal of Vestibular Research : Equilibrium & Orientation*, *20*(1), 71–77. https://doi.org/10.3233/VES-2010-0347

Nouri, S., & Karmali, F. (2018). Variability in the Vestibulo-Ocular Reflex and Vestibular Perception. *Neuroscience*, *393*, 350–365. https://doi.org/10.1016/j.neuroscience.2018.08.025

Okumura, T., Horii, A., Kitahara, T., Imai, T., Uno, A., Osaki, Y., & Inohara, H. (2015). Somatosensory shift of postural control in dizzy patients. *Acta Oto-Laryngologica*, *135*(9), 925–930. https://doi.org/10.3109/00016489.2015.1040172

Priesol, A. J., Valko, Y., Merfeld, D. M., & Lewis, R. F. (2014). Motion perception in patients with idiopathic bilateral vestibular hypofunction. *Otolaryngology - Head and Neck Surgery (United States)*, *150*(6), 1040–1042. https://doi.org/10.1177/0194599814526557

Seemungal, B. M., Gunaratne, I. A., Fleming, I. O., Gresty, M. A., Bronstein, A. M., & Seemungal, B.M., Gunaratne, I.A., Fleming, I.O., Gresty, M.A., B. A. M. (2004). Perceptual and nystagmic thresholds of vestibular function in yaw. *Journal of Vestibular Research: Equilibrium and Orientation*, *14*(6), 461–466. https://doi.org/10.3233/VES-2009-0366

Soyka, F., Bülthoff, H. H., & Barnett-Cowan, M. (2015). Integration of Semi-Circular Canal and Otolith Cues for Direction Discrimination during Eccentric Rotations. *PloS One*, *10*(8), e0136925. https://doi.org/10.1371/journal.pone.0136925

Tarnutzer, A. A., Bockisch, C. J., & Straumann, D. (2009). Head roll dependent variability of subjective visual vertical and ocular counterroll. *Experimental Brain Research*, *195*(4), 621–626. https://doi.org/10.1007/s00221-009-1823-4

van de Berg, R., Rosengren, S., & Kingma, H. (2018). Laboratory examinations for the vestibular system. *Current Opinion in Neurology*, *31*(1), 111–116. https://doi.org/10.1097/WCO.0000000000000526

Chapter 6 How to optimize the electrical stimulation for VI: Geometry of the labyrinth

ABSTRACT

Objective: to conduct precise measurements and analyze the geometric parameters of the rat vestibular organ based on high-resolution micro-CT images.

Methods: images of the rat vestibular organ were obtained using micro-CT with a resolution of 4 micrometers. The images were reconstructed in 3D, segmented, and transformed into a 3D model to obtain geometric dimensions and calculate the dynamic characteristics of vestibular angular acceleration sensors.

Results: geometric parameters of rat semicircular canals and ampullae were determined and compared with human data. Dynamic characteristics of rat semicircular canals were calculated.

Conclusion: It was shown that most of the geometric parameters of the rat vestibular labyrinth are similar to the human data available. The achieved accuracy of measurements of geometric parameters and an obtained thorough anatomic structure of the rat inner ear implies the possibility to conduct experimental studies and simulations to investigate the physiological properties of the vestibular labyrinth.

Chapter 6

INTRODUCTION

The vestibular system is a sensory system responsible for maintaining the balance, orientation in space and gaze stabilization (Kingma & van de Berg, 2016). The vestibular system, also called a labyrinth, is a part of the inner ear located in the left and right temporal bones. It is a multicomponent heterogeneous medium with a complex anatomical and chemical composition, significantly different physical characteristics, including electrical conductive and dielectric properties (Demkin et al., 2018; Demkin, Melnichuk, Shchetinin, et al., 2019).

Last decade the first vestibular prosthesis that restores the absent vestibular function via the electrical stimulation of the semicircular canal (SCC) ampullae was successfully implanted in human (Pelizzone et al., 2014). This was possible due to a number of experimental studies on stimulation of the vestibular afferents performed in animals (Merfeld & Lewis, 2012). In order to enhance the credibility of the models, experimental studies on electroconductivity were performed in guinea pigs and rats (Demkin et al., 2018, 2020a). Both the most advanced 3D finite element models (FEM) and electroconductivity experiments require a known geometrical model for simulations and data validation. Moreover, existing models of the vestibular system are different in their complexity and limitations (Momani & Cardullo, 2018). For instance, the FEM models are supposed to be highly sensitive to the initial data including the dimensions of the vestibular organ, the variance of which (Curthoys et al., 1977; Das et al., 2014; Shinomori et al., 2001) will lead to simulation errors. Therefore, the precise geometry is crucial in the 3D FEM of the vestibular organ that is used to optimize the electrical stimulation by the vestibular implant (Handler et al., 2017; Hayden et al., 2011; Marianelli et al., 2015).

Among non-invasive and non-destructive methods, microCT is one of the most popular ("Micro-Computed Tomogr. Med. Eng.," 2020). It is a widely used technique that is mainly able to visualize dense substances like a bone. The existing microCT devices produce images with a high resolution that can reach the value of 1 um. Therefore, this technique is useful for obtaining a very detailed 3-dimensional model of the inner ear.

This study aims to construct 3D models of the guinea pig and rat inner ear based on high resolution microCT images, and to measure the dimensions of the semicircular canals.

MATERIALS AND METHODS

All procedures performed in studies involving animals were in accordance with the ethical standards of the institution at which the studies were conducted and ethical approval was obtained from the Bioethics Committee of the Institute of Biology at Tomsk State University, registration No34, minute No18 dated December 2, 2019.

In this study, a single periotic bone of a rat (Rattus) weighing 342 grams and a single periotic bone of a guinea pig weighing 947 grams were used. Before the study, the animals were kept in standard vivarium conditions with water and food *ad libitum*. All procedures were performed following the European Convention for the Protection of Vertebrate Animals.

The animals were decapitated under ether anesthesia to conduct micro-CT. Soft tissues of the periotic region and craniotomy were removed due to the limited volume of

the measuring chamber of the tomograph. The bones of the tympanic cavity and the periotic capsule were removed with the preserved native structure of the vestibulocochlear nerve leaving this capsule through the internal auditory opening. The samples were not fixed. The studies were carried out on fresh tissue samples not later than an hour after decapitation. The micro-CT Skyscan1172 (Bruker Corporation, USA) was used to obtain images of the bone labyrinth. An average voltage of 80 kV and a current of 124 µA were used for scanning with an aluminum filter 0.5 mm thick. The pixel size before reconstruction was equal to 4 µm, and the exposure time was set at 1.23 seconds. After reconstruction, the pixel size was 32 micrometers.

On the reconstructed sections, the bony labyrinth was clearly visible as a network of connected tunnels in the periotic bone (Figure 6.1). The reconstructed into 3D images were imported into 3D Slicer 4.11 (Fedorov et al., 2012) for the bony labyrinth segmentation. The segmentation was carried out manually; the resulting segments were assembled into a 3D model. Processing of 3D models included anti-aliasing to eliminate small inaccuracies made as a result of manual segmentation.
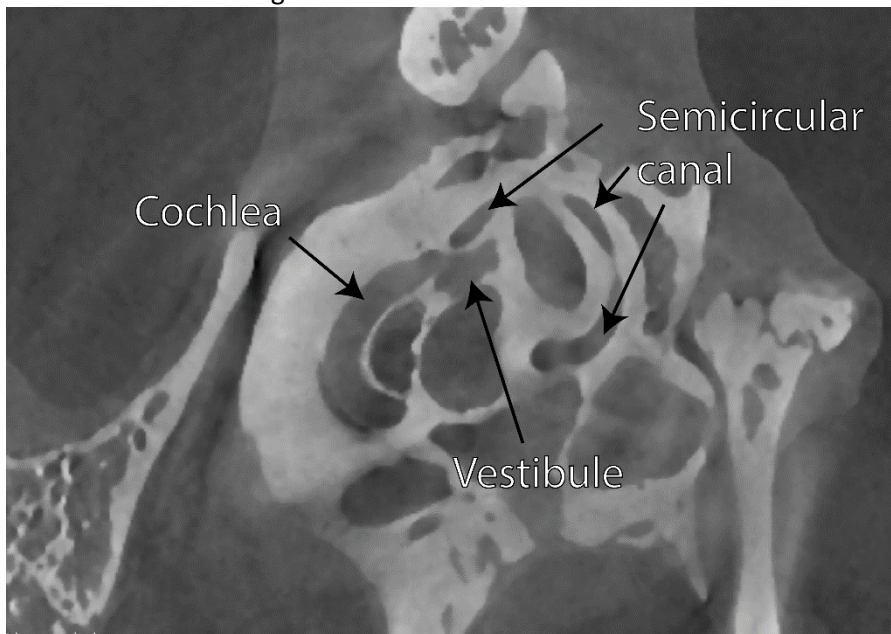
Figure 6.1 The microCT image of the rat temporal bone. Bone is visible as a light region, soft tissues and cavities are visible as dark regions.

All measurements were carried out manually on a 3D-model using free software 3D Slicer 4.11. The shape of the lateral (LSSC), anterior (ASSC), and posterior (PSSC) semicircular canals of the rat, the cross-section of the canal, and the ampulla were approximated by an ellipse (Curthoys & Oman, 1987). Thus, the length of minor (A) and major (B) axes was measured for each semicircular canal, semicircular canal cross-section, and ampulla (Figure 6.2). Semicircular canal cross-section was measured at the beginning (close to the ampulla), in the middle, and at the end (far from the ampulla) of each canal (Figure 6.3). Ampulla dimensions were measured as dimensions perpendicular to the canal

plane. Each measurement was repeated 5 times, then the mean value and the standard deviations were calculated.
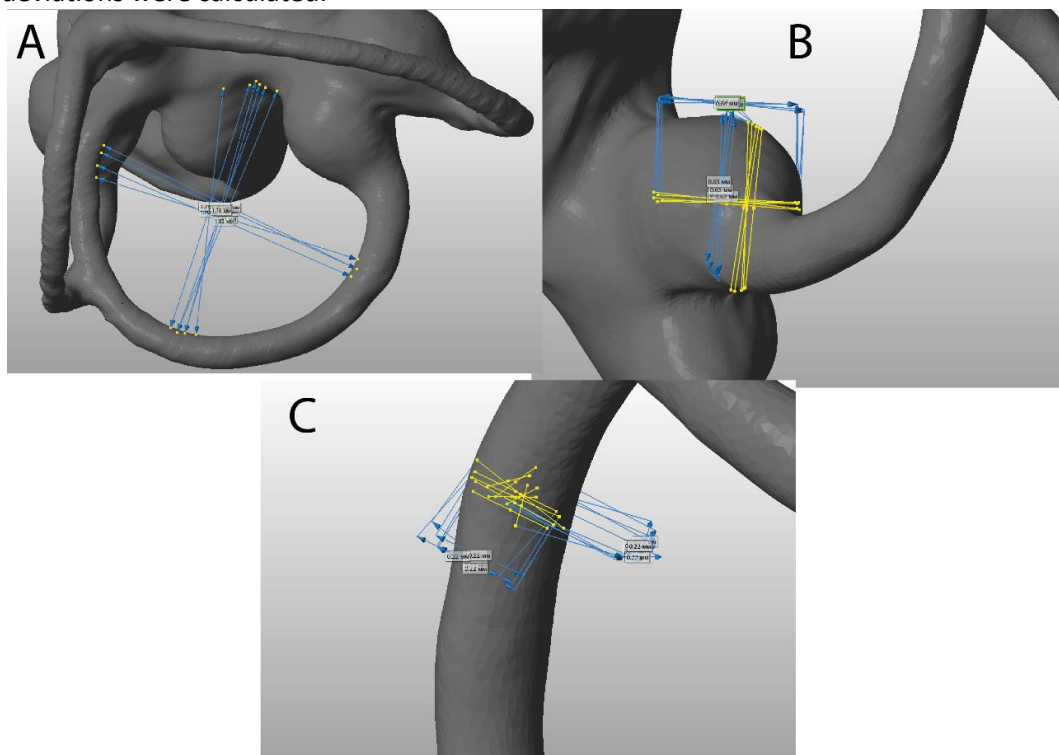
Figure 6.2 3D-geometric model of the rat inner ear. A – measuring the LSCC canal dimensions; B – measuring the LSCC ampulla dimensions; C – measuring the LSCC cross-section dimensions.
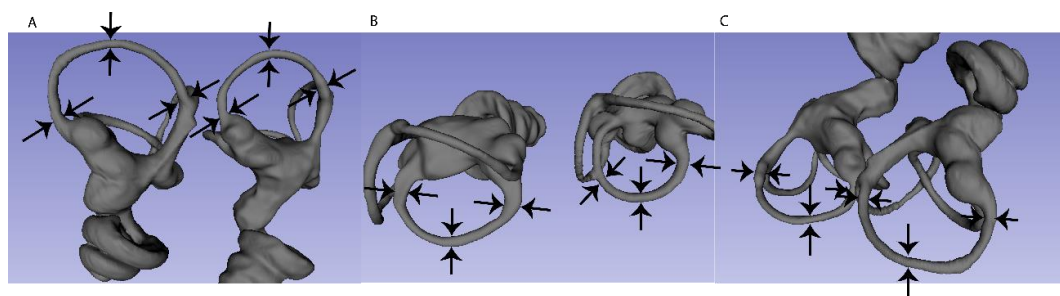
Figure 6.3 The location of the semicircular canal cross-section measurements. A - anterior, B – lateral, C – posterior semicircular canal.

RESULTS

The 3D models of the inner ear of guinea pig and rat were constructed (Figure 6.4) and selected structures of the inner ear were measured. Apparently, the bony labyrinths of the guinea pig and rat are of the comparable size, despite the guinea pig labyrinth is slightly bigger.

The measured dimensions of SCC, ampullae are shown in Table 6.1, the SCC cross-section dimensions are given in Table 6.2. The standard deviations in each measurement did not exceed 30 um. The ampulla dimensions in the guinea pig are 0.1-0.3 mm bigger than in the rat, whereas the cross-sections are only 0.05 mm bigger. The canal cross-section become thinner in the middle both in rat and guinea pig. Among other semicircular canals the maximal cross-section area is observed for the LSSC in the rat as well as in the guinea pig.
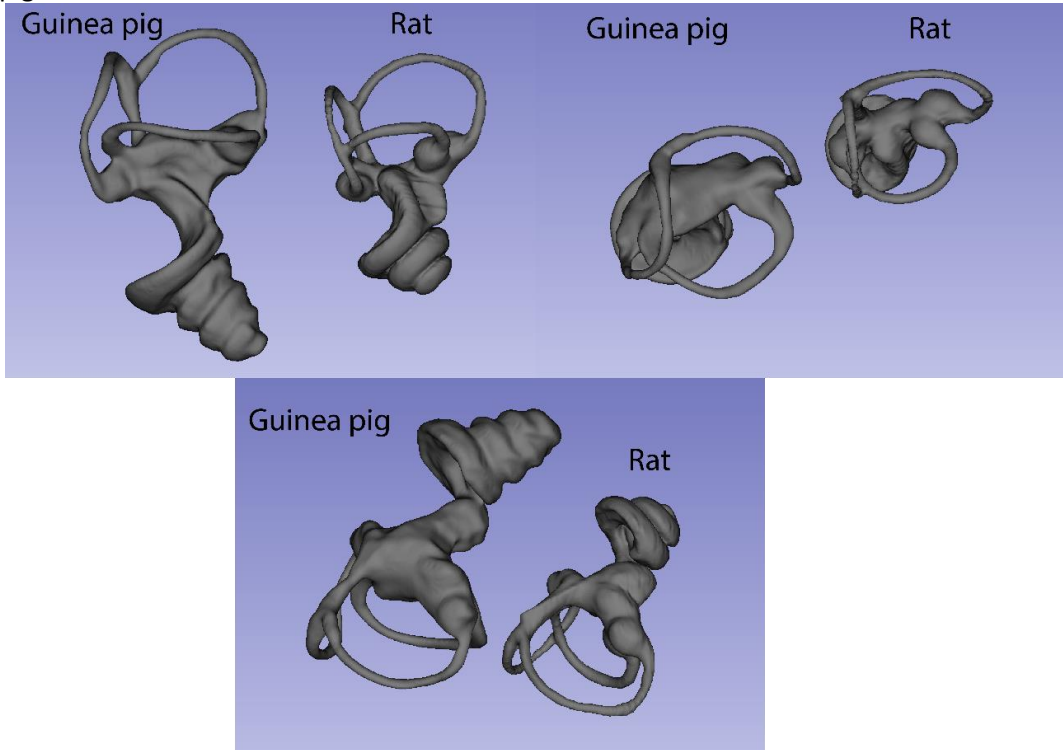
Figure 6.4 3D geometry models of the guinea pig and rat bony labyrinths obtained from segmentation of the microCT images in three different projections.

Table 6.1 Dimensions of the ampullae and semicircular canals in the rat and guinea pig: length of the major (B) and minor (A) axes (mean ± standard deviation). LSCC, ASCC, PSCC – are lateral, anterior and posterior semicircular canals respectively. Units: mm.

Canal	Parameter	Rat		Guinea pig	
		Ampulla	Canal	Ampulla	Canal
LSCC	*A*	0.64±0.01	1.76±0.03	0.71±0.03	1.48±0.02
	B	0.64±0.01	1.83±0.03	0.75±0.01	2.48±0.01
ASCC	*A*	0.69±0.01	1.75±0.02	0.72±0.02	2.14±0.01
	B	0.74±0.01	2.51±0.02	0.73±0.01	2.67±0.02
PSCC	*A*	0.63±0.01	1.57±0.01	0.73±0.01	1.96±0.01
	B	0.74±0.01	1.83±0.02	0.98±0.02	2.16±0.01

Table 6.2 Dimensions of the SCC cross-sections in the rat and guinea pig measured at the beginning (next to ampulla), in the middle, and at the end (far from ampulla) of each SCC: length of the major (B) and minor (A) axes (mean ± standard deviation). LSCC, ASCC, PSCC – are lateral, anterior and posterior semicircular canals respectively. Units: mm.

		Rat			Guinea pig		
		Start	Middle	End	Start	Middle	End
LSCC	*A*	0.24±0.01	0.21±0.01	0.19±0.01	0.40±0.01	0.21±0.01	0.36±0.01
	B	0.23±0.01	0.22±0.01	0.23±0.01	0.25±0.01	0.26±0.01	0.23±0.01
ASCC	*A*	0.21±0.01	0.17±0.01	0.21±0.01	0.19±0.01	0.2±0.01	0.31±0.01
	B	0.23±0.01	0.18±0.01	0.22±0.01	0.24±0.01	0.23±0.01	0.30±0.01
PSCC	*A*	0.23±0.01	0.16±0.01	0.24±0.01	0.25±0.01	0.22±0.01	0.28±0.01
	B	0.23±0.01	0.2±0.01	0.22±0.01	0.19±0.01	0.25±0.01	0.32±0.01

DISCUSSION

The 3D geometry models of the bony labyrinth of the rat and guinea pig were constructed based on microCT images. It was shown that the bony labyrinths of the guinea pig and rat are comparable to each other despite the guinea pig labyrinth is slightly bigger. The human labyrinth is apparently bigger compared with the animals under study (Cox & Jeffery, 2010).

In all measurements the standard deviation did not exceed 30 um, whereas the measurement tolerance calculated as 95% confidence interval was at the order of 10 um already at 5 measurements done. The systematic error propagated from the resolution of the reconstructed microCT image was equal to 30 um, that ultimately defined the overall measurement accuracy. Using advanced reconstruction techniques allows to get the resolution up to 1 um (Glueckert et al., 2018; Metscher, 2009) which will increase the accuracy even more.

The dimensions of canal cross-sections and ampullae of the guinea pig and rat are similar but not identical to the data presented in (Curthoys & Oman, 1987), since the choice of the measurement spot would play a significant role in the outcome. This is related to the non-uniform thickness of the canal along its length. On top of that, this study investigated only one single sample unlike (Curthoys & Oman, 1987), where intersubject variations can be significant.

The measured dimensions of the animal inner ears will help to design the experimental studies in the electroconductivity properties. The obtained cross-sectional values of canals in laboratory animals imply that the electrode cannot be inserted via the canal (van de Berg et al., 2012) like during the vestibular implantation procedure, but should be directly placed in the ampulla to perform the measurements. Firstly, it means that the electrode contact tip should not exceed 0.6 mm in diameter for the rat and 0.7 mm for guinea pig to fit in the ampulla. Secondly, different surgical approaches to reach the ampulla in human (van de Berg et al., 2012) and in laboratory animals (Demkin et al., 2018, 2020b; Demkin, Melnichuk, Svetlik, et al., 2019) might lead to the different electroconductivity outcomes due to: 1) (partial) ampulla destruction in the case of animal models; and 2) the presence of the electrode in the canal space blocking one path of current spread in human.

Eventually, the obtained morphological similarities of semicircular canals show that using the rat and/or guinea pig for experimental and modeling studies of the vestibular system can contribute to the vestibular implant studies (Hayden et al., 2011).

This circumstance should be taken into account when designing prosthetics of the vestibular apparatus and placing electrodes in ampullae, because the transfer function of the vestibular implant depends on the configuration of the vestibular organ and location of the stimulating electrodes (Demkin, Melnichuk, Svetlik, et al., 2019).

CONCLUSION

It was shown that the geometric dimensions of the vestibular organs of the rat and guinea pig do not have significant differences that could change the physiology of vestibular functions, nevertheless the guinea pig labyrinth is slightly bigger which makes access for implantation easier. The obtained images and 3D models can serve as a basis for 1) designing the surgical approach in animals for electroconductivity experiments; 2) designing the electrodes that would fit in the animal ampullae during electroconductivity experiments; and 3) further finite element modeling.

REFERENCES

Cox, P. G., & Jeffery, N. (2010). Semicircular canals and agility: The influence of size and shape measures. *Journal of Anatomy*, *216*(1), 37–47. https://doi.org/10.1111/j.1469-7580.2009.01172.x

Curthoys, I. S., Blanks, R. H. I. I., & Markham, C. H. (1977). Semicircular canal radii of curvature (R) in cat, guinea pig and man. *Journal of Morphology*, *151*(1), 1–15. https://doi.org/10.1002/jmor.1051510102

Curthoys, I. S., & Oman, C. M. (1987). Dimensions of the horizontal semicircular duct, ampulla and utricle in rat and guinea pig. *Acta Oto-Laryngologica*, *103*(3–4), 254–261. https://doi.org/10.3109/00016488709107280

Das, D., Kamil, F. A., Biswas, K., & Das, S. (2014). Evaluation of single cell electrical parameters from bioimpedance of a cell suspension. *RSC Advances*, *4*(35), 18178–18185. https://doi.org/10.1039/c4ra00400k

Demkin, V. P., Kingma, G., Mel'nichuk, S. V., Svetlik, M. V., Rudenko, T. V., Akinina, M. D., & Suyundukova, A. T. (2020a). Effect of Leakage Currents on the Formation of Electrical Pulse for the Vestibular Nerve Stimulation. *Russian Physics Journal*, *62*(12), 2228–2234. https://doi.org/10.1007/s11182-020-01970-3

Demkin, V. P., Kingma, G., Mel'nichuk, S. V., Svetlik, M. V., Rudenko, T. V., Akinina, M. D., & Suyundukova, A. T. (2020b). Effect of Leakage Currents on the Formation of Electrical Pulse for the Vestibular Nerve Stimulation. *Russian Physics Journal*, *62*(12), 2228–2234. https://doi.org/10.1007/s11182-020-01970-3

Demkin, V. P., Melnichuk, S. V., Shchetinin, P. P., Kingma, H., & Van de Berg, R. (2019). Electrophysical Properties and Determination of the Impedance of Vestibular Labyrinth Tissues. *Russian Physics Journal*, *61*(11), 2019–2027. https://doi.org/10.1007/s11182-019-01632-z

Demkin, V. P., Melnichuk, S. V., Svetlik, M. V., Shchetinin, P. P., Kingma, H., Van de Berg, R., Demkin, O. V., & Udut, E. V. (2019). Experimental Investigation of Electric Signal Transmission Through Vestibular Organ Tissues. *Russian Physics Journal*, *61*(12), 2264–2267. https://doi.org/10.1007/s11182-019-01665-4

Demkin, V. P., Udut, V. V., Shchetinin, P. P., Svetlik, M. V., Mel'nichuk, S. V., Shchetinina, A. P., Pleshkov, M. O., Starkov, D. N., Demkin, O. V., & Kingma, H.

(2018). Electrophysiological Properties of Rat Vestibular Labyrinth and Their Effect on Parameters of Transmitted Voltage Pulses. *Bulletin of Experimental Biology and Medicine*, *164*(6), 707–711. https://doi.org/10.1007/s10517-018-4063-4

Fedorov, A., Beichel, R., Kalpathy-Cramer, J., Finet, J., Fillion-Robin, J. C., Pujol, S., Bauer, C., Jennings, D., Fennessy, F., Sonka, M., Buatti, J., Aylward, S., Miller, J. V, Pieper, S., & Kikinis, R. (2012). 3D Slicer as an image computing platform for the Quantitative Imaging Network. *Magnetic Resonance Imaging*, *30*(9), 1323–1341. https://doi.org/10.1016/j.mri.2012.05.001

Glueckert, R., Johnson Chacko, L., Schmidbauer, D., Potrusil, T., Pechriggl, E. J., Hoermann, R., Brenner, E., Reka, A., Schrott-Fischer, A., & Handschuh, S. (2018). Visualization of the Membranous Labyrinth and Nerve Fiber Pathways in Human and Animal Inner Ears Using MicroCT Imaging. *Frontiers in Neuroscience*, *12*, 501. https://doi.org/10.3389/fnins.2018.00501

Handler, M., Schier, P. P., Fritscher, K. D., Raudaschl, P., Chacko, L. J., Glueckert, R., Saba, R., Schubert, R., Baumgarten, D., & Baumgartner, C. (2017). Model-based vestibular afferent stimulation: Modular workflow for analyzing stimulation scenarios in patient specific and statistical vestibular anatomy. *Frontiers in Neuroscience*, *11*(DEC), 713. https://doi.org/10.3389/fnins.2017.00713

Hayden, R., Sawyer, S., Frey, E., Mori, S., Migliaccio, A. A., & Della Santina, C. C. (2011). Virtual labyrinth model of vestibular afferent excitation via implanted electrodes: Validation and application to design of a multichannel vestibular prosthesis. *Experimental Brain Research*, *210*(3–4), 623–640. https://doi.org/10.1007/s00221-011-2599-x

Kingma, H., & van de Berg, R. (2016). Anatomy, physiology, and physics of the peripheral vestibular system. In J. M. Lempert & T. Furman (Eds.), *Handbook of Clinical Neurology* (Vol. 137, pp. 1–16). Elsevier B.V. https://doi.org/10.1016/B978-0-444-63437-5.00001-7

Marianelli, P., Capogrosso, M., Luciani, L. B., Panarese, A., Bassi Luciani, L., Panarese, A., & Micera, S. (2015). A Computational Framework for Electrical Stimulation of Vestibular Nerve. *IEEE Transactions on Neural Systems and Rehabilitation Engineering*, *23*(5), 897–909. https://doi.org/10.1109/TNSRE.2015.2407861

Merfeld, D. M., & Lewis, R. F. (2012). Replacing semicircular canal function with a vestibular implant. In *Current Opinion in Otolaryngology and Head and Neck Surgery* (Vol. 20, Issue 5, pp. 386–392). Curr Opin Otolaryngol Head Neck Surg. https://doi.org/10.1097/MOO.0b013e328357630f

Metscher, B. D. (2009). Micro CT for comparative morphology: Simple staining methods allow high-contrast 3D imaging of diverse non-mineralized animal tissues. *BMC Physiology*, *9*(1). https://doi.org/10.1186/1472-6793-9-11

Micro-computed Tomography (micro-CT) in Medicine and Engineering. (2020). In *Micro-computed Tomography (micro-CT) in Medicine and Engineering*. Springer International Publishing. https://doi.org/10.1007/978-3-030-16641-0

Momani, A., & Cardullo, F. (2018). A review of the recent literature on the

mathematical modeling of the vestibular system. *AIAA Modeling and Simulation Technologies Conference, 2018*, *209959*, 1–35. https://doi.org/10.2514/6.2018-0114

Pelizzone, M., Fornos, A. P., Guinand, N., van de Berg, R., Kos, I., Stokroos, R., Kingma, H., & Guyot, J. P. (2014). First functional rehabilitation via vestibular implants. In *Cochlear Implants International* (Vol. 15, Issue SUPPL. 1). Maney Publishing. https://doi.org/10.1179/1467010014Z.000000000165

Shinomori, Y., Spack, D. S., Jones, D. d., & Kimura, R. S. (2001). Volumetric and dimensional analysis of the guinea pig inner ear. *Annals of Otology, Rhinology and Laryngology*, *110*(1), 91–98. https://doi.org/10.1177/000348940111000117

van de Berg, R., Guinand, N., Guyot, J.-P., Kingma, H., & Stokroos, R. J. (2012). The modified ampullar approach for vestibular implant surgery: feasibility and its first application in a human with a long-term vestibular loss. *Frontiers in Neurology*, *3*, 18. https://doi.org/10.3389/fneur.2012.00018

Chapter 7 How to optimize the electrical stimulation for VI: Electrical properties

ABSTRACT

Objective. Several lumped and distributed parameter models of the inner ear have been proposed to improve vestibular implant stimulation. The models should account for all significant physical phenomena that influence the current propagation, such as the electrical double layer (EDL) and medium polarization. The electrical properties of the medium are reflected in the electrical impedance; therefore, the study aimed to measure the impedance in the guinea pig inner ear and construct its equivalent circuit.

Approach. The electrical impedance was measured from 100 Hz to 50 kHz between a pair of platinum electrodes immersed in 0.9% NaCl saline solution using sinusoidal voltage signals. The Randles circuit was fitted to the measured impedance in the saline solution in order to estimate the EDL parameters ($C, W, and\ R_{ct}$) of the electrode interface in saline. Then, the electrical impedance was measured between all combinations of the electrodes located in the semicircular canal ampullae and the vestibular nerve in the guinea pig *in vitro*. The extended Randles circuit considering the medium polarization (R_i, R_e, C_m) together with EDL parameters (C, R_{ct}) obtained from the saline solution was fitted to the measured impedance of the guinea pig inner ear. The Warburg element was assumed negligible and was not considered in the guinea pig model.

Main results. For the set-up used, the obtained EDL parameters were: $C = 27.09 * 10^{-8} F, R_{ct} = 18.75\ k\Omega$. The average values of intra-, extracellular resistances, and membrane capacitance were $R_i = 4.74\ k\Omega$, $R_e = 45.05\ k\Omega$, $C_m = 9.69 * 10^{-8}\ F$, respectively.

Significance. The obtained values of the model parameters can serve as a good estimation of the EDL for modelling work. The EDL, together with medium polarization, plays a significant role in the electrical impedance of the guinea pig inner ear, therefore, they should be considered in electrical conductivity models to increase the credibility of the simulations.

INTRODUCTION

The vestibular system – also called the vestibular labyrinth – is a pair of balance organs located in the left and right temporal bones. Each vestibular organ consists of three semicircular canals (SCCs) that detect head angular acceleration and two otolith organs that detect head linear acceleration, including gravity. Head motion information obtained by the vestibular organs is then transferred via nerves to the brain and used to stabilize gaze, facilitate orientation in space, and maintain balance (Kingma & van de Berg, 2016). For some reasons, the vestibular function can be decreased or completely lost (Lucieer et al., 2016), which significantly worsens the quality of patients' lives and brings a considerable economic burden (Sun et al., 2014).

Research groups have shown that vestibular function in a population with severe bilateral vestibular loss can be partially restored using an investigational vestibular prosthesis – the vestibular implant (VI) (Boutros et al., 2019; Perez Fornos et al., 2017). The concept of the VI is to replace the impaired vestibular end-organ with an electrical stimulator using a set of gyroscopes. Currently, VIs for the semicircular canals consist of three electrode branches, each of which is inserted into one SCC with the stimulating contact targeting the center of the ampulla (Seppen et al., 2019; van de Berg et al., 2012). Head rotation is measured by gyroscopes and processed by the VI. Information about head motion is encoded using modulated biphasic charge-balanced square electrical pulses. It is then sent directly into the vestibular nerves through the electrodes - one of each electrode pair being located in the respective SCC, the other located either nearby (bipolar stimulation) or remotely (monopolar stimulation).

In recent years, several distributed parameter models (Handler et al., 2017; Hayden et al., 2012; Marianelli et al., 2015) together with lumped parameter models (Demkin et al., 2018, 2020) have been proposed for investigation of the current propagation in the tissues of the human and animal inner ear to optimize the VI stimulation. The abovementioned distributed parameter models mainly consider the interelectrode space to be purely resistive. However, medium polarization (C. Gabriel et al., 1996; S. Gabriel et al., 1996) and the electrical double layer (EDL) present in the electrode-tissue interface could influence the shape and amplitude of the voltage waveform (Grant & Lowery, 2009). In contrast, lumped parameter models already include the capacitive effects of biological membranes of the cells building up the living tissue.

The EDL represents a small but highly resistive layer at the electrode surface that may influence the current in the range of low frequencies (Cantrell et al., 2008; Grant & Lowery, 2009). In a simplified representation, the EDL can be described as a capacitor preventing the flow of low frequency components of the stimulus. On the other hand, medium polarization (of tissues external to the electrode) can occur at different frequencies. For example, the electronic, ionic, and orientational polarization is present at frequencies higher than the MHz range (gamma

dispersion). In contrast, the polarization of cell membranes and macrostructures can arise starting in the range of Hz (alpha dispersion) (Grimnes & Martinsen, 2010; SCHWAN, 1957).

The electrical impedance measurements followed by the equivalent circuit fitting approach is widely used in biology studies, including *ex vitro* measurements of isolated animal tissues (Dean et al., 2008), *in vivo* measurements of plants (Bar-On et al., 2021), and *ex vivo* human dental (Herencsar et al., 2020) and cardiac (Fischer et al., 2019) tissues. The most accurate physical models used to optimize the VI should account for all significant physical phenomena of current transmission in the inner ear. Thus, in this study, we performed the following steps: The 0.9% NaCl saline solution was chosen to measure the electrical impedance between a pair of platinum half exposed ball electrodes of 0.5 mm diameter in a frequency range from 100 Hz to 50 kHz. Medium polarization was neglected in this case since the saline solution does not include any tissue and the chosen frequency range is too low to cause gamma dispersion. For this case, the Randles equivalent circuit representing a purely resistive medium and the reactive EDL were the features chosen to fit the measured impedance. Next, the electrical impedances were measured in the guinea pig inner ear between each pair of ampullae and vestibular nerve using the same conditions as in the case of saline solution. All measurements were performed at room temperature T=298K. Finally, an extended Randles circuit including the reactive component of tissue impedance (instead of purely resistive) and the EDL parameters identified from saline solution measurements were used to fit the measured impedances in the guinea pig.

The first aim of this study was to determine electrical impedances between a pair of electrodes immersed in saline solution to estimate their EDL parameters under such conditions from the fitted Randles circuit. The second aim was to determine electrical impedances between each pair of electrodes, with contacts located close to the center of each ampulla of each SCC and adjacent to the vestibular nerve in the guinea pig inner ear. This was done *in vitro* using sinusoidal voltage signals in a frequency range from 100 Hz to 50 kHz. Finally, the aim was to fit the measured interelectrode electrical impedance, including the EDL and medium polarization, to the Randles circuit using a squared error minimization algorithm.

MATERIALS AND METHODS

Sample

This study used 10 ml of 0.9% NaCl saline solution stored in a disposable plastic container (1.71 x 1.25 x 4.5 cm) and the periotic bone of a guinea pig weighing 947 grams. Before the study, the animal was kept in standard vivarium conditions with water and food *ad libitum*. All procedures were performed following the European Convention for the Protection of Vertebrate Animals. The animal was decapitated under ether anesthesia. The bones of the tympanic cavity and the periotic capsule were removed, with the preserved native structure of the vestibulocochlear nerve

leaving this capsule through the internal auditory opening. The study was carried out on a fresh tissue sample no later than an hour after decapitation. The sample was not fixed.

Equipment

A set of platinum electrodes was used to measure the impedances. The platinum ball contact branches fabricated by Med-EL are made by flaming the end of a wire into a ball contact. The size of the ball contact is checked to be within a $\pm 0.05\ mm$ range of tolerance. Each electrode branch was fabricated with a ball contact at the tip with a diameter of 0.5 mm, half exposed, resulting in an estimated contact area of $S_e = \frac{\pi d^2}{2} = 0.39\ mm^2$. The remaining electrode surface was insulated with silicone rubber. The measured active electrical resistance of each electrode was below 2 Ω and thus was considered negligible compared to the EDL. First, two electrodes were inserted parallel to each other in a plastic container filled with 10 ml 0.9% NaCl saline solution, positioned at a distance of 35 mm from each other. Next, three electrodes were each inserted into the fenestrations of one of the three SCC ampullae of the vestibular organ, and one electrode was attached to the vestibulocochlear nerve stump. All electrodes were fixed at their positions using cyanoacrylate (superglue).

The measurement circuit is presented in Figure 7.1. Only two out of four inserted electrodes were used at a time in each of six measurements: one electrode provided the voltage, another served as a ground node. The AC voltage generator (Gen) provided a sinusoidal signal with an amplitude of 0.2 V in the case of saline solution and 0.4 V in guinea pig inner ear, both in a frequency range of 100 Hz to 50 kHz. The chosen magnitude of the load resistor (R) should not interfere with the target impedance. On the other hand, the load resistance should be big enough to register the voltage applied. Thus, in the present study, the load resistor was $R = 960\ \Omega$ (1% resistance accuracy) for guinea pig measurements and $R = 100\ \Omega$ (1% resistance accuracy) for saline solution measurements. During the measurements, the total current flowing in the circuit did not exceed 90 μA. The RIGOL DS1054 oscilloscope (Osc) simultaneously registered the voltage applied between the stimulating electrode EL1 and the ground GND (V_{gen}), and the voltage applied between the registering electrode EL2 and the ground GND (V_{load}). The measurements were performed at room temperature T=298 K.
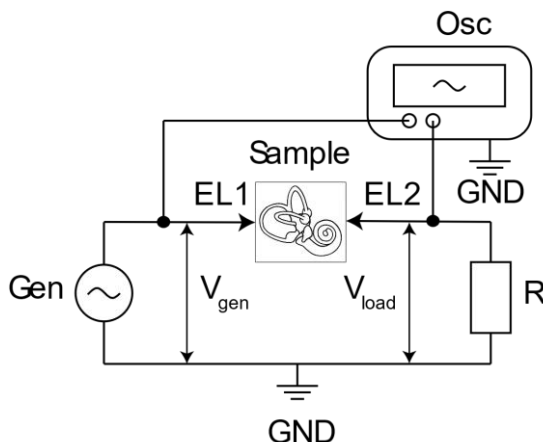
Figure 7.1 Schematic picture of the impedance measurement circuit. Gen – voltage signal source; Osc – oscilloscope; R – load resistor; EL1 and EL2 – implanted platinum electrodes; GND – ground node; V_{gen} – voltage provided by generator; V_{load} – voltage measured at the load resistor.

Electrical impedance calculation

The measurement circuit was considered a closed one (insignificant current flow to and from oscilloscope); therefore, the electrical current was assumed to be the same at any point of the (model) circuit and was determined as $I = \frac{V_{load}}{R}$. Taking into account the previously mentioned assumption and the energy conservation law, the voltage applied to the sample was then calculated simply as a difference between the voltage provided by the generator and the voltage drop over the load resistor: $V_s = V_{gen} - V_{load}$. The electrical impedance magnitude was then calculated at each measured frequency via Ohm's law as the ratio of the voltage and current amplitudes: $|Z(f)| = \frac{|V_s|}{|I|}$. The phase shift $\Delta\varphi = \varphi_2 - \varphi_1$ was determined by comparing the harmonic signal applied from generator $V_{gen} = A_1 sin(\omega t + \varphi_1)$ and the harmonic signal received at the load $V_{load} = A_2 sin(\omega t + \varphi_2)$. Both signals underwent Fast Fourier Transform, then the dominant harmonic component was identified in each signal as having the highest magnitude. The phases φ_1 and φ_2 were calculated in each signal using Euler's formula, and finally, their difference resulted in the overall phase shift $\Delta\varphi$ expressed in radians.

Equivalent circuit model: saline solution

The Randles circuit (Randles, 1947) was chosen to simulate the electrical impedance between the electrodes immersed in the saline solution and estimate the EDL parameters since the saline solution does not include any biological tissues or cell membranes. The medium impedance in the saline solution was considered to be purely resistive (R_s) due to the absence of biological tissues in the measurement. The EDL was represented by a capacitor (C) connected in parallel to a Warburg

element (W) and an active resistance (R_{ct}) describing the charge transfer through the EDL (Figure 7.2). The Warburg element was represented as a constant phase element with an impedance equal to $Z_W = \frac{1}{A*(i*2*\pi*f)^p}$, where A is the inverse magnitude of Warburg element impedance; i is the imaginary unit, f is linear frequency, and p is a real number in the range between 0 and 1 (Taylor & Gileadi, 1995).
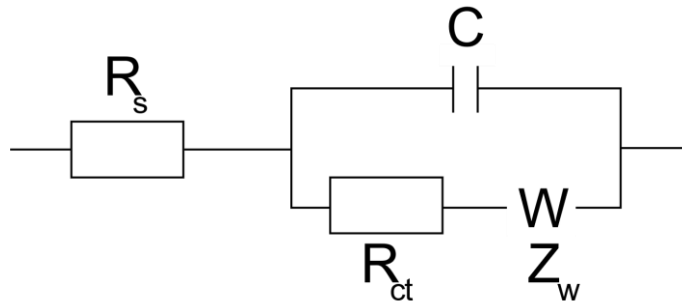
Figure 7.2 Randles circuit used for fitting the measured impedance in saline solution. R_s – the interelectrode medium resistance, R_{ct} – charge transfer resistance, C – EDL capacitance, W – Warburg element, Z_W – Warburg element impedance.

Equivalent circuit model: guinea pig inner ear

An extended equivalent Randles circuit was used to fit the measured electrical impedance in the guinea pig inner ear tissue (Figure 7.3). The Randles equivalent circuit was chosen because of the simplicity in its interpretation (impact of the EDL compared with the biological tissue) and lower ambiguity in parameter identification compared with the equivalent circuits incorporating more elements (Demkin et al., 2020). The equivalent circuit consists of a simplified EDL circuit without the Warburg element (R_{ct}, C) describing electrode-tissue interface and a tissue circuit representing the inner ear tissue in terms of extracellular resistance (R_e) in parallel with membrane capacitance (C_m) and intracellular resistance (R_i). The Warburg element was omitted due to the small impedance magnitude compared with other resistances and for the simplicity of further simulations. The EDL parameters were taken from the result obtained from the saline solution simulation, whereas the tissue parameters were identified by fitting the tissue circuit to the measured data.
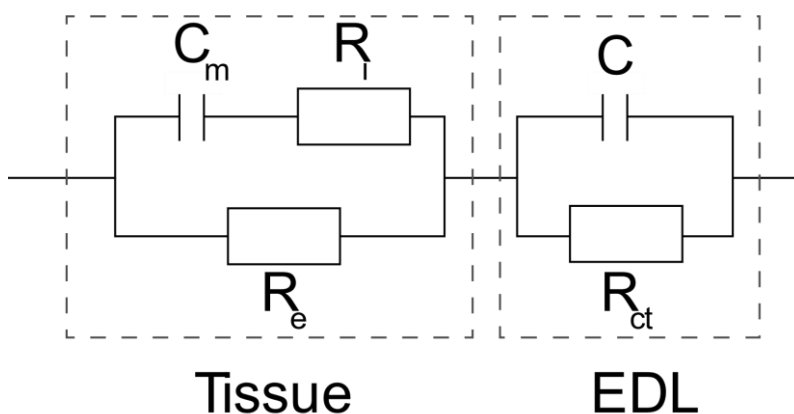
Figure 7.3 Randles circuit with extended tissue model (excluding Warburg element) used for fitting the measured impedance in the guinea pig inner ear. Tissue circuit: R_i – resistance of the intracellular medium, C_m – membrane capacitance, R_e – resistance of the extracellular medium; EDL circuit: R_{ct} – charge transfer resistance, C – EDL capacitance; EDL – electrical double layer.

A custom-made algorithm to find the best combination of parameters has been implemented in Matlab 2014b (Mathworks, Natick, USA). The algorithm fitted the desired equivalent circuit to the experimentally determined electrical impedance in the complex form using the iterative method of minimizing the squared error between the fit and the measurements. The initial values of the different parameters and their chosen upper range are listed in Table 7.1; the lower range was always set at 0, since the considered parameters must be non-negative.

Table 7.1 The range of the equivalent circuit parameters used for the model fit.

	Medium				EDL			
	Guinea pig tissue			Saline				
	R_i (Ω)	C_m (F)	R_e (Ω)	R_s (Ω)	C (F)	R_{ct} (Ω)	$A(\frac{1}{\Omega})$	p
Starting point	$2 * 10^4$	10^{-9}	$2 * 10^4$	$2 * 10^4$	10^{-9}	$4 * 10^3$	0.06	0.5
Upper limit	10^6	10^{-6}	10^6	10^6	10^{-6}	10^6	Inf	1

RESULTS

Impedance measurements: saline solution

Figure 7.4 shows the magnitude and phase shift of the total electrical impedance for both measured and fitted parameters for the saline solution. The impedance magnitude becomes horizontally asymptotic at approximately 30 kHz

with a value of about 1 $k\Omega$. The originally negative phase shift tends to 0 degrees with increasing external field frequency and reaches 0 degrees at around 50 kHz.

Figure 7.4 Measured and fitted electrical impedance in the saline solution. Measured impedance (blue crosses), fitted impedance (blue solid line), measured phase shift (red circles), and simulated phase shift (red dashed line).

Equivalent circuit simulation: saline solution

Table 7.2 shows the best Randles circuit parameters (Figure 7.2) obtained from the fitting algorithm by using the total measured impedance of the saline solution. The maximum value of Warburg element impedance does not exceed the magnitude of 0.05 Ω and, therefore, can be neglected compared with saline resistance R_s (809.49 Ω) and charge transfer resistance R_{ct} (18.75 $k\Omega$). Thus, the fitted values of EDL (C, R_{ct}) will be used for further simulations of stimulation through real electrodes in the guinea pig inner ear.

The capacitive impedance (X_C) acts according to the expression $X_C = \frac{1}{i\omega C}$. It forms the low frequency impedance that decays with increasing the stimulation frequency. In contrast, active resistance of saline (R_s) is frequency independent and determines the plateau value at high frequency range (Figure 7.4).

Table 7.2 Fitted parameters of the impedance in the saline solution. R_s – resistance of the interelectrode medium; R_{ct} – charge transfer resistance; C – electrical double layer capacitance; A – the inverse magnitude of Warburg element impedance; p – the power of the phase part of Warburg element impedance.

	Medium	EDL			
	R_s (Ω)	$C*10^{-8}$ (F)	R_{ct} $(k\Omega)$	A $(\frac{1}{\Omega})$	p
saline	809.49	27.09	18.75	0.06	0.89

Impedance measurements: guinea pig

Both measured and fitted magnitudes and phase shifts of a total electrical impedance in the guinea pig inner ear are shown in Figure 7.5. Both the magnitude and phase shift indicate a nonlinear frequency dependence. The measured impedance magnitude becomes horizontally asymptotic at approximately 10 kHz with an average value of 4.6 $k\Omega$. The value of the asymptote also includes the load resistor (960 Ω), which is in series to the measured impedance. The absolute value of phase shift tends to decrease to 0 degrees at approximately the same frequency of 10 kHz.
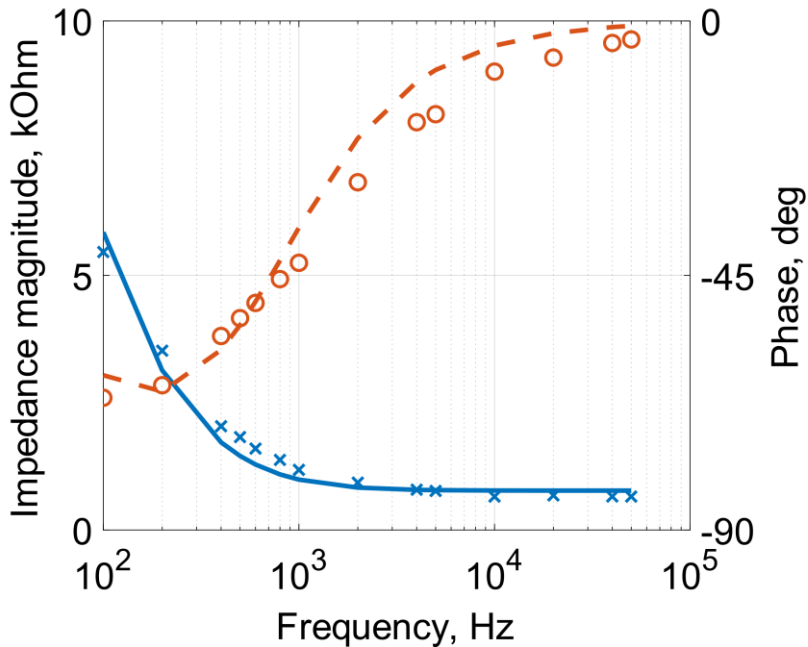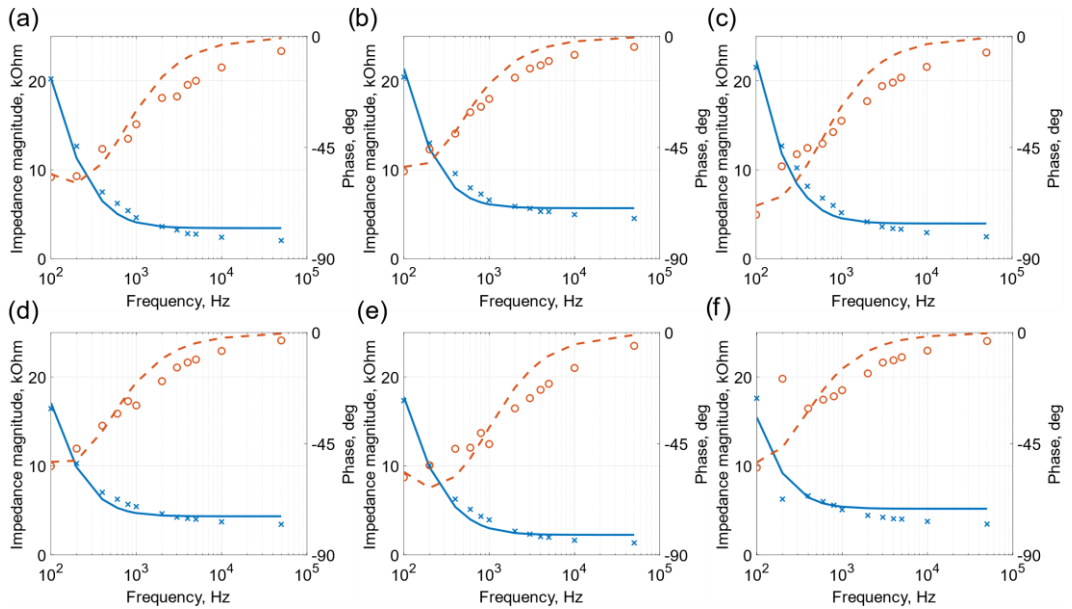
Figure 7.5 Measured and fitted electrical impedance in the guinea pig inner ear. Measured impedance (blue crosses), fitted impedance (blue solid line), measured phase shift (red circles), and simulated phase shift (red dashed line) between: (a) ASCC-LSCC; (b) ASCC-VN; (c) ASCC-PSCC; (d) LSCC-VN; (e) LSCC-PSCC; (f) PSCC-VN in guinea pig. Abbreviations: ASCC, PSCC, LSCC – are anterior, posterior and lateral semicircular canals, respectively; VN – vestibular nerve.

Equivalent circuit simulation: guinea pig

The extended equivalent Randles circuit was fitted to the measured data to take into account medium polarization, using the circuit shown in Figure 7.3 (including the extended tissue model but without the Warburg element). The other EDL parameters (C and R_{ct}) are defined to be the same as in the saline solution simulations (Table 7.2). The (small magnitude) Warburg element was not considered in this equivalent circuit since the simulations showed that the absence of the Warburg element does not worsen the goodness of fit. The best fit coefficients are shown in Table 7.3. The fitted intracellular resistance (R_i) between a pair of ampullae is slightly lower than the resistance between an ampulla and the vestibular nerve stump at the location of the recording electrode.

Table 7.3 The fitted impedance parameters in the guinea pig inner ear: Randles circuit with extended tissue. ASCC, PSCC, LSCC – are anterior, posterior, and lateral semicircular canals, respectively; VN – vestibular nerve; R_i – resistance of the intracellular medium; C_m – membrane capacitance; R_e – resistance of the extracellular medium; R_{ct} – resistance of the diffusion layer; C – electrical double layer capacitance; SD – standard deviation. EDL parameters are fixed in this case at levels obtained from the saline solution measurements.

	Medium			EDL	
	R_i $(k\Omega)$	C_m $* 10^{-8}$ (F)	R_e $(k\Omega)$	$C * 10^{-8}$ (F)	R_{ct} $(k\Omega)$
ASCC-LSCC	3.88	8.44	33.34		
ASCC-VN	6.76	7.79	35.12		
ASCC-PSCC	4.31	9.50	134.65	27.09	18.75
LSCC-VN	5.30	9.94	23.24		
LSCC-PSCC	2.69	9.84	22.86		
PSCC-VN	5.50	12.60	24.08		
Average	4.74	9.69	45.05	-	-
SD	1.42	1.68	44.16	-	-

DISCUSSION

In the present study, the electrical impedance was determined in the saline solution and between the selected structures of the guinea pig inner ear: the three SCC ampullae and the vestibular nerve. The parameters of the Randles circuit were fitted to the measured values of the electrical impedance in the saline solution to estimate the EDL parameters. The obtained magnitude of the Warburg element is considerably smaller than the other elements in the equivalent circuit. Therefore, the Warburg element could be neglected. The extended Randles circuit parameters, including intra- and extracellular resistance and cell membrane capacitance (Figure 7.3) were fitted to the measured electrical impedances in the guinea pig inner ear. A good match between the model and the measurements for both magnitude and phase shift was obtained. A better fit can be obtained by adding more elements in the circuit, but this should be done concerning their physical interpretation.

The data suggest that the capacitive component of the electrical impedance in the guinea pig inner ear is significant in the range of relatively low frequencies up to 10 kHz. At higher frequencies, the impedance of both capacitors present in the extended Randles circuit approaches zero, allowing the current to bypass the charge transfer resistance and the extracellular resistance and to flow through the intracellular resistance and the membrane capacitance (Figure 7.3). Consequently, the overall magnitude of the electrical impedance approaches (at high frequencies)

the total active resistance - equal to the sum of the intracellular resistance and the load resistor with increasing frequency in the model.

The EDL capacitance per unit area can be assumed to be in the range of $\frac{C}{S} = 10 - 20 \frac{\mu F}{cm^2}$ for a metal electrode immersed in liquid (Merrill et al., 2005), which has the same order of magnitude as the findings of this study $\frac{C}{S} = \frac{C}{2S_e} = 34.73 \, \mu F/cm^2$. The electrode contact area in these experiments is, in fact, twice the area of single contact since the model creates one capacitance value that accounts for the capacitance C for both electrodes; therefore, the direct comparison between literature and fitted values cannot be established.

In vivo vs. in vitro

It has been shown in the literature that there are differences between *in vitro* and *in vivo* results, indicating a slight decrease in the conductivity and permittivity in *in vitro* cases (Schwartz & Mealing, 1985). Even though the ionic composition of endo- and perilymphatic liquids equalizes *post mortem* due to the diffusion process (Rodgers et al., 1966), it does not change the overall liquid conductivity and active resistance R_e. Finally, the tissue properties can change with temperature (Edd et al., 2005; Fischer et al., 2019), with the trend to increase when lowering the temperature in the positive temperature range. Thus, the measured impedance evaluated in this paper could be a slight overestimation of the real in vivo situation.

Relation to a human inner ear

When considering the human inner ear space, the value of the EDL capacitance will probably vary from the findings of this study due to the bigger sizes of vestibular labyrinths (in particular, of the SCCs and the ampullae). Electrode dimensions used in humans can be bigger or smaller than in the *in-vitro* experiments of this study on guinea pigs. This might lead to different contact surface areas and, consequently, different EDL capacitances - C, which in its way affects the impedance in the low frequency range. The electrode size issue can be resolved in each particular case by direct measurement of the implant electrode tip and a consecutive scaling the EDL capacitance.

In addition, the human ampullae are located farther from each other and from the vestibular nerve than in the guinea pig, which will probably increase the active resistance - R_e. On the other hand, the cross-sections of human semicircular canals are approximately 20 times bigger than in the guinea pig (Curthoys et al., 1977) that will probably reduce the active resistance - R_e according to the cylinder resistance equation (if the canal can be assumed as a conductive cylinder).

This study presents the electrical impedances not only between each pair of ampullae but also between the ampullae and vestibular nerve, which is crucial to understand the nerve fiber stimulation processes and cross-talk between stimulated ampullae. The presented methodology to evaluate fitting parameters by matching

the measured *in vitro* electroconductive properties of the guinea pig inner ear could improve modelling the electrode-tissue interface and evaluate simulations. The obtained values of the EDL parameters (C, W, R_{ct}) can serve as a good estimate of the EDL to use in future electrical modelling, including other electrode dimensions, even though they might change with different electrode contact areas. Unlike the EDL, the medium impedance would change with different interelectrode distances and tissues present between the electrodes, such as bone, membrane, or cupula. Eventually, the physical phenomena described in this article remain the same for guinea pig and human inner ear can be used for modeling purposes.

Future prospective

In the future, *in vivo* experiments measuring the interelectrode impedance in laboratory animals (and potentially in VI patients) will be very useful for validating the presented results.

A (micro-)Computed Tomography scan of the implanted site after impedance measurements would allow for the reconstruction of the entire geometry and determine the precise distance between electrodes located in the inner ear. Together with the obtained impedances in the inner ear, the known geometry would allow for the construction of 3D FEM models and calculation of the distributed parameters such as electrical conductivity and dielectric permittivity of the tissues involved (Fischer et al., 2019).

The measured electrical impedances of the guinea pig inner ear and obtained equivalent circuits shown in this study can also be used to improve and optimize already existing 3D FEM models by considering the EDL in the simulations. In addition, impedance measurements from various isolated tissues of the inner ear and identification of their distributed electrical parameters might be essential to get more realistic localized results from the 3D FEM simulations.

CONCLUSION

The EDL, together with medium polarization, plays a significant role in the electrical impedance of the guinea pig inner ear. Thus, when trying to predict the performance of electrical stimulation using electrical conductivity models, the EDL and medium polarization should be considered in these models to increase the credibility of the simulation outcomes.

ACKNOWLEDGEMENTS

ETHICAL STATEMENT

All procedures performed in studies involving animals were in accordance with the ethical standards of the institution at which the studies were conducted and ethical approval was obtained from the Bioethics Committee of the Institute of

Biology at Tomsk State University, registration No34, minute No18 dated December 2, 2019.

REFERENCES

Bar-On, L., Garlando, U., Sophocleous, M., Jog, A., Motto Ros, P., Sade, N., Avni, A., Shacham-Diamand, Y., & Demarchi, D. (2021). Electrical Modelling of In-Vivo Impedance Spectroscopy of Nicotiana tabacum Plants. *Frontiers in Electronics*, *0*, 14. https://doi.org/10.3389/FELEC.2021.753145

Boutros, P. J., Schoo, D. P., Rahman, M., Valentin, N. S., Chow, M. R., Ayiotis, A. I., Morris, B. J., Hofner, A., Rascon, A. M., Marx, A., Deas, R., Fridman, G. Y., Davidovics, N. S., Ward, B. K., Treviño, C., Bowditch, S. P., Roberts, D. C., Lane, K. E., Gimmon, Y., … della Santina, C. C. (2019). Continuous vestibular implant stimulation partially restores eye-stabilizing reflexes. *JCI Insight*, *4*(22). https://doi.org/10.1172/jci.insight.128397

Cantrell, D. R., Inayat, S., Taflove, A., Ruoff, R. S., & Troy, J. B. (2008). Incorporation of the electrode-electrolyte interface into finite-element models of metal microelectrodes. *Journal of Neural Engineering*, *5*(1), 54–67. https://doi.org/10.1088/1741-2560/5/1/006

Curthoys, I. S., Markham, C. H., & Curthoys, E. J. (1977). Semicircular duct and ampulla dimensions in cat, guinea pig and man. *Journal of Morphology*, *151*(1), 17–34. https://doi.org/10.1002/jmor.1051510103

Dean, D. A., Ramanathan, T., Machado, D., & Sundararajan, R. (2008). Electrical Impedance Spectroscopy Study of Biological Tissues. *Journal of Electrostatics*, *66*(3–4), 165. https://doi.org/10.1016/J.ELSTAT.2007.11.005

Demkin, V. P., Kingma, G., Mel'nichuk, S. V., Svetlik, M. V., Rudenko, T. V., Akinina, M. D., & Suyundukova, A. T. (2020). Effect of Leakage Currents on the Formation of Electrical Pulse for the Vestibular Nerve Stimulation. *Russian Physics Journal*, *62*(12), 2228–2234. https://doi.org/10.1007/s11182-020-01970-3

Demkin, V. P., Shchetinin, P. P., Melnichuk, S. V., Kingma, H., Van de Berg, R., Pleshkov, M. O., & Starkov, D. N. (2018). Electric Current Transmission Through Tissues of the Vestibular Labyrinth of a Patient: Perfection of the Vestibular Implant. *Russian Physics Journal*, *60*(11), 2019–2024. https://doi.org/10.1007/s11182-018-1318-5

Edd, J. F., Horowitz, L., & Rubinsky, B. (2005). Temperature dependence of tissue impedivity in electrical impedance tomography of cryosurgery. *IEEE Transactions on Biomedical Engineering*, *52*(4), 695–701. https://doi.org/10.1109/TBME.2005.844042

Fischer, G., Handler, M., Johnston, P. R., & Baumgarten, D. (2019). Impedance and conductivity of bovine myocardium during freezing and thawing at slow rates - implications for cardiac cryo–ablation: Impedance of bovine myocardium during freezing and thawing. *Medical Engineering and Physics*, *74*, 89–98. https://doi.org/10.1016/j.medengphy.2019.09.017

Gabriel, C., Gabriel, S., & Corthout, E. (1996). The dielectric properties of biological tissues: I. Literature survey. *Physics in Medicine and Biology*, *41*(11), 2231–2249. https://doi.org/10.1088/0031-9155/41/11/001

Gabriel, S., Lau, R. W., & Gabriel, C. (1996). The dielectric properties of biological tissues: II. Measurements in the frequency range 10 Hz to 20 GHz. *Physics in Medicine and Biology*, *41*(11), 2251–2269. https://doi.org/10.1088/0031-9155/41/11/002

Grant, P. F., & Lowery, M. M. (2009). Effects of the electrical double layer and dispersive tissue properties in a volume conduction model of deep brain stimulation. *Proceedings of the 31st Annual International Conference of the IEEE Engineering in Medicine and Biology Society: Engineering the Future of Biomedicine, EMBC 2009*, *c*, 6497–6500. https://doi.org/10.1109/IEMBS.2009.5333592

Grimnes, S., & Martinsen, Ø. G. (2010). Alpha-dispersion in human tissue. *Journal of Physics: Conference Series*, *224*(1). https://doi.org/10.1088/1742-6596/224/1/012073

Handler, M., Schier, P. P., Fritscher, K. D., Raudaschl, P., Chacko, L. J., Glueckert, R., Saba, R., Schubert, R., Baumgarten, D., & Baumgartner, C. (2017). Model-based vestibular afferent stimulation: Modular workflow for analyzing stimulation scenarios in patient specific and statistical vestibular anatomy. *Frontiers in Neuroscience*, *11*(DEC), 713. https://doi.org/10.3389/fnins.2017.00713

Hayden, R., Sawyer, S., Frey, E., Mori, S., Migliaccio, A. A., & Della Santina, C. C. (2012). Virtual Labyrinth model of vestibular afferent excitation via implanted electrodes – Validation and application to design of a multichannel vestibular prosthesis. *Experimental Brain Research*, *210*(3–4), 623–640. https://doi.org/10.1007/s00221-011-2599-x.Virtual

Herencsar, N., Freeborn, T. J., Kartci, A., & Cicekoglu, O. (2020). A Comparative Study of Two Fractional-Order Equivalent Electrical Circuits for Modeling the Electrical Impedance of Dental Tissues. *Entropy*, *22*(10), 1–19. https://doi.org/10.3390/E22101117

Kingma, H., & van de Berg, R. (2016). Anatomy, physiology, and physics of the peripheral vestibular system. In J. M. Lempert & T. Furman (Eds.), *Handbook of Clinical Neurology* (Vol. 137, pp. 1–16). Elsevier B.V. https://doi.org/10.1016/B978-0-444-63437-5.00001-7

Lucieer, F., Vonk, P., Guinand, N., Stokroos, R., Kingma, H., & van de Berg, R. (2016). Bilateral vestibular hypofunction: Insights in etiologies, clinical subtypes, and diagnostics. *Frontiers in Neurology*, *7*(MAR), 26. https://doi.org/10.3389/fneur.2016.00026

Marianelli, P., Capogrosso, M., Luciani, L. B., Panarese, A., Bassi Luciani, L., Panarese, A., & Micera, S. (2015). A Computational Framework for Electrical Stimulation of Vestibular Nerve. *IEEE Transactions on Neural Systems and Rehabilitation Engineering*, *23*(5), 897–909. https://doi.org/10.1109/TNSRE.2015.2407861

Merrill, D. R., Bikson, M., & Jefferys, J. G. R. (2005). Electrical stimulation of excitable

tissue: Design of efficacious and safe protocols. *Journal of Neuroscience Methods*, *141*(2), 171–198. https://doi.org/10.1016/j.jneumeth.2004.10.020

Perez Fornos, A., Cavuscens, S., Ranieri, M., van de Berg, R., Stokroos, R., Kingma, H., Guyot, J.-P., & Guinand, N. (2017). The vestibular implant: A probe in orbit around the human balance system. *Journal of Vestibular Research*, *27*(1), 51–61. https://doi.org/10.3233/VES-170604

Randles, J. E. B. (1947). Kinetics of rapid electrode reactions. *Discussions of the Faraday Society*, *1*(11), 11–19. https://doi.org/10.1039/df9470100011

Rodgers, K., Chou, J. T., & Rodgers, B. K. (1966). CONCENTRATIONS OF INORGANIC IONS IN GUINEA-PIG INNER EAR FLUIDS. II. POST-MORTEM CHANGES IN THE IONIC COMPOSITION OF UTRICULAR ENDOLYMPH AND PERILYMPH. *The Journal of Laryngology and Otology*, *80*(9), 885–889. https://doi.org/10.1017/s0022215100066159

SCHWAN, H. P. (1957). Electrical properties of tissue and cell suspensions. In *Advances in biological and medical physics* (Vol. 5). ACADEMIC PRESS INC. https://doi.org/10.1016/b978-1-4832-3111-2.50008-0

Schwartz, J. L., & Mealing, G. A. R. (1985). Dielectric properties of frog tissues in vivo and in vitro. *Physics in Medicine and Biology*, *30*(2), 117–124. https://doi.org/10.1088/0031-9155/30/2/001

Seppen, B. F., van Hoof, M., Stultiens, J. J. A., van den Boogert, T., Guinand, N., Guyot, J. P., Kingma, H., Fornos, A. P., Handschuh, S., Glueckert, R., Jacobi, L., Schrott-Fischer, A., Johnson Chacko, L., & van de Berg, R. (2019). Drafting a Surgical Procedure Using a Computational Anatomy Driven Approach for Precise, Robust, and Safe Vestibular Neuroprosthesis Placement-When One Size Does Not Fit All. *Otology & Neurotology : Official Publication of the American Otological Society, American Neurotology Society [and] European Academy of Otology and Neurotology*, *40*(5S Suppl 1), S51–S58. https://doi.org/10.1097/MAO.0000000000002211

Sun, D. Q., Ward, B. K., Semenov, Y. R., Carey, J. P., & Della Santina, C. C. (2014). Bilateral Vestibular Deficiency: Quality of Life and Economic Implications. *JAMA Otolaryngology-- Head & Neck Surgery*, *140*(6), 527–534. https://doi.org/10.1001/jamaoto.2014.490

Taylor, S. R., & Gileadi, E. (1995). Physical interpretation of the Warburg impedance. *Corrosion*, *51*(9), 664–671. https://doi.org/10.5006/1.3293628

van de Berg, R., Guinand, N., Guyot, J.-P., Kingma, H., & Stokroos, R. J. (2012). The modified ampullar approach for vestibular implant surgery: feasibility and its first application in a human with a long-term vestibular loss. *Frontiers in Neurology*, *3*, 18. https://doi.org/10.3389/fneur.2012.00018

Chapter 8 How to optimize the electrical stimulation for VI: Modeling of electrical conductivity

INTRODUCTION

The vestibular system facilitates three main functions of the human body: spatial orientation, balance control and gaze stabilization (Kingma & van de Berg, 2016). Vestibular function loss due to a variety of reasons (Lucieer et al., 2016; Van De Berg et al., 2015) is very difficult to treat. The solution is the vestibular implant (VI) that is able to restore the lost vestibular function (Fornos et al., 2019; Guinand et al., 2011). At current, VIs incorporate 3 electrodes located inside of the semicircular canal (SCC) ampullae (van de Berg et al., 2012, 2017), that provide the electrical current stimulation of the nearby vestibular afferents replacing in such a way the damaged endorgan (van de Berg et al., 2015).

The process of the vestibular implant development and improvement naturally includes the modelling approach since *in silico* experiments are much simpler than *in vitro* and particularly *in vivo* experiments. The most advanced models present are the 3D finite element models (FEM) including such geometrical volume domains as the temporal bone, endo and perilymphatic spaces as a whole, and the vestibular nerve together with nerve excitation model (Handler et al., 2017; Hayden et al., 2011; Hedjoudje et al., 2019; Marianelli et al., 2015). Each of the abovementioned geometry domains has a pair of electrical properties: conductivity and permittivity, resulting in the resistance and capacitance respectively. Both conductivity and permittivity result in an electrical impedance that determines the current propagation through the medium under study. Understanding of the electrical properties of the simulated medium is crucial for obtaining the reliable results.

The goal of this study is to construct the 3D FEM model reflecting the measured electrical impedance in the guinea pig inner ear incorporating the electrical double layer and to investigate the significance of the surrounding temporal bone.

MATERIALS AND METHODS

Sample and impedance measurement

Electrical impedance measured in the 0.9% NaCl saline solution and in the guinea pig inner ear: all combinations between each pair of SCC ampullae and vestibular nerve. Here we give only a brief outline of experimental procedures, since they were described in detail in the chapter 7.

Constructing the 3D model: electrodes

Each electrode was presented as a sphere with radius $r_{electrode} = 0.25$ mm surrounded by a larger sphere with the radius $r_{EDL} = 0.251$ mm representing the EDL of 1 um thick (Figure 8.1). The spheres were considered to be half-insulated to match the experimental conditions where the metal electrode tip was only half-exposed.
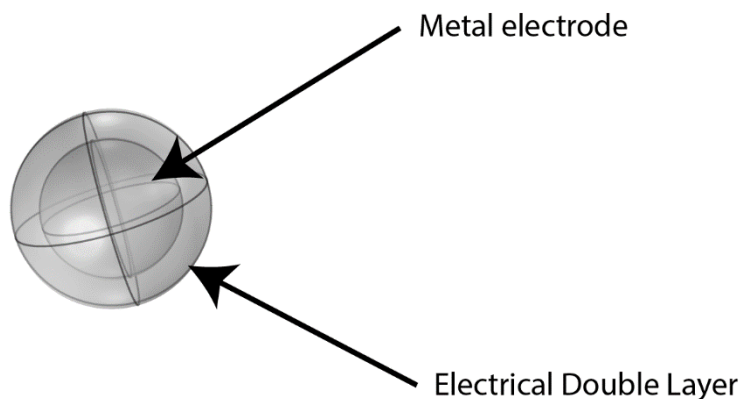
Figure 8.1 3D geometry of the platinum electrode with EDL.

Constructing the 3D model: saline solution

Figure 8.2 shows the 3D geometry of the experiment in the saline solution. A block with the dimensions 46.7 x 12.5 x 17.1 mm represented the cavity with the saline solution.
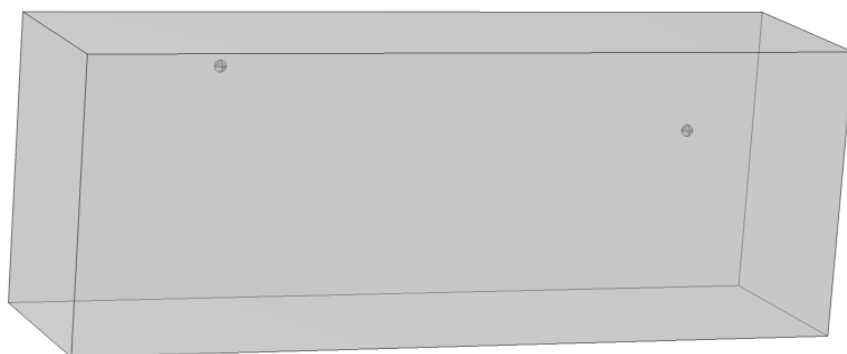
Figure 8.2 3D geometry of the saline solution container with two spherical electrodes immersed in it.

Constructing the 3D model: guinea pig

In this study, the periotic bone of a guinea pig weighing 947 grams were used. Before the study, the animal was kept in standard vivarium conditions with water and food *ad libitum*. All procedures were performed following the European Convention for the Protection of Vertebrate Animals. The animal was decapitated

under ether anesthesia. The bones of the tympanic cavity and the periotic capsule were removed with the preserved native structure of the vestibulocochlear nerve leaving this capsule through the internal auditory opening. The sample was not fixed.

The imaging was carried out on fresh tissue sample not later than an hour after decapitation. The micro-CT Skyscan1172 (Bruker Corporation, USA) was used to obtain images of the bone labyrinth. An average voltage of 80 kV and a current of 124 µA were used for scanning with an aluminum filter 0.5 mm thick. The pixel size before reconstruction was 4 µm, and the exposure time was set at 1.23 seconds. After reconstruction, the pixel size was 32 micrometers.

On the reconstructed sections, the bony labyrinth was clearly visible as a network of connected tunnels in the periotic bone. The recovered images were imported into 3D Slicer 4.8.1 for the bony labyrinth segmentation (Fedorov et al., 2012). The segmentation was carried out manually; the resulting segments were assembled into a 3D model. Processing of 3D models included anti-aliasing to eliminate small inaccuracies made as a result of manual segmentation. The obtained 3D model of the guinea pig bony labyrinth was then imported in Comsol software and was surrounded by a rectangular block of the size 9 x 10 x 7 mm (Figure 8.3).
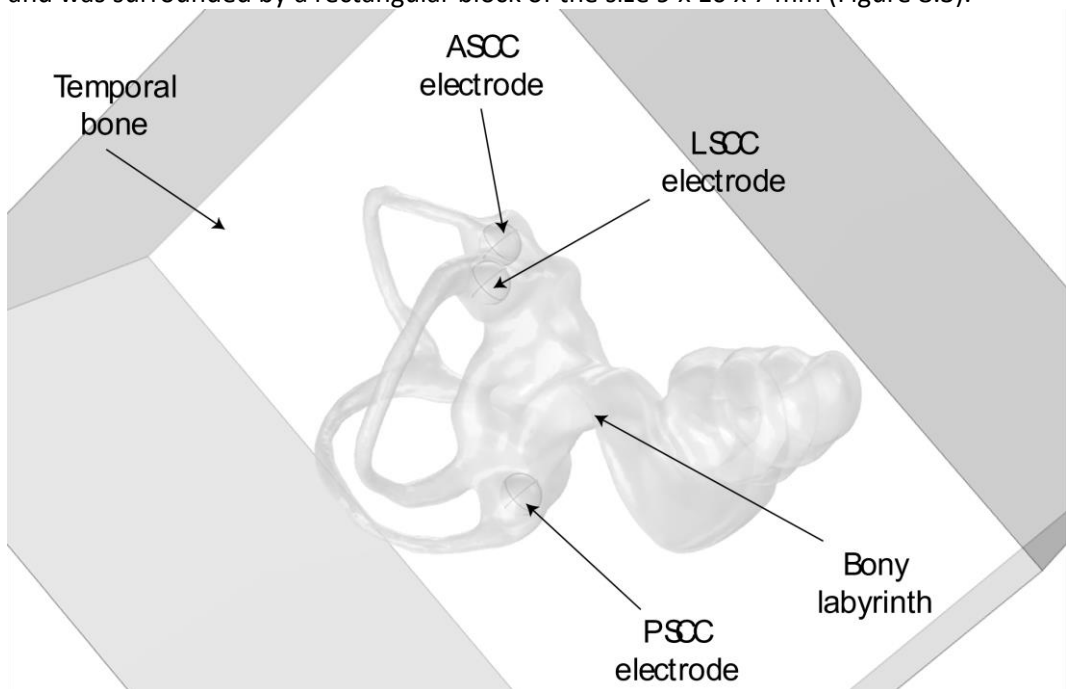
Figure 8.3 3D geometry of the guinea pig bony labyrinth with spherical electrodes located in each SCC ampullae surrounded by a temporal bone block.

Electroconductivity parameters

In the Electric Currents module, necessary parameters of the electrical conductivity such as dielectric permittivity (ε) and electrical conductivity (σ) were assigned to each volume domain of 3D model (Table 8.1).

Table 8.1 Values of electrical conductivity for endo- and perilymph domain, and for platinum electrodes used for simulation.

	$\sigma \left(\dfrac{S}{m}\right)$	ε
Bone	0.01	10000
Saline solution	2.216	81
Endo- and peri-lymph	1.5	81
Platinum	$8.9 * 10^6$	1

The dielectric permittivity of the electrolyte liquids (saline and endo- and perilymph) was considered to be the same as for the water $\varepsilon = 78$, corresponding to room temperature of 25 $°C$ (Malmberg & Maryott, 1956). Hence, dielectric permittivity does not make sense for a conductive medium and, therefore, its value should be equal to 1. Nevertheless, the simulations showed, that changing the value of ε for liquids present in the model in the range from 1 to 100 does not make any impact to the result. The conductivity of the endo and perilymphatic liquids and the bone is taken from the literature (Handler et al., 2017; Hayden et al., 2012; Kosterich et al., 1983; Marianelli et al., 2015). The calculation of the conductivity of saline solution is given in the Appendix 2.

Adding physics

The combination of "Electric currents" and "Electrical Circuit" modules in Comsol 5.6 software was used in this study.

Electrical Circuit module comprised the ground node connected in series with the load resistor R_{load} having the resistance of 100 Ω for saline solution and 960 Ω for guinea pig models. The electrical circuit was connected to the receiving electrode in the 3D model of Electric currents module.

The initial conditions applied in the whole 3D volume under study were set as 0V. Voltage source with an amplitude of 0.1 V was connected to one of the electrodes. The simulations were conducted in a frequency domain from 50 Hz to 50 kHz with a step of 50 Hz which corresponds to the frequencies of the VI (Appendix 3). Measured value – electrical current flowing through the load resistor R_{load}.

Identifying the distributed EDL parameters

The distributed electroconductivity parameters of EDL remain unknown, so the method of parameter estimation was applied. It is known that EDL is a small highly resistive dielectric layer, therefore it should probably have a relatively low

conductivity and relatively high dielectric permittivity to reveal the features of a capacitor. Thus, a grid search was performed for all combinations of parameters shown in Table 8.2, which means the potential distribution and the current flowing through the load resistor were calculated for each combination of signal frequency, EDL permittivity and EDL conductivity. Then the impedances were calculated again for each combination of permittivity and conductivity of EDL and compared with measured impedances.

Table 8.2 The range of the EDL parameters used for grid search.

	$\varepsilon\ EDL$	$\sigma\ EDL\ (\frac{S}{m})$
Lower bound	10^3	10^{-5}
Upper bound	10^7	1
Step	$1/5\ Log(10)$	$1/5\ Log(10)$

In the end, the root mean squared error normalized by the mean (NRMSE) was used to estimate the goodness of fit when compared the experimental and fitted electrical impedance in complex form. NRMSE values range from 0 to infinity, where 0 means a perfect match and infinity means a complete mismatch. It is difficult to treat the absolute value of NRMSE, but it can be used to compare fitted models between each other, where the closer to zero value means a better fit.

RESULTS

Saline solution impedance simulation

The magnitude of saline solution conductivity was decreased down to 1.8 S/m to make simulated impedance match the experimental results in the range of high frequencies over 10 kHz. The best estimated electroconductivity parameters of EDL after applying the grid search approach are shown in Table 8.3. The simulated impedance was compared with the measured one in the complex form and resulted in NRMSE=1.41.

Table 8.3 Best estimated parameters of the EDL in the saline solution

	$\sigma_{EDL}\ (\frac{S}{m})$	ε_{EDL}
EDL	$6 \cdot 10^{-4}$	$1.1 \cdot 10^5$
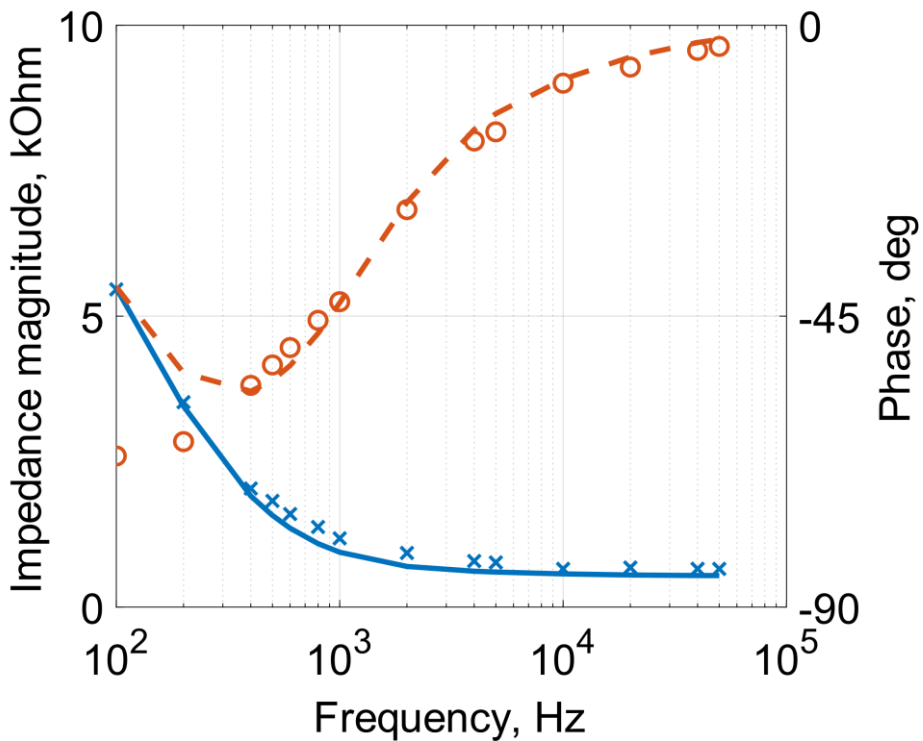
Figure 8.4 Measured and simulated electrical impedance in the saline solution. Measured impedance (blue crosses), fitted impedance (blue solid line), measured phase shift (red circles), and simulated phase shift (red dashed line). Comsol simulation with EDL parameters taken from Table 8.3.

Bone significance

The presence of the bone tissue around the vestibular system influences the magnitude and phase shift of the electrical impedance in the guinea pig model in the range of relatively low frequencies despite its low conductivity and high permittivity compared with endolymph/perilymph liquid (Figure 8.5).
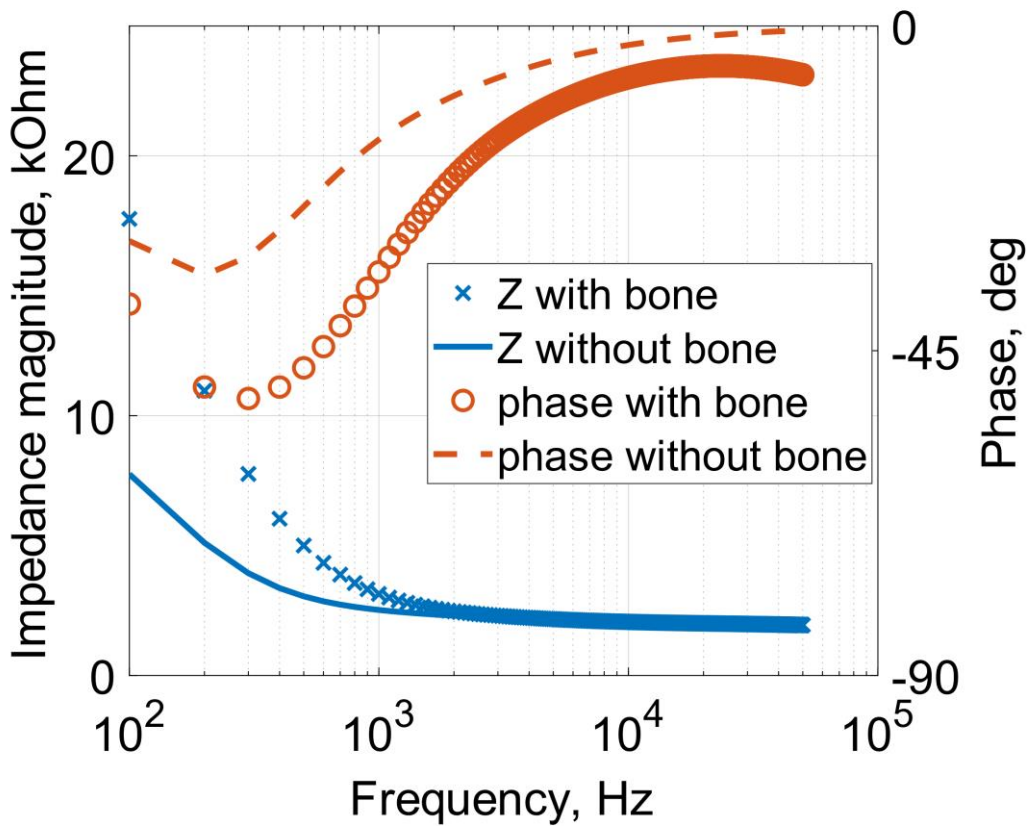
Figure 8.5 Simulated impedance and phase shift in the guinea pig inner ear between anterior and posterior ampullae: comparing models including and excluding the temporal bone.

Guinea pig impedance simulation
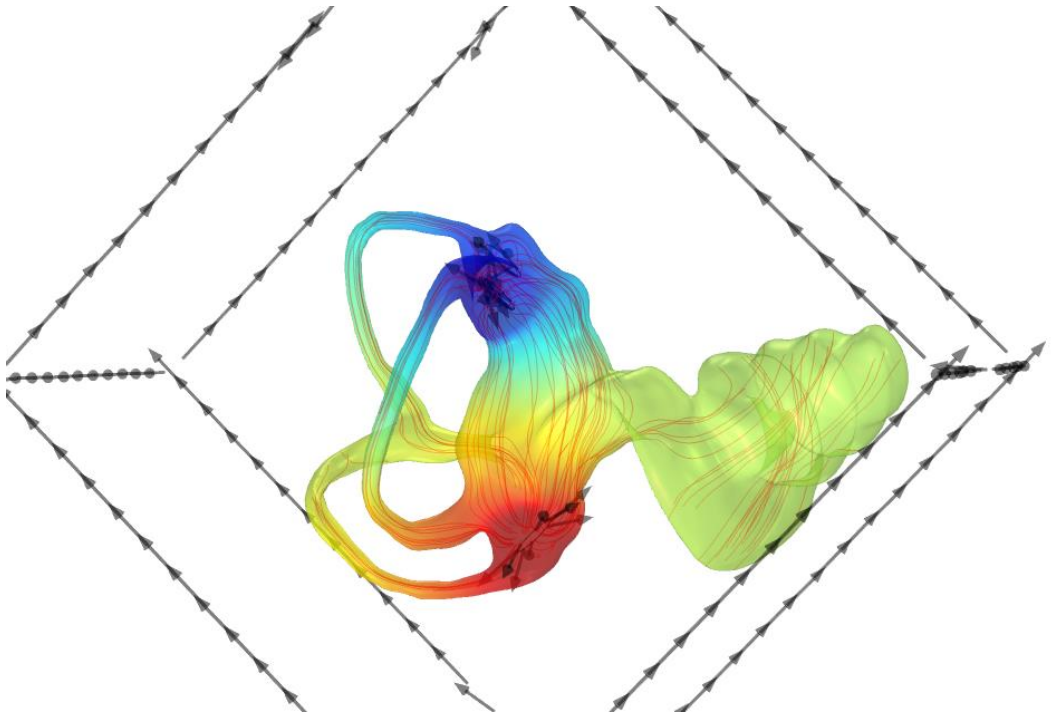
Figure 8.6 Electrical potential distribution (in color); and electrical current flow (black arrows and red lines) through the guinea pig inner ear.

The measured and simulated impedance of the guinea pig ampullae is shown on Figure 8.7. The magnitude of the simulated impedance matches the measurement quite well except the mid frequency range around 1 kHz, where the simulated impedance decreases steeper. In its way, the simulated phase shift indicates a non-monotonous behavior in a low frequency range below 500 Hz unlike the measured experimentally. Apparently, this can be related to a capacitive part of the impedance, viz with the dielectric properties of the interelectrode medium.
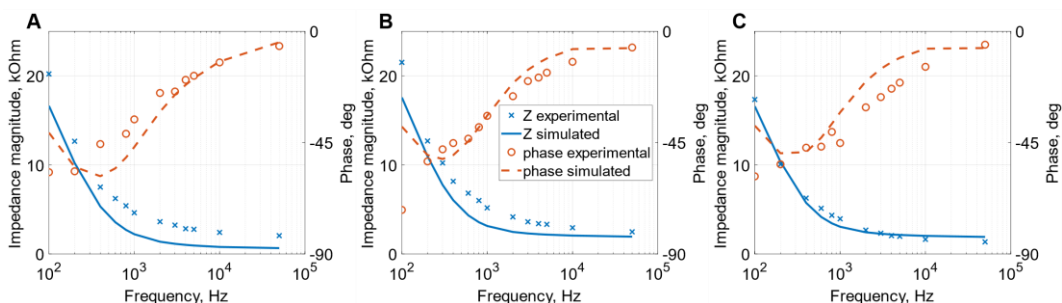
Figure 8.7 Measured (solid and dashed lines) and simulated (circles and crosses) impedance and phase shift in the guinea pig inner ear. A - between ASCC and LSCC, B – between ASCC and PSCC, C -between PSCC and LSCC.

The obtained values of NRMSE for the complex impedance are shown in Table 8.4. On average the obtained values of NRMSE for the guinea pig impedance are lower than for the saline solution, indicating a slightly better fit. Nevertheless, the NRMSE values obtained in Comsol simulation are an order of magnitude higher than equivalent circuit model which reveals the advantages of the optimization algorithm over grid search.

Table 8.4 NRMSE for electrical impedance measured between each pair of SCC ampullae in guinea pig.

Electrode location	NRMSE
ASCC-PSCC	1.39
ASCC-LSCC	1.16
PSCC-LSCC	1.27

Current propagation

Simulated propagation of the rectangular biphasic voltage pulse through the guinea pig inner ear tissues are shown in Figure 8.8 and Figure 8.9. The biphasic voltage pulse propagating through the inner ear tissues is distorted and transformed into a tri-phasic, where the first cathodic phase is lower than the positive phase resulting in less tissue stimulation.

Figure 8.8 Comsol simulation: square voltage pulse provided by a PSCC electrode and the voltage registered at the load resistor.

Figure 8.9 Comsol simulation: electrical current flowing through the resistor.

DISCUSSION

This study presents the development of the finite element model for the guinea pig inner ear incorporating the 1um electrical double layer surrounding electrodes. Such an approach allows to match the experimentally measured electrical impedance quite well. The val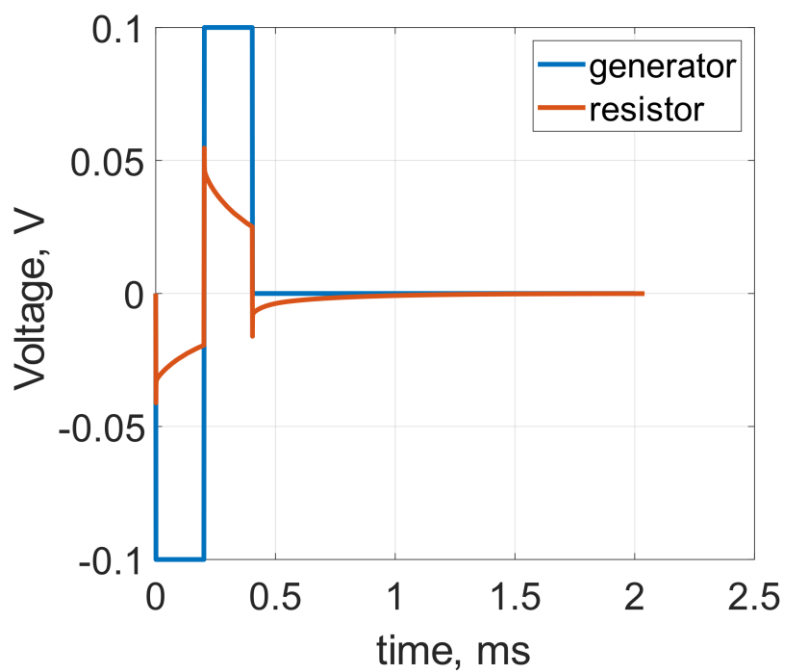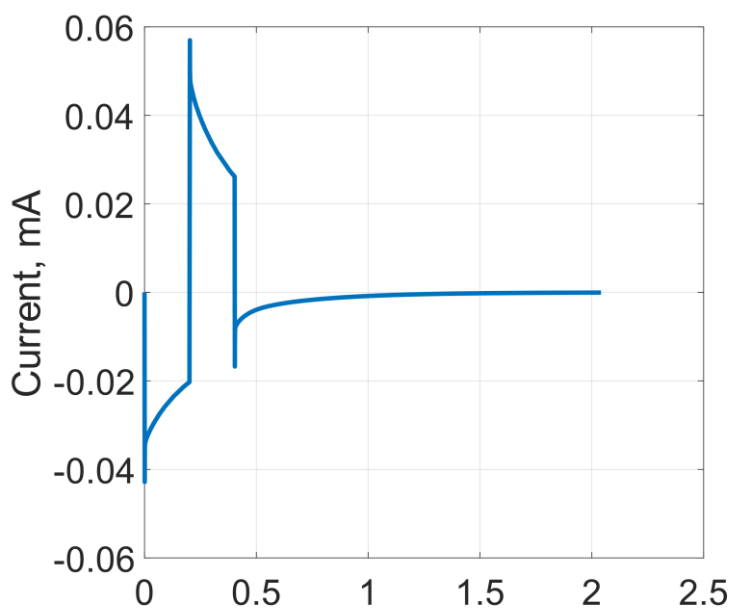ues of dielectric permittivity and conductivity of 1um thick EDL layer have been identified using the grid search approach, $\sigma_{EDL}\left(\frac{S}{m}\right) = 6 \cdot 10^{-4} \, S/m$ and $\varepsilon_{EDL} = 1.1 \cdot 10^5$. It should also be noted that the obtained values should be adjusted in the case of another EDL thickness, since they are size dependent.

The value of the medium conductivity influences the high frequency part of the impedance, i.e. saturation part: the higher is the medium conductivity the lower is the impedance. The value of EDL conductivity influences the low frequency part of the impedance. Finally, dielectric permittivity of EDL is responsible for the steepness of the impedance decay.

The obtained values of the EDL electroconductivity allow to calculate the lumped parameters and compare them with obtained ones in the previous chapter. The formation of EDL around the half-exposed spherical electrode can be presented as a spherical capacitor. The capacitance of a single electrode EDL is then can be found by the following expression:

$$C_{sph} = \varepsilon\varepsilon_0 S/d \qquad (1)$$

where $\varepsilon_0 = 8.85 * 10^{-12} \frac{F}{m}$ is vacuum permittivity, ε is the dielectric permittivity of the capacitor dielectric or EDL in our case (see Table 8.3), S is the sphere area, and d is the distance between capacitor plates or EDL thickness in our case. Substituting all numeric values in the equation we get $C_{EDL} = 38.22 \cdot 10^{-8} \, F$. The value is at least if the same order of magnitude as described in the literature for the metal electrode immersed in liquid (Merrill et al., 2005). Assuming the EDL capacitances to be connected in series, the obtained value should be halved resulting in a good match with the literature data.

Since EDL has a non-zero conductivity, it is possible to calculate the overall resistance of a single electrode EDL using the following expression for the cylindrical resistor:

$$R = \rho\frac{l}{S} = \frac{d}{\sigma \cdot S} \qquad (2)$$

where σ is the electroconductivity, the rest parameters are as before. Substituting the numerical values, we get $R_{EDL} = 4.244 \, kOhm$. The obtained lumped parameters are of the same magnitude as in the chapter 2, nevertheless the direct comparison cannot be established since in the equivalent circuit the parameters were defined for two electrodes at the same time.

Bone presence influences the result significantly despite the bone material is less conductive, has high permittivity, and only surrounds the electrolytic space in the inner ear. It therefore can be hypothesized that the structures that are present

inside of the inner are like cupula and membraneous labyrinth may affect the current propagation even stronger. Unfortunately, there is no information in the literature about the dielectric properties of these structures.

Better accuracy in terms of matching the measured electrical impedance can be reached by increasing the amount of steps in the grid search algorithm or by developing the parameter optimization algorithms.

There are different ways to implement EDL in FEM, in particular in Comsol: contact impedance, electrochemistry, or by connecting an equivalent circuit of EDL to one of the electrodes (Cantrell et al., 2008).

Each tissue should be measured separately in order to identify the conductivity and permittivity.

Study limitations

The precise electrode locations remain hypothesized. Nevertheless, a slight change in the electrode position should not change the simulation drastically as soon as the electrode tip is still immersed in the liquid which is justified in this study. The situation can be more complicated when the electrode tip is surrounded not only by liquid but also by air due to the canal fenestration or when the electrode tip is touching the bone. These particular cases should be studied separately.

The model does not include the geometry of the vestibular nerve because it was not visible of the CT image, therefore it is not possible to calculate the potential distribution in the nerve. On top of that, no fine structures of the labyrinth such as cupula and membranous labyrinth are not visible as well, which still can play a significant role in the electric current propagation creating the alpha polarization on the tissue borders.

Therefore, the model can be extended by performing the micro-CT imaging with a high spatial resolution down to 1 um, high intensity resolution of 16 bit and staining techniques using such substances as OsO4 or PTA (Ertl & Boegle, 2019; Glueckert et al., 2018; Schulz-Mirbach et al., 2013; van den Boogert et al., 2018) to other visualize structures of the inner ear. For example, staining allows to see neural fibers which normally are not visible in a CT. Both high spatial and intensity resolution will potentially allow to visualize membraneous labyrinth and otolith organs.

CONCLUSION

The electrical impedance measured in saline solution and between each pair of ampullae of the guinea pig inner ear was simulated using 3D FEM modelling in Comsol Multiphysics. The conductivity and permittivity of EDL have been identified from saline solution measurements using 1um thick EDL approximation. It was shown that the bone affects the propagation of the electrical currents significantly which implies that the absence of the fine structures inside of the inner ear like cupula and membraneous labyrinth may also distort the simulated electrical impedance. Therefore, more detailed images of the inner ear should be used for construction of more precise electrocounductivity models. On top of that, the study

on the electroconductivity parameters of the tissues involved in necessary in the future.

REFERENCES

Cantrell, D. R., Inayat, S., Taflove, A., Ruoff, R. S., & Troy, J. B. (2008). Incorporation of the electrode-electrolyte interface into finite-element models of metal microelectrodes. *Journal of Neural Engineering*, *5*(1), 54–67. https://doi.org/10.1088/1741-2560/5/1/006

Ertl, M., & Boegle, R. (2019). Investigating the vestibular system using modern imaging techniques-A review on the available stimulation and imaging methods. *Journal of Neuroscience Methods*, *326*, 108363. https://doi.org/10.1016/j.jneumeth.2019.108363

Fedorov, A., Beichel, R., Kalpathy-Cramer, J., Finet, J., Fillion-Robin, J. C., Pujol, S., Bauer, C., Jennings, D., Fennessy, F., Sonka, M., Buatti, J., Aylward, S., Miller, J. V, Pieper, S., & Kikinis, R. (2012). 3D Slicer as an image computing platform for the Quantitative Imaging Network. *Magnetic Resonance Imaging*, *30*(9), 1323–1341. https://doi.org/10.1016/j.mri.2012.05.001

Fornos, A. P., Van De Berg, R., Sommerhalder, J., & Guinand, N. (2019). Designing artificial senses: Steps from physiology to clinical implementation. *Swiss Medical Weekly*, *149*(21–22). https://doi.org/10.4414/smw.2019.20061

Glueckert, R., Johnson Chacko, L., Schmidbauer, D., Potrusil, T., Pechriggl, E. J., Hoermann, R., Brenner, E., Reka, A., Schrott-Fischer, A., & Handschuh, S. (2018). Visualization of the Membranous Labyrinth and Nerve Fiber Pathways in Human and Animal Inner Ears Using MicroCT Imaging. *Frontiers in Neuroscience*, *12*, 501. https://doi.org/10.3389/fnins.2018.00501

Guinand, N., Guyot, J. P., Kingma, H., Kos, I., & Pelizzone, M. (2011). Vestibular implants: The first steps in humans. *2011 Annual International Conference of the IEEE Engineering in Medicine and Biology Society*, *2011*, 2262–2264. https://doi.org/10.1109/IEMBS.2011.6090569

Handler, M., Schier, P. P., Fritscher, K. D., Raudaschl, P., Chacko, L. J., Glueckert, R., Saba, R., Schubert, R., Baumgarten, D., & Baumgartner, C. (2017). Model-based vestibular afferent stimulation: Modular workflow for analyzing stimulation scenarios in patient specific and statistical vestibular anatomy. *Frontiers in Neuroscience*, *11*(DEC), 713. https://doi.org/10.3389/fnins.2017.00713

Hayden, R., Sawyer, S., Frey, E., Mori, S., Migliaccio, A. A., & Della Santina, C. C. (2011). Virtual labyrinth model of vestibular afferent excitation via implanted electrodes: Validation and application to design of a multichannel vestibular prosthesis. *Experimental Brain Research*, *210*(3–4), 623–640. https://doi.org/10.1007/s00221-011-2599-x

Hayden, R., Sawyer, S., Frey, E., Mori, S., Migliaccio, A. A., & Della Santina, C. C. (2012). Virtual Labyrinth model of vestibular afferent excitation via implanted electrodes – Validation and application to design of a multichannel vestibular prosthesis. *Experimental Brain Research*, *210*(3–4), 623–640.

https://doi.org/10.1007/s00221-011-2599-x.Virtual

Hedjoudje, A., Hayden, R., Dai, C., Ahn, J. H., Rahman, M., Risi, F., Zhang, J., Mori, S., & Della Santina, C. C. (2019). Virtual Rhesus Labyrinth Model Predicts Responses to Electrical Stimulation Delivered by a Vestibular Prosthesis. *JARO - Journal of the Association for Research in Otolaryngology*, *20*(4), 313–339. https://doi.org/10.1007/s10162-019-00725-3

Kingma, H., & van de Berg, R. (2016). Anatomy, physiology, and physics of the peripheral vestibular system. In J. M. Lempert & T. Furman (Eds.), *Handbook of Clinical Neurology* (Vol. 137, pp. 1–16). Elsevier B.V. https://doi.org/10.1016/B978-0-444-63437-5.00001-7

Kosterich, J. D., Foster, K. R., & Pollack, S. R. (1983). Dielectric permittivity and electrical conductivity of fluid saturated bone. *IEEE Transactions on Bio-Medical Engineering*, *30*(2), 81–86. http://www.ncbi.nlm.nih.gov/pubmed/6832795

Lucieer, F., Vonk, P., Guinand, N., Stokroos, R., Kingma, H., & van de Berg, R. (2016). Bilateral vestibular hypofunction: Insights in etiologies, clinical subtypes, and diagnostics. *Frontiers in Neurology*, *7*(MAR), 26. https://doi.org/10.3389/fneur.2016.00026

Malmberg, C. G., & Maryott, A. A. (1956). Dielectric constant of water from 0 to 100 C. *Journal of Research of the National Bureau of Standards*, *56*(1), 1. https://doi.org/10.6028/jres.056.001

Marianelli, P., Capogrosso, M., Luciani, L. B., Panarese, A., Bassi Luciani, L., Panarese, A., & Micera, S. (2015). A Computational Framework for Electrical Stimulation of Vestibular Nerve. *IEEE Transactions on Neural Systems and Rehabilitation Engineering*, *23*(5), 897–909. https://doi.org/10.1109/TNSRE.2015.2407861

Merrill, D. R., Bikson, M., & Jefferys, J. G. R. (2005). Electrical stimulation of excitable tissue: Design of efficacious and safe protocols. *Journal of Neuroscience Methods*, *141*(2), 171–198. https://doi.org/10.1016/j.jneumeth.2004.10.020

Schulz-Mirbach, T., Heß, M., & Metscher, B. D. (2013). Sensory epithelia of the fish inner ear in 3D: studied with high-resolution contrast enhanced microCT. *Frontiers in Zoology*, *10*(1), 63. https://doi.org/10.1186/1742-9994-10-63

van de Berg, R., Guinand, N., Guyot, J.-P., Kingma, H., & Stokroos, R. J. (2012). The modified ampullar approach for vestibular implant surgery: feasibility and its first application in a human with a long-term vestibular loss. *Frontiers in Neurology*, *3*, 18. https://doi.org/10.3389/fneur.2012.00018

van de Berg, R., Guinand, N., Khoa Nguyen, T. A., Ranieri, M., Cavuscens, S., Guyot, J. P., Stokroos, R., Kingma, H., & Perez-Fornos, A. (2015). The vestibular implant: Frequency-dependency of the electrically evoked vestibulo-ocular reflex in humans. *Frontiers in Systems Neuroscience*, *8*(JAN), 255. https://doi.org/10.3389/fnsys.2014.00255

van de Berg, R., Lucieer, F., Guinand, N., van Tongeren, J., George, E., Guyot, J.-P., Kingma, H., van Hoof, M., Temel, Y., van Overbeeke, J., Perez-Fornos, A., & Stokroos, R. (2017). The Vestibular Implant: Hearing Preservation during Intralabyrinthine Electrode Insertion-A Case Report. *Frontiers in Neurology*, *8*,

137. https://doi.org/10.3389/fneur.2017.00137

Van De Berg, R., Van Tilburg, M., & Kingma, H. (2015). Bilateral Vestibular Hypofunction: Challenges in Establishing the Diagnosis in Adults. In *ORL* (Vol. 77, Issue 4, pp. 197–218). ORL J Otorhinolaryngol Relat Spec. https://doi.org/10.1159/000433549

van den Boogert, T., van Hoof, M., Handschuh, S., Glueckert, R., Guinand, N., Guyot, J. P., Kingma, H., Perez-Fornos, A., Seppen, B., Chacko, L. J., Schrott-Fischer, A., & van de Berg, R. (2018). Optimization of 3D-visualization of micro-anatomical structures of the human inner ear in osmium tetroxide contrast enhanced micro-CT scans. *Frontiers in Neuroanatomy*, *12*(May), 1–11. https://doi.org/10.3389/fnana.2018.00041

Chapter 9 Final discussion and valorization

THE AIM AND FINDINGS OF THIS THESIS

Many people worldwide suffer from bilateral vestibulopathy (BVP) which prevalence is estimated at 0.03% in the whole population (Ward et al., 2013) (Agrawal et al., 2009). Patients with BVP usually report lower health-related quality of life (HRQoL) (Guinand et al., 2012; Sun et al., 2014). Unfortunately, BVP is still often misdiagnosed due to diagnostic challenges like the lack of standardization in vestibular testing (Van De Berg et al., 2015). Furthermore, treatment options are currently limited and with low yield (Van de Berg et al., 2011). Therefore, this thesis aimed to improve the diagnostics and optimize treatment of BVP by electrical stimulation based on investigation of underlying physical principles. Topics considered in this thesis included the following: patterns of the vestibular dysfunction in BVP patients, video head impulse testing using electro-oculography, assessment of self-motion perception, and electrical properties of the inner ear that are used in electrophysiological models for optimizing electrical stimulation by a vestibular implant (VI).

In this thesis, it was demonstrated that:

- Only three quarters of patients diagnosed with bilateral vestibulopathy are eligible for vestibular implantation because it requires a careful examination of all five vestibular end organs to ensure safe implantation of the vestibular implant.
- Electro-oculography detecting the electrical potential of an eye is an accurate alternative to video-oculography in head impulse testing.
- Thresholds of self-motion perception can quickly be determined in a clinical setting using a six degrees of freedom motion platform, but different testing paradigms need different normative values.
- The electrical double layer of inner ear tissues, together with medium polarization, plays a significant role in the electrical impedances, and should be considered in electrical conductivity models to optimize vestibular implant stimulation.

FINAL DISCUSSION AND VALORIZATION

Bilateral vestibulopathy (BVP) is a chronic disease characterized by a bilaterally reduced or absent vestibular function (Hain et al., 2013; Lucieer et al., 2016; Strupp et al., 2017). According to Barany Society criteria, BVP is diagnosed based on symptoms (e.g. unsteadiness and oscillopsia) combined with a bilaterally reduced vestibular function as measured by at least one of the following tests: caloric test, torsion swing test, and head impulse test (HIT) (Strupp et al., 2017). However, these tests only measure the vestibulo-ocular reflex of the horizontal semicircular canals, while BVP is not a homogeneous disorder: abnormalities can also be found in the vertical semicircular canals and otolith organs. Therefore, to better understand BVP, it is recommended to evaluate the function of all five end organs. This will also facilitate decision making regarding vestibular implantation. After all, since surgically

implanting the vestibular system can cause significant damage to the vestibular system, other sensors than the horizontal semicircular canals also need to show deficits. By this, the vestibular system is not additionally damaged by vestibular implantation (van de Berg et al., 2020). Moreover, regarding diagnosis of BVP, the caloric test and video head impulse test seem to have a higher sensitivity for detecting vestibular hypofunction: 80% of BVP patients were diagnosed based on only the caloric test, only video head impulse testing, or both tests (Chapter 2).

Vestibular test procedures based on the vestibulo-ocular reflex, mainly use recording of eye movements (oculography) (Blakley & Chan, 2015; Eggert, 2007; Siddiqui & Shaikh, 2013). The gold standard of eye movement recording, the scleral coil technique, is almost never used in clinic due to its inconvenience for the patient. Video-oculography is most widely used, but it has drawbacks related to pupil detection, calibration, goggle slippage, and fitting the predefined geometry of the goggles to a patient's face (Heuberger et al., 2018; MacDougall et al., 2009; Suh et al., 2017; Weber et al., 2009). Electro-oculography is nowadays less commonly used in clinic, but it is still a complementary technique which can reliably be used for eye movement recordings during the caloric test and during rotatory chair testing (Gananca et al., 2010; López et al., 2016; Merino et al., 2010; Pietkiewicz et al., 2012). The feasibility of using electro-oculography for video head impulse testing, was not yet investigated. This thesis demonstrated that electro-oculography is an accurate technique to record eye movements during horizontal video head impulse testing: results are not significantly different from video-oculography (Chapter 3).

Many vestibular testing procedures rely on vestibular reflexes (Lang & McConn Walsh, 2010; van de Berg et al., 2018), while the function of the vestibular system goes beyond facilitating reflexes. Testing reflexes only, implies that the vestibular system is not fully tested by current clinical tests (Merfeld et al., 2014). Therefore, an additional vestibular test was proposed: testing of self-motion perception thresholds (Dupuits et al., 2019). Self-motion perception is a much more complicated mechanism than vestibular reflexes, since it the end-result of a multisensory integration of signals, including input from the audiovestibular, visual and somatosensory systems, which are modulated by cognition (Merfeld et al., 2005; Nouri & Karmali, 2018). In addition, the surrounding three-dimensional space allows 12 different motion types and directions: six translations along three orthogonal axes and six rotations around the same orthogonal axes. Each of these directions is sensed by different vestibular end organs, and, therefore, motion sensitivity will be different for each type of motion. In research setting, test duration is one of the most fundamental problems when measuring the 'true' self-motion perception thresholds. After all, a long test procedure leads to decreased attention, compromising test results. In this thesis, a relatively fast (<1 hour) procedure was described to determine self-motion perceptual thresholds in clinic. It was demonstrated that self-motion perceptual thresholds could reliably be obtained and that thresholds increase with age, probably indicating the decay in the vestibular function. Another study recently found that BVP patients demonstrate significantly

higher self-motion perceptual thresholds for certain movement types and directions (van Stiphout et al., 2021). This might imply that self-motion perceptual thresholds can become another functional outcome (in line with DVA (Starkov, Snelders, et al., 2020) and fHIT (Starkov, Guinand, et al., 2020; van Dooren et al., 2019)) related to vestibulopathy, complementing the vestibular test battery. (Chapter 4).

It should be noted that for self-motion perceptual thresholds, the chosen testing paradigm influences the thresholds. It was shown that reducing the number of choices leads to a decrease of the self-motion perceptual thresholds (Grabherr et al., 2008; Priesol et al., 2014). Most likely, this is mainly the result of a higher chance to guess the correct type and direction of movement. This means that if 12 possible options are presented, an 8% chance to guess the right threshold is present, and with only two options, this chance increases up to 50%. However, an additional psychometric influence cannot be ruled out. This latter was not investigated, since the subject of the study in this thesis was related to clinical outcomes (yes or no a decrease of thresholds), not to the full underlying mechanism of the change in threshold between two testing paradigms (12 options versus 2 options). The findings of this thesis imply that normative data should be collected for each testing paradigm. Therefore, when using self-motion perceptual thresholds in future diagnostic procedures and studies, findings should be related to the testing paradigm specific normative values (Chapter 5).

Since the vestibular implant (partially) restores vestibular function by electrically stimulating the vestibular system, it seems necessary to gain more insights in how the electrical current flows through the vestibular system. After all, having a deeper understanding of this current flow, might allow more safe and effective stimulation of the vestibular system. For this purpose, electrophysiological modelling of the inner ear is imperative (Handler et al., 2017; Hayden et al., 2012; Marianelli et al., 2015). Several factors are involved in optimizing the accuracy of such a model. First, the geometry, structure and size of the inner ear need to be determined with high resolution (micro)CT scanning techniques (Ertl & Boegle, 2019; Glueckert et al., 2018; van den Boogert et al., 2018) (Chapter 6). In case of creating a personalized model for already implanted patients, electrode position can be checked postoperatively, using e.g. three-dimensional X-ray tomography. Other factors that influence the current flow are the electrical properties of the inner ear that can be described in terms of the electrical impedance (Chapter 7). Although research in animals might not fully represent the human situation, it can still provide essential insights about current flow to validate existing models. In this thesis, the guinea pig inner ear's measured impedances identified the key physical phenomena that influence the current flow: electrode and medium polarization. Eventually, the impedance will determine whether stimulation is possible or not: a high impedance most probably indicates a suboptimal contact between one of the stimulating electrodes and the tissue it aims to stimulate, compromising effective electrical stimulation.

Finally, the precise pathway of current flow in the inner ear, and the amount of current delivered to the target nerve, can be obtained from these three-dimensional electrophysiological models. The existing models described in literature have different complexity, incorporating more or fewer tissues. These models strongly rely on the electroconductive parameters of every tissue, while it is known that these parameters are not precise. Combining the 3D geometric model of the inner ear and the experimental measurements described in Chapter 7, allows more precise estimates of the required parameters (electroconductivity and permittivity of the double layer, endo- and perilymph, and temporal bone) and evaluates the significance of the presence or absence of every tissue in the model: the presence of the temporal bone around the inner ear significantly changes the electrical impedance measured inside of the inner ear. The resulting experimentally validated electrophysiological models might aid in determining the best electrode position and stimulation paradigm, in order to improve safe and effective stimulation of the vestibular system using a vestibular implant (Chapter 8).

FUTURE RESEARCH

Bilateral vestibulopathy and its relation to underlying etiologies

Despite existing diagnostic criteria for diagnosing bilateral vestibulopathy, the use of different equipment and data processing algorithms might result in different outcomes and diagnoses (e.g., a patient might not be classified as BVP even though the disease is present). Therefore, vestibular testing should also include normative data related to the system used and standards regarding vestibular test procedures should be formulated world-wide. Collecting a more extensive and complete database of BVP patients, including the function of all five end organs, might improve understanding of BVP in general and in particular the idiopathic etiology.

Reliability of the electro-oculography method in head impulse testing

Development of a light-weight electro-oculography based device that includes gyroscopes, a multichannel amplifier and signal processing and analysis software, could result in a new type of head impulse testing device, complementary to the video-oculography devices. For that purpose, the following is required: 1) testing the applicability of electro-oculography in vertical head impulse testing; 2) testing the applicability of electro-oculography in patients with vestibular hypofunction. If successful, electro-oculography might especially be a useful alternative for patients in which video-oculography is challenging (e.g. difficulties with pupil detection). Furthermore, costs might not be as high as for the video-oculography devices, although that should still be determined.

Self-motion perception testing and the vestibular implant

At current, it was demonstrated that the vestibular implant is able to restore the vestibulo-ocular reflex, dynamic visual acuity, and spatial orientation.

Nevertheless, how much the vestibular implant contributes to motion perception, remains unknown. Testing of self-motion perceptual thresholds in bilateral vestibulopathy patients fitted with a vestibular implant, might therefore indicate whether the vestibular implant is also able to improve self-motion perception. In addition to this, testing self-motion perception during electrical vestibular stimulation might also bring new insights into the interaction between the peripheral vestibular end organs and the brain. After all, the advantage of the vestibular implant is the fact that it can (relatively) selectively stimulate different parts of the vestibular organ. Whether this eventually results in specific improvements of self-motion perception, still needs to be determined.

Optimization of electrical stimulation of the vestibular afferents

Investigating in vivo the electrical impedances in bilateral vestibulopathy patients fitted with a vestibular implant, can give additional insights in the tissue properties and how to improve the electrophysiological models' accuracy. By developing more precise models of the inner ear's electroconductivity (in terms of substructures and their electrical properties) could eventually lead to a more personalized and effective stimulation paradigm in vestibular implant patients. Furthermore, otolith structures should be included in the electrophysiological human models, to facilitate the electrode design, surgical approach and stimulation paradigm which are necessary for electrical stimulation of the otolith organs.

This thesis demonstrates the importance of developing and implementing new diagnostic tools and treatment options in routine clinical practice. Moreover, an efficient and cost-effective approach to restore vestibular function using a vestibular implant will reduce patients' suffering and socio-economic burdens on societies. This thesis and future projects will aim at developing, identifying, improving, and implementing efficient diagnostic tools and treatment options in practice, to improve quality of life in patients with vestibular hypofunction.

REFERENCES

Agrawal, Y., Carey, J. P., Della Santina, C. C., Schubert, M. C., & Minor, L. B. (2009). Disorders of balance and vestibular function in US adults: data from the National Health and Nutrition Examination Survey, 2001-2004. *Archives of Internal Medicine*, *169*(10), 938–944. https://doi.org/10.1001/archinternmed.2009.66

Blakley, B. W., & Chan, L. (2015). Methods considerations for nystagmography. *Journal of Otolaryngology - Head & Neck Surgery 2015 44:1*, *44*(1), 1–5. https://doi.org/10.1186/S40463-015-0078-2

Dupuits, B., Pleshkov, M., Lucieer, F., Guinand, N., Fornos, A. P., Guyot, J. P., Kingma, H., & Van De Berg, R. (2019). A new and faster test to assess vestibular perception. *Frontiers in Neurology*, *10*(JUL), 707. https://doi.org/10.3389/fneur.2019.00707

Eggert, T. (2007). Eye movement recordings: Methods. In *Developments in*

Ophthalmology (Vol. 40, pp. 15–34). Dev Ophthalmol. https://doi.org/10.1159/000100347

Ertl, M., & Boegle, R. (2019). Investigating the vestibular system using modern imaging techniques-A review on the available stimulation and imaging methods. *Journal of Neuroscience Methods*, *326*, 108363. https://doi.org/10.1016/j.jneumeth.2019.108363

Gança, M. M., Caovilla, H. H., & Gança, F. F. (2010). Electronystagmography versus videonystagmography. *Brazilian Journal of Otorhinolaryngology*, *76*(3), 399–403. http://www.ncbi.nlm.nih.gov/pubmed/20658023

Glueckert, R., Johnson Chacko, L., Schmidbauer, D., Potrusil, T., Pechriggl, E. J., Hoermann, R., Brenner, E., Reka, A., Schrott-Fischer, A., & Handschuh, S. (2018). Visualization of the Membranous Labyrinth and Nerve Fiber Pathways in Human and Animal Inner Ears Using MicroCT Imaging. *Frontiers in Neuroscience*, *12*. https://doi.org/10.3389/fnins.2018.00501

Grabherr, L., Nicoucar, K., Mast, F. W., & Merfeld, D. M. (2008). Vestibular thresholds for yaw rotation about an earth-vertical axis as a function of frequency. *Experimental Brain Research*, *186*(4), 677–681. https://doi.org/10.1007/s00221-008-1350-8

Guinand, N., Boselie, F., Guyot, J.-P. P., & Kingma, H. (2012). Quality of life of patients with bilateral vestibulopathy. *Annals of Otology, Rhinology and Laryngology*, *121*(7), 471–477. https://doi.org/10.1177/000348941212100708

Hain, T. C., Cherchi, M., & Yacovino, D. A. (2013). Bilateral vestibular loss. *Seminars in Neurology*, *33*(3), 195–203. https://doi.org/10.1055/s-0033-1354597

Handler, M., Schier, P. P., Fritscher, K. D., Raudaschl, P., Chacko, L. J., Glueckert, R., Saba, R., Schubert, R., Baumgarten, D., & Baumgartner, C. (2017). Model-based vestibular afferent stimulation: Modular workflow for analyzing stimulation scenarios in patient specific and statistical vestibular anatomy. *Frontiers in Neuroscience*, *11*(DEC), 713. https://doi.org/10.3389/fnins.2017.00713

Hayden, R., Sawyer, S., Frey, E., Mori, S., Migliaccio, A. A., & Della Santina, C. C. (2012). Virtual Labyrinth model of vestibular afferent excitation via implanted electrodes – Validation and application to design of a multichannel vestibular prosthesis. *Experimental Brain Research*, *210*(3–4), 623–640. https://doi.org/10.1007/s00221-011-2599-x.Virtual

Heuberger, M., Grill, E., Saglam, M., Ramaioli, C., Müller, M., Strobl, R., Holle, R., Peters, A., Schneider, E., & Lehnen, N. (2018). Usability of the video head impulse test: Lessons from the population-based prospective KORA study. *Frontiers in Neurology*, *9*(AUG), 659. https://doi.org/10.3389/FNEUR.2018.00659/BIBTEX

Lang, E. E., & McConn Walsh, R. (2010). Vestibular function testing. *Irish Journal of Medical Science*, *179*(2), 173–178. https://doi.org/10.1007/S11845-010-0465-7

López, A., Ferrero, F. J., Valledor, M., Campo, J. C., & Postolache, O. (2016). A study on electrode placement in EOG systems for medical applications. *2016 IEEE*

International Symposium on Medical Measurements and Applications, MeMeA 2016 - Proceedings, 6–10. https://doi.org/10.1109/MeMeA.2016.7533703

Lucieer, F., Vonk, P., Guinand, N., Stokroos, R., Kingma, H., & van de Berg, R. (2016). Bilateral vestibular hypofunction: Insights in etiologies, clinical subtypes, and diagnostics. *Frontiers in Neurology*, *7*(MAR), 26. https://doi.org/10.3389/fneur.2016.00026

MacDougall, H. G., Weber, K. P., McGarvie, L. A., Halmagyi, G. M., & Curthoys, I. S. (2009). The video head impulse test: Diagnostic accuracy in peripheral vestibulopathy. *Neurology*, *73*(14), 1134–1141. https://doi.org/10.1212/WNL.0b013e3181bacf85

Marianelli, P., Capogrosso, M., Luciani, L. B., Panarese, A., Bassi Luciani, L., Panarese, A., & Micera, S. (2015). A Computational Framework for Electrical Stimulation of Vestibular Nerve. *IEEE Transactions on Neural Systems and Rehabilitation Engineering*, *23*(5), 897–909. https://doi.org/10.1109/TNSRE.2015.2407861

Merfeld, D. M., Park, S., Gianna-Poulin, C., Black, F. O., & Wood, S. (2005). Vestibular Perception and Action Employ Qualitatively Different Mechanisms. I. Frequency Response of VOR and Perceptual Responses During *Translation* and *Tilt*. *Journal of Neurophysiology*, *94*(1), 186–198. https://doi.org/10.1152/jn.00904.2004

Merfeld, D. M., Priesol, A., Lee, D., Lewis, R. F., & Daniel M. Merfelda,, Adrian Priesola, Daniel Leea, and R. F. L. (2014). Potential solutions to several vestibular challenges facing clinicians. *Journal of Vestibular Research: Equilibrium and Orientation*, *154*(11), 2262–2265. https://doi.org/10.1016/j.pain.2013.06.005.Re-Thinking

Merino, M., Rivera, O., Gómez, I., Molina, A., & Dorronzoro, E. (2010). A method of EOG signal processing to detect the direction of eye movements. *Proceedings - 1st International Conference on Sensor Device Technologies and Applications, SENSORDEVICES 2010*, 100–105. https://doi.org/10.1109/SENSORDEVICES.2010.25

Nouri, S., & Karmali, F. (2018). Variability in the Vestibulo-Ocular Reflex and Vestibular Perception. *Neuroscience*, *393*, 350–365. https://doi.org/10.1016/j.neuroscience.2018.08.025

Pietkiewicz, P., Pepaś, R., Sułkowski, W., Zielińska-Bliźniewska, H., Olszewski, J., P, P., R, P., WJ, S., H, Z.-B., & J, O. (2012). Electronystagmography versus videonystagmography in diagnosis of vertigo. *International Journal of Occupational Medicine and Environmental Health*, *25*(1), 59–65. https://doi.org/10.2478/s13382-012-0002-1

Priesol, A. J., Valko, Y., Merfeld, D. M., & Lewis, R. F. (2014). Motion perception in patients with idiopathic bilateral vestibular hypofunction. *Otolaryngology - Head and Neck Surgery (United States)*, *150*(6), 1040–1042. https://doi.org/10.1177/0194599814526557

Siddiqui, U., & Shaikh, A. N. (2013). An Overview of "Electrooculography." *International Journal of Advanced Research in Computer and Communication*

Engineering, *2*(11), 4328–4330. www.ijarcce.com

Starkov, D., Guinand, N., Lucieer, F., Ranieri, M., Cavuscens, S., Pleshkov, M., Guyot, J. P., Kingma, H., Ramat, S., Perez-Fornos, A., & Van De Berg, R. (2020). Restoring the high-frequency dynamic visual acuity with a vestibular implant prototype in humans. *Audiology and Neurotology*, *25*(1–2), 91–95. https://doi.org/10.1159/000503677

Starkov, D., Snelders, M., Lucieer, F., Janssen, A. M. L., Pleshkov, M., Kingma, H., van Rompaey, V., Herssens, N., Hallemans, A., Vereeck, L., McCrum, C., Meijer, K., Guinand, N., Perez-Fornos, A., & van de Berg, R. (2020). Bilateral vestibulopathy and age: experimental considerations for testing dynamic visual acuity on a treadmill. *Journal of Neurology*, *267*(0123456789), 265–272. https://doi.org/10.1007/s00415-020-10249-z

Strupp, M., Kim, J. S., Murofushi, T., Straumann, D., Jen, J. C., Rosengren, S. M., Della Santina, C. C., & Kingma, H. (2017). Bilateral vestibulopathy: Diagnostic criteria consensus document of the classification committee of the barany society. *Journal of Vestibular Research: Equilibrium and Orientation*, *27*(4), 177–189. https://doi.org/10.3233/VES-170619

Suh, M. W., Park, J. H., Kang, S. Il, Lim, J. H., Park, M. K., & Kwon, S. K. (2017). Effect of Goggle Slippage on the Video Head Impulse Test Outcome and Its Mechanisms. *Otology & Neurotology : Official Publication of the American Otological Society, American Neurotology Society [and] European Academy of Otology and Neurotology*, *38*(1), 102–109. https://doi.org/10.1097/MAO.0000000000001233

Sun, D. Q., Ward, B. K., Semenov, Y. R., Carey, J. P., & Della Santina, C. C. (2014). Bilateral Vestibular Deficiency: Quality of Life and Economic Implications. *JAMA Otolaryngology-- Head & Neck Surgery*, *140*(6), 527–534. https://doi.org/10.1001/jamaoto.2014.490

Van de Berg, R., Guinand, N., Stokroos, R. J., Guyot, J. P., & Kingma, H. (2011). The vestibular implant: Quo vadis? *Frontiers in Neurology*, *AUG*. https://doi.org/10.3389/fneur.2011.00047

van de Berg, R., Ramos, A., van Rompaey, V., Bisdorff, A., Perez-Fornos, A., Rubinstein, J. T., Phillips, J. O., Strupp, M., Della Santina, C. C., & Guinand, N. (2020). The vestibular implant: Opinion statement on implantation criteria for research. *Journal of Vestibular Research*, *30*(3), 213–223. https://doi.org/10.3233/ves-200701

van de Berg, R., Rosengren, S., & Kingma, H. (2018). Laboratory examinations for the vestibular system. *Current Opinion in Neurology*, *31*(1), 111–116. https://doi.org/10.1097/WCO.0000000000000526

Van De Berg, R., Van Tilburg, M., & Kingma, H. (2015). Bilateral Vestibular Hypofunction: Challenges in Establishing the Diagnosis in Adults. In *ORL* (Vol. 77, Issue 4, pp. 197–218). ORL J Otorhinolaryngol Relat Spec. https://doi.org/10.1159/000433549

van den Boogert, T., van Hoof, M., Handschuh, S., Glueckert, R., Guinand, N., Guyot,

J. P., Kingma, H., Perez-Fornos, A., Seppen, B., Chacko, L. J., Schrott-Fischer, A., & van de Berg, R. (2018). Optimization of 3D-visualization of micro-anatomical structures of the human inner ear in osmium tetroxide contrast enhanced micro-CT scans. *Frontiers in Neuroanatomy*, *12*(May), 1–11. https://doi.org/10.3389/fnana.2018.00041

van Dooren, T. S., Lucieer, F. M. P., Duijn, S., Janssen, A. M. L., Guinand, N., Pérez Fornos, A., Van Rompaey, V., Kingma, H., Ramat, S., & van de Berg, R. (2019). The Functional Head Impulse Test to Assess Oscillopsia in Bilateral Vestibulopathy. *Frontiers in Neurology*, *10*, 365. https://doi.org/10.3389/fneur.2019.00365

van Stiphout, L., Lucieer, F., Pleshkov, M., Van Rompaey, V., Widdershoven, J., Guinand, N., Pérez Fornos, A., Kingma, H., & van de Berg, R. (2021). Bilateral vestibulopathy decreases self-motion perception. *Journal of Neurology*, *0123456789*. https://doi.org/10.1007/s00415-021-10695-3

Ward, B. K., Agrawal, Y., Hoffman, H. J., Carey, J. P., & Della Santina, C. C. (2013). Prevalence and impact of bilateral vestibular hypofunction: Results from the 2008 US national health interview survey. *JAMA Otolaryngology - Head and Neck Surgery*, *139*(8), 803–810. https://doi.org/10.1001/jamaoto.2013.3913

Weber, K. P., MacDougall, H. G., Halmagyi, G. M., & Curthoys, I. S. (2009). Impulsive testing of semicircular-canal function using video-oculography. *Annals of the New York Academy of Sciences*, *1164*, 486–491. https://doi.org/10.1111/j.1749-6632.2008.03730.x

Chapter 10 Summary

Summary

Chapter 2 describes a group of patients diagnosed with bilateral vestibulopathy (BVP) according to the Bárány Society diagnostic criteria. It was demonstrated that due to the heterogeneity of this disorder, different results are obtained with different vestibular tests. Therefore, it is imperative to standardize diagnostic tests and to obtain laboratory-specific normative values. In addition, it was shown that the caloric test and video head impulse test are most sensitive to detect vestibular function impairment. In contrast, the torsion swing test is more suited to measure the residual function. Finally, it was demonstrated that 76% of BV patients were eligible for vestibular implantation. Therefore, a thorough assessment of the vestibular function of all five end organs (two otoliths and three semicircular canals) is essential before vestibular implantation is possible.

Chapter 3 shows that the electro-oculography (EOG) method can be potentially applied to perform the head impulse test. Comparison of simultaneously performed EOG and video-oculography (VOG) during testing of horizontal saccades and during horizontal head impulse testing (HIT) showed a good concordance regarding recorded eye velocities in a group of healthy volunteers. The EOG method has several advantages over the VOG method, such as the absent phenomenon of goggle slippage and no pupil detection problems. Therefore, an EOG-based head impulse test device might be considered as an alternative to video HIT, especially in cases when pupil detection or goggle fixation is not possible.

Chapter 4 presents a new and fast approach for testing motion perception in clinical practice. A six degrees of freedom motion platform was used to estimate six rotational (yaw left-right, pitch forward-backward, and roll left-right) and six translational self-motion perception thresholds (translations forward-backward, left-right, and up-down) within an hour. This test for vestibular perception showed comparable patterns in perceptual thresholds compared to more research-oriented, lengthy tests. This might pave the way for self-motion perception testing in clinic, in order to diagnose vestibular dysfunction, or to assess effects of therapy (e.g., rehabilitation, vestibular implant) on self-motion perception.

Chapter 5 compares two clinical approaches for assessing self-motion perception: the 2-option and 12-option approach. The thresholds measured using the 2-option paradigm were lower than those measured with the 12-option paradigm, most likely because of the higher chance of guessing in the first case (8% vs. 50%, respectively), although the additional psychometric influence cannot be ruled out. These findings imply that each approach to assess self-motion perception, should have its own normative values.

Chapter 6 shows the morphometric parameters of the semicircular canals in the guinea pig and rat. The obtained 3D models of the bony labyrinths can serve as a basis for precise morphometric measurements and future finite element modeling.

Chapter 7 presents the electrical impedance measurements in the guinea pig inner ear *in vitro* and its simulation using the equivalent circuit model. The most significant physical phenomena determining the electrical impedance of the inter-electrode space where quantified: electrode polarization (electrical double layer)

and medium polarization (alpha-dispersion at low frequencies due to cell membranes and tissue-tissue interface). Electrical double layer properties were identified in a saline solution experiment. The Randles equivalent circuit was fitted to the measured impedance and was used for simulating the propagation of the electrical pulses through the inner ear tissues. The capacitive effects present in the interelectrode space distorted the voltage pulses passing the interelectrode space, which might hinder electrical stimulation of vestibular afferents.

Chapter 8 demonstrates another approach for modelling electro-conductivity of the inner ear, including two compartments (the bony labyrinth and the temporal bone) and using the 3D Finite Element approach. It was shown that the FEM approach matched the previously measured impedances (Chapter 7) relatively well using the "grid search algorithm", although the "least squares method" applied in the equivalent circuit model eventually showed a better fit. However, in contrast to the equivalent circuit model, the FEM approach provided more detailed information on the electrical potential distribution, e.g. for each neural branch separately. Furthermore, it was found that the presence of the temporal bone surrounding the bony labyrinth, significantly influences the electrical parameters of the whole system, when the bony labyrinth is stimulated. Not only the conductivity, but also the permittivity properties of the tissues are essential for accurate simulations of the electrical current propagation through the inner ear tissues. Eventually, from a clinical perspective, the electrical impedances measured between electrodes in the vestibular organ are the crucial parameters determining whether electrical stimulation will result in the desired neural response.

Curriculum Vitae

Maksim Pleshkov, MSc

Maksim Pleshkov was born on July 20th 1992 in Tomsk, Russia. He studied Physics at Tomsk State University (TSU) from 2009 until 2015. In 2013 he graduated from the plasma physics department with obtaining the Bachelor degree. At the second year of his Master in 2014-2015 he took part in the exchange program together with Maastricht University (MU), where he was involved in the research project on measuring the thresholds of the translational motion under supervision of professor Herman Kingma from MU and professor Vladimir Demkin from TSU.

Directly after graduation he was enrolled in 4-year postgraduate study in TSU. Meanwhile he started to work as a teaching assistant at the department of general and experimental physics of the physics faculty in TSU. Among other teaching activities he delivered a practical training course "Special physics practice" in the frames of Double degree Master program implemented together at MU and TSU in English from 2015 until 2018. From 2018 until 2021 he was also involved in development of Tomsk International Science Program bachelor program in TSU.

In 2017 he applied for a grant provided by Russian government and "Skolkovo" organization for the PhD study in MU for a duration of 4 years.

His research interests are vestibular implant, biophysics, mathematical modeling, data analysis.

LinkedIn: https://www.linkedin.com/in/max-pleshkov-942781b3/

List of publications

1. Dupuits, B., **Pleshkov, M.**, Lucieer, F., Guinand, N., Fornos, A. P., Guyot, J. P., Kingma, H., & Van De Berg, R. (2019). A new and faster test to assess vestibular perception. *Frontiers in Neurology*, *10*(JUL), 707. https://doi.org/10.3389/fneur.2019.00707

2. **Pleshkov, M. O.**, D'Alessandro, S., Svetlik, M., Starkov, D., Zaytsev, V., Handler, M., Baumgarten, D., Saba, R., van de Berg, R., Demkin, V., & Kingma, H. (2022). Fitting the determined impedance in the guinea pig inner ear to randles circuit using square error minimization in the range of 100 Hz to 50 kHz. *Biomedical Physics & Engineering Express*, *8*(2), 25005. https://doi.org/10.1088/2057-1976/ac4c4a

3. **Pleshkov, M.**, Rondas, N., Lucieer, F., van Stiphout, L., Janssen, M., Guinand, N., Perez-Fornos, A., Demkin, V., van Rompaey, V., Kingma, H., & van de Berg, R. (2022). Reported thresholds of self-motion perception are influenced by testing paradigm. *Journal of Neurology*, *0123456789*. https://doi.org/10.1007/s00415-022-11032-y

4. Zaytsev, V. A., **Pleshkov, M. O.**, Starkov, D. N., Demkin, V. P., Rudenko, T. V., & Kingma, H. (2022). Comparative Analysis of Oculography Methods For The Diagnosis Of The Vestibular System. *Russian Physics Journal*, *64*(10), 55–59. https://doi.org/10.1007/s11182-022-02525-4

5. van Stiphout, L., **Pleshkov, M.**, Lucieer, F., Dobbels, B., Mavrodiev, V., Guinand, N., Pérez Fornos, A., Widdershoven, J., Strupp, M., Van Rompaey, V., & van de Berg, R. (2022). Patterns of Vestibular Impairment in Bilateral Vestibulopathy and Its Relation to Etiology. *Frontiers in Neurology*, *13*(March), 1–14. https://doi.org/10.3389/fneur.2022.856472

6. Starkov, D., Vermorken, B., Van Dooren, T. S., Van Stiphout, L., Janssen, M., **Pleshkov, M.**, Guinand, N., Pérez Fornos, A., Van Rompaey, V., Kingma, H., & Van de Berg, R. (2021). The Effect of Different Head Movement Paradigms on Vestibulo-Ocular Reflex Gain and Saccadic Eye Responses in the Suppression Head Impulse Test in Healthy Adult Volunteers. *Frontiers in Neurology*, *12*. https://doi.org/10.3389/fneur.2021.729081

7. van Stiphout, L., Lucieer, F., **Pleshkov, M.**, Van Rompaey, V., Widdershoven, J., Guinand, N., Pérez Fornos, A., Kingma, H., & van de Berg, R. (2021). Bilateral vestibulopathy decreases self-motion

perception. *Journal of Neurology*, *0123456789*. https://doi.org/10.1007/s00415-021-10695-3

8. Kobyakova, O. S., Deev, I. A., Kulikov, E. S., Tyufilin, D. S., **Pleshkov, M. O.**, Homyakov, K. V., Levko, A. N., Balaganskaya, M. V., & Zagromova, T. A. (2021). The medical nurses: the factors of professional burning-out. *Problemy Sotsial'noi Gigieny, Zdravookhraneniia i Istorii Meditsiny*, *29*(2), 353–358. https://doi.org/10.32687/0869-866X-2021-29-2-353-358

9. Starkov, D., Snelders, M., Lucieer, F., Janssen, A. M. L., **Pleshkov, M.**, Kingma, H., van Rompaey, V., Herssens, N., Hallemans, A., Vereeck, L., McCrum, C., Meijer, K., Guinand, N., Perez-Fornos, A., & van de Berg, R. (2020). Bilateral vestibulopathy and age: experimental considerations for testing dynamic visual acuity on a treadmill. *Journal of Neurology*, *267*(0123456789), 265–272. https://doi.org/10.1007/s00415-020-10249-z

10. Starkov, D., Strupp, M., **Pleshkov, M.**, Kingma, H., & van de Berg, R. (2020). Diagnosing vestibular hypofunction: an update. *Journal of Neurology*, *1*, 3. https://doi.org/10.1007/s00415-020-10139-4

11. Starkov, D., Guinand, N., Lucieer, F., Ranieri, M., Cavuscens, S., **Pleshkov, M.**, Guyot, J. P., Kingma, H., Ramat, S., Perez-Fornos, A., & Van De Berg, R. (2020). Restoring the high-frequency dynamic visual acuity with a vestibular implant prototype in humans. *Audiology and Neurotology*, *25*(1–2), 91–95. https://doi.org/10.1159/000503677

12. Demkin, V. P., Shchetinin, P. P., Melnichuk, S. V., Kingma, H., Van de Berg, R., **Pleshkov, M. O.**, & Starkov, D. N. (2018). Electric Current Transmission Through Tissues of the Vestibular Labyrinth of a Patient: Perfection of the Vestibular Implant. *Russian Physics Journal*, *60*(11), 2019–2024. https://doi.org/10.1007/s11182-018-1318-5

13. Demkin, V. P., Udut, V. V., Shchetinin, P. P., Svetlik, M. V., Mel'nichuk, S. V., Shchetinina, A. P., **Pleshkov, M. O.**, Starkov, D. N., Demkin, O. V., & Kingma, H. (2018). Electrophysiological Properties of Rat Vestibular Labyrinth and Their Effect on Parameters of Transmitted Voltage Pulses. *Bulletin of Experimental Biology and Medicine*, *164*(6), 707–711. https://doi.org/10.1007/s10517-018-4063-4

14. Udut, E. V., Shchetinin, P. P., Rudenko, T. V., Lucieer, F., Kingma, H., Shchetinina, A. P., **Pleshkov, M. O.**, Demkin, V. P., & Udut, V. V. (2018). Pathogenetic Role of Endothelial Dysfunction in Idiopathic Vestibulopathy. *Bulletin of Experimental Biology and Medicine*, *164*(6), 726–729. https://doi.org/10.1007/s10517-018-4067-0

Appendix 1. Supplementary material for chapter 2
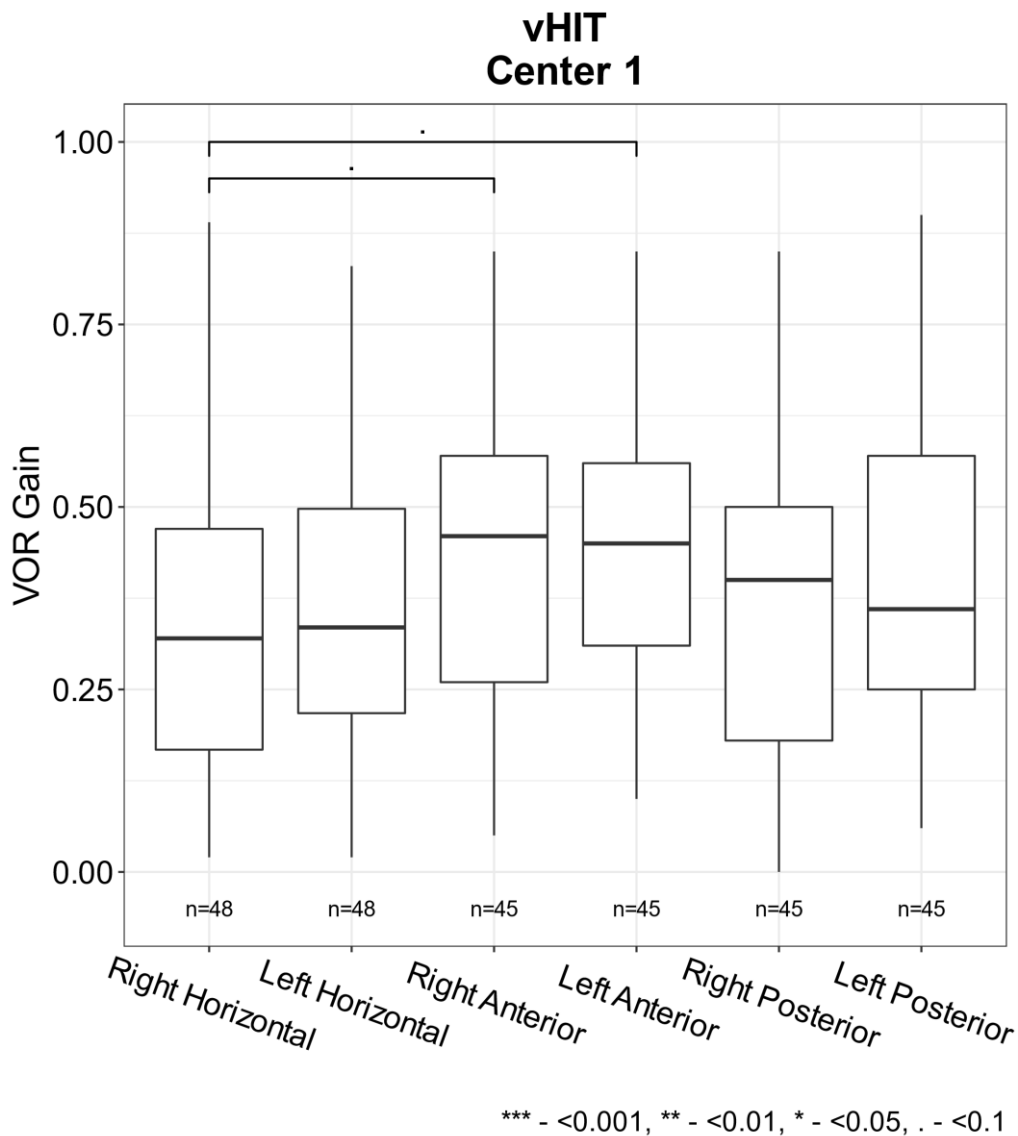
Figure 1. Vestibular Ocular Reflex (VOR) gain of all six semi-circular canals measured with the video Head Impulse Test (vHIT) in center 1. Each box plot represents the 25 to 75 percentiles and bold black lines the median.

Appendix 1. Supplementary material for chapter 2

Table 1. The vestibular reflex tests performed in each center. (vHIT = video Head Impulse Test, cVEMP = cervical vestibular evoked myogenic potential, oVEMP = ocular vestibular evoked myogenic potential).

|	Caloric test	Torsion swing test		vHIT			cVEMP	oVEMP
		0.1 Hz	0.05 Hz	Horizontal	Anterior	Posterior		
Center 1 (n=50)	+	+		+	+	+	+	+
Center 2 (n=58)	+		+	+	+	+	+	
Center 3 (n=65)	+			+				

vHIT
Center 2

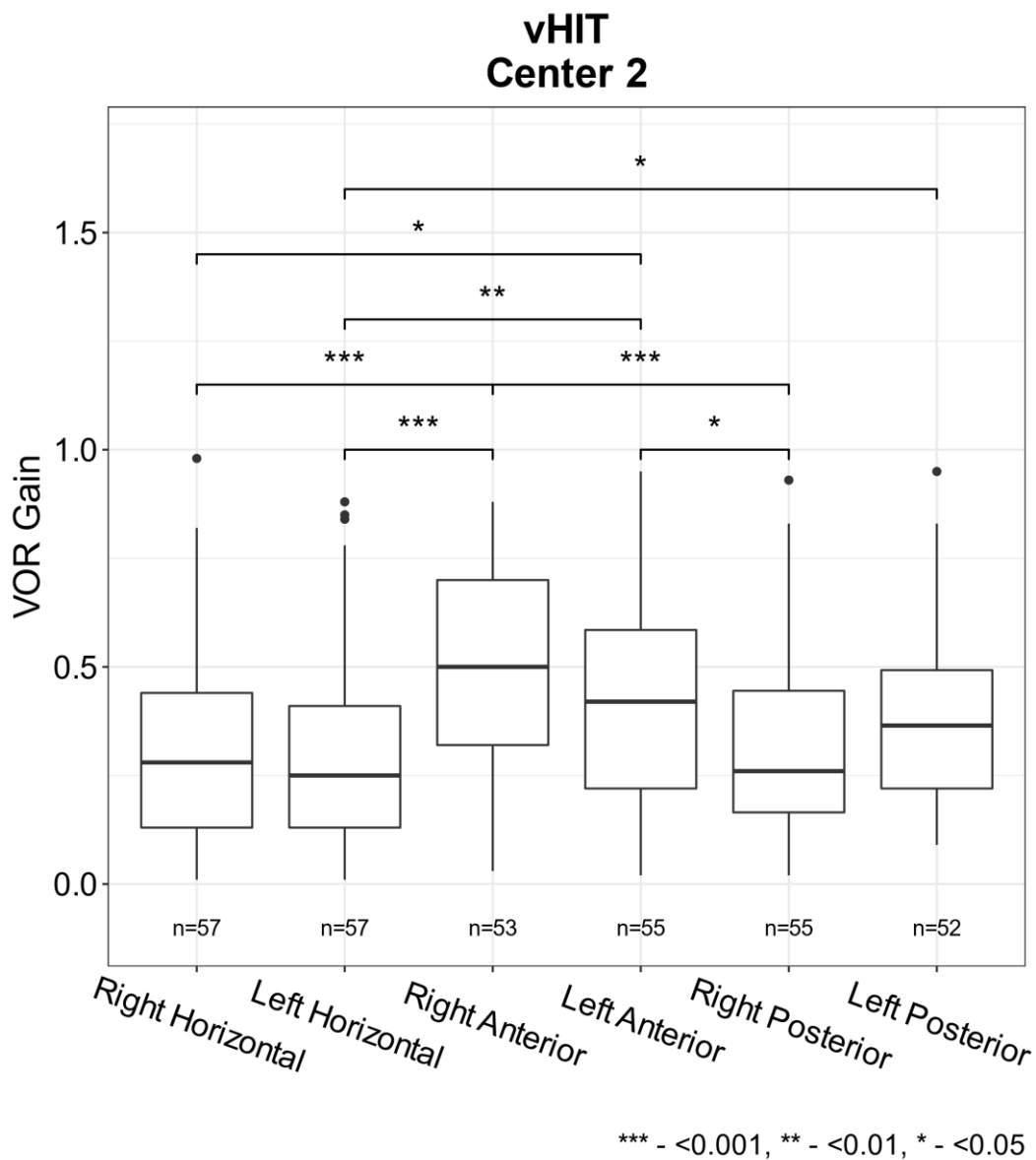*** - <0.001, ** - <0.01, * - <0.05

Figure 2. Vestibular Ocular Reflex (VOR) gain of all six semi-circular canals measured with video Head Impulse Test (vHIT) for center 2. Each box plot represents the 25 to 75 percentiles, bold black lines the median, dots the outliers and asterisks (*) illustrate statistically significant differences.

Table 2. Statistical results from pairwise comparisons between the six semi-circular canals of all three centers combined and per center separately (center 1 and 2) using post-hoc Dunn test with Benjamini Hochberg correction for multiple testing. Significant p-values are shown in bold font. (LA = Left Anterior, RA = Right Anterior, LH = Left Horizontal, RH = Right Horizontal, LP = Left Posterior, RP = Right Posterior)

	All 3 centers		Center 1		Center 2	
	Z	*p*-value	Z	*p*-value	Z	*p*-value
LA - LH	3,520	**0,002**	1,845	0,325	3,365	**0,003**
LA - LP	1,244	0,291	1,110	0,445	0,622	0,572
LH - LP	-2,101	0,067	-0,718	0,591	-2,689	**0,018**
LA - RA	-1,053	0,366	0,302	0,817	-1,611	0,146
LH - RA	-4,671	**<0.001**	-1,539	0,31	-4,958	**<0.001**
LP - RA	-2,282	**0,048**	-0,808	0,571	-2,205	0,052
LA - RH	3,235	**0,004**	2,852	0,065	2,703	**0,021**
LH - RH	-0,328	0,857	1,023	0,459	-0,668	0,582
LP - RH	1,819	0,115	1,724	0,318	2,037	0,069
RA - RH	4,388	**<0.001**	2,545	0,082	4,302	**<0.001**
LA - RP	2,895	**0,009**	1,664	0,288	2,408	**0,034**
LH - RP	-0,29	0,827	-0,155	0,877	-0,935	0,437
LP - RP	1,629	0,155	0,554	0,669	1,752	0,120
RA - RP	3,932	**<0.001**	1,362	0,371	3,997	**<0.001**
RH - RP	-0,005	0,996	-1,161	0,461	-0,273	0,785

Table 3. Kruskal-Wallis H test results for comparison of median vestibular test results for caloric test, torsion swing test and 3D-video Head Impulse Test between etiologies. Significant p-values are shown in bold font. (X^2 = Chi-squared statistic, Df = Degrees of freedom, vHIT = video Head Impulse Test)

		X^2	Df	*p*-value
Etiology – Caloric test	center 1	4.685	6	0.585
	center 2	6.557	8	0.585
	center 3	11.004	7	0.138
Etiology – Torsion swing test	center 1	3.213	6	0.782
	center 2	21.83	9	0.009*
Etiology – vHIT Anterior	All 3 centers	14.434	9	0.103
	center 1	2.142	6	0.906
	center 2	17.234	9	0.045*
Etiology – vHIT Horizontal	All 3 centers	32.389	9	<0.001*
	center 1	5.623	6	0.467
	center 2	17.387	9	0.043*

	center 3	24.491	7	<0.001*
Etiology – vHIT Posterior	All 3 centers	16.047	9	0.066
	center 1	4.564	6	0.601
	center 2	17.670	9	0.039*

* Significant results from Kruskal-Wallis H test were further analyzed with pairwise comparisons using post-hoc Dunn test with Benjamini Hochberg correction for multiple testing, shown in table 4.

Table 4. Statistical results from pairwise comparisons of torsion swing test results from center 2, horizontal vHIT results from all three centers, 3D vHIT results from center 2 and horizontal vHIT results from center 3, between different etiologies using post-hoc Dunn test with Benjamini Hochberg correction for multiple testing. Significant p-values are shown in bold font. (vHIT = video Head Impulse Test)

	Torsion swing test center 2		Horizontal vHIT all 3 centers		Anterior vHIT center 2		Horizontal vHIT center 2		Posterior vHIT center 2		Horizontal vHIT center 3	
	Z	p-value	Z	p-value	Z	p-value	Z	p-value	Z	p-value	Z	p-value
Autoimmune Congenital	1,651	0,371	0,037	1,000	0,412	1,000	0,064	0,971	0,513	0,804	1,204	0,376
Autoimmune Genetic	0,555	0,723	1,096	0,372	1,136	0,823	0,341	0,868	1,012	0,610	-	-
Congenital Genetic	1,730	0,418	1,145	0,378	0,568	0,987	0,430	0,883	0,305	0,900	-	-
Autoimmune Idiopathic	1,232	0,491	0,231	0,897	0,659	0,997	0,252	0,901	0,977	0,592	1,174	0,374
Congenital Idiopathic	1,011	0,540	0,181	0,918	0,101	0,985	0,338	0,848	0,282	0,898	0,386	0,784
Genetic - Idiopathic	2,007	0,336	3,096	0,022	1,259	0,721	0,233	0,895	0,051	0,981	-	-
Autoimmune Infectious	1,726	0,380	0,020	0,984	0,048	0,984	0,689	1,000	1,680	0,299	1,620	0,268
Congenital Infectious	0,489	0,760	0,028	1,000	0,601	0,986	0,603	0,983	0,991	0,603	0,388	0,814

	-		-		-		-		-			
Genetic - Infectious Idiopathic	3,183	0,065	2,079	0,121	3,005	0,119	2,734	0,094	1,792	0,299	-	-
Infectious Autoimmune	- -	-			-		-		-			
	1,218	0,478	0,426	0,773	1,645	0,500	2,201	0,312	1,671	0,266	1,161	0,362
Menière's Disease Congenital	-		-			-		-		-		
	0,959	0,524	1,096	0,384	0,019	0,985	0,000	1,000	1,715	0,324	0,125	0,900
Menière's Disease Genetic - Menière's	-		-		-		-		-			
Disease Idiopathic	1,063	0,518	1,052	0,388	0,486	0,973	0,078	0,981	1,086	0,567	1,598	0,257
	-		-		-		-		-			
	0,880	0,550	3,459	0,008	1,841	0,492	0,568	0,917	1,508	0,348	-	-
Menière's Disease Infectious	-		-		-		-		-			
	0,270	0,908	1,583	0,232	1,024	0,860	0,404	0,883	1,474	0,351	2,185	0,101
Menière's Disease Autoimmune	-		-		-		-		-			
	1,067	0,559	1,690	0,195	0,108	1,000	1,090	0,730	0,314	0,917	2,495	0,071
Mixed	- -	-		-		-		-		-		
	2,126	0,503	1,163	0,380	0,397	0,973	0,984	0,770	1,886	0,296	-	-
Congenital - Mixed	-	-		-		-		-		-		
	0,220	0,885	1,133	0,373	0,872	0,957	0,910	0,816	1,293	0,420	-	-
Genetic - Mixed	-	-		-		-		-		-		
	2,762	0,129	2,178	0,110	2,221	0,296	2,107	0,316	1,705	0,305	-	-
Idiopathic - Mixed	-	-		-		-		-		-		
	1,731	0,470	1,234	0,376	1,528	0,569	1,910	0,316	1,678	0,280	-	-
Infectious - Mixed	-	-		-		-		-		-		
	1,004	0,526	1,346	0,321	0,557	0,963	0,612	1,000	-0,69	0,669	-	-
Menière's Disease - Mixed	-	-		-		-		-		-		
	1,639	0,350	0,478	0,749	0,556	0,930	1,320	0,600	0,362	0,897	-	-

Appendix 1. Supplementary material for chapter 2

```
Autoimmune        - -                                              -
Neurodegenerative 1,905 0,365 1,918 0,155 0,229 0,996 0,533 0,891 1,424 0,366 2,459 0,065
Congenital        - -                                              -
Neurodegenerative 0,254 0,878 1,957 0,151 0,183 0,986 0,596 0,953 0,910 0,583 1,471 0,282
Genetic           - -                                              -
Neurodegenerative 2,081 0,421 1,450 0,276 0,821 0,927 0,396 0,842 0,948 0,572 -     -
Idiopathic        - -                                              -
Neurodegenerative 1,356 0,438 3,017 0,023 0,349 0,962 0,469 0,871 0,951 0,591 2,923 0,032
Infectious        - -                                              -
Neurodegenerative 0,830 0,555 2,608 0,045 0,355 0,985 1,404 0,555 0,230 0,898 1,326 0,345
Menière's Disease - -                                              -
Neurodegenerative 1,374 0,449 3,573 0,016 0,262 1,000 0,652 1,000 0,029 0,977 3,893 0,003
Mixed             - -
Neurodegenerative 0,073 0,942 2,742 0,039 0,661 1,000 1,599 0,412 0,243 0,909 -     -
Autoimmune        - -                                              -
Toxic             1,063 0,540 0,479 0,768 0,093 0,969 0,513 0,882 0,438 0,850 1,902 0,178
                                                                   -
Congenital - Toxic 0,959 0,543 0,528 0,747 0,411 0,988 0,591 0,924 0,191 0,910 0,665 0,644
                   -           -           -
Genetic - Toxic   1,075 0,578 1,196 0,372 1,703 0,499 0,398 0,864 0,856 0,588 -     -
                                          -
Idiopathic - Toxic 0,085 0,953 1,579 0,224 0,892 0,986 0,506 0,862 0,789 0,605 2,250 0,098
Infectious - Toxic 0,888 0,562 0,91  0,467 0,237 1,000 1,978 0,359 1,898 0,371 0,300 0,823
Menière's Disease - -
Toxic             0,147 0,925 2,483 0,059 0,106 1,000 0,726 1,000 1,805 0,320 3,428 0,009
Mixed - Toxic     1,508 0,395 1,722 0,191 0,650 0,967 1,969 0,315 1,976 0,433 -     -
```

|												
Neurodegenerative - Toxic	1,270	0,483	2,100	0,124	0,187	1,000	0,139	0,953	1,305	0,432	1,306	0,335
Autoimmune - Trauma	0,631	0,699	1,750	0,190	1,365	0,705	1,209	0,638	0,181	0,896	1,843	0,183
Congenital - Trauma	1,391	0,462	1,790	0,183	0,860	0,923	1,287	0,594	0,810	0,607	0,716	0,632
Genetic - Trauma	0,262	0,892	1,215	0,374	0,660	1,000	1,706	0,360	2,002	0,509	-	-
Idiopathic - Trauma	0,858	0,550	2,913	0,027	1,362	0,650	1,739	0,410	1,887	0,333	1,545	0,264
Infectious - Trauma	1,636	0,327	2,464	0,056	2,439	0,331	3,183	0,065	2,970	0,134	0,416	0,825
Menière's Disease - Trauma	0,464	0,761	3,487	0,011	1,903	0,513	1,710	0,393	2,681	0,110	2,726	0,045
Mixed - Trauma	2,055	0,359	2,617	0,050	2,258	0,359	2,849	0,099	2,760	0,130	-	-
Neurodegenerative - Trauma	1,702	0,363	0,260	0,894	1,084	0,835	0,557	0,897	1,924	0,407	0,812	0,583
Toxic - Trauma	0,611	0,696	1,917	0,146	1,798	0,464	0,984	0,813	0,876	0,591	0,218	0,858
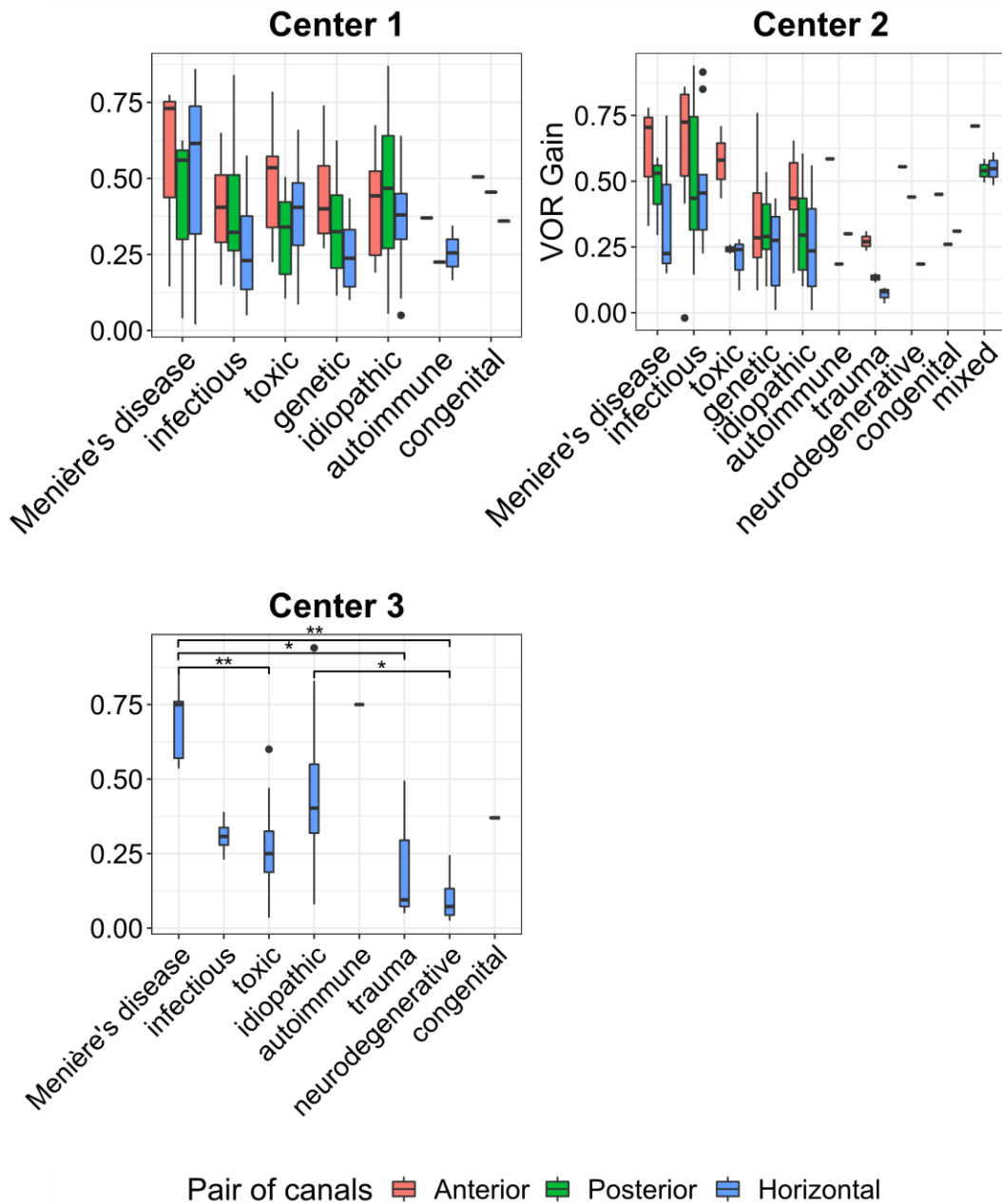
Figure 3. Vestibular Ocular Reflex (VOR) gain per etiology for all three pairs of semi-circular canals (i.e. horizontal, anterior and posterior canals) measured with video Head Impulse Test, presented per center. Each box plot represents the 25 to 75 percentiles, bold black lines the median, and dots the outliers.
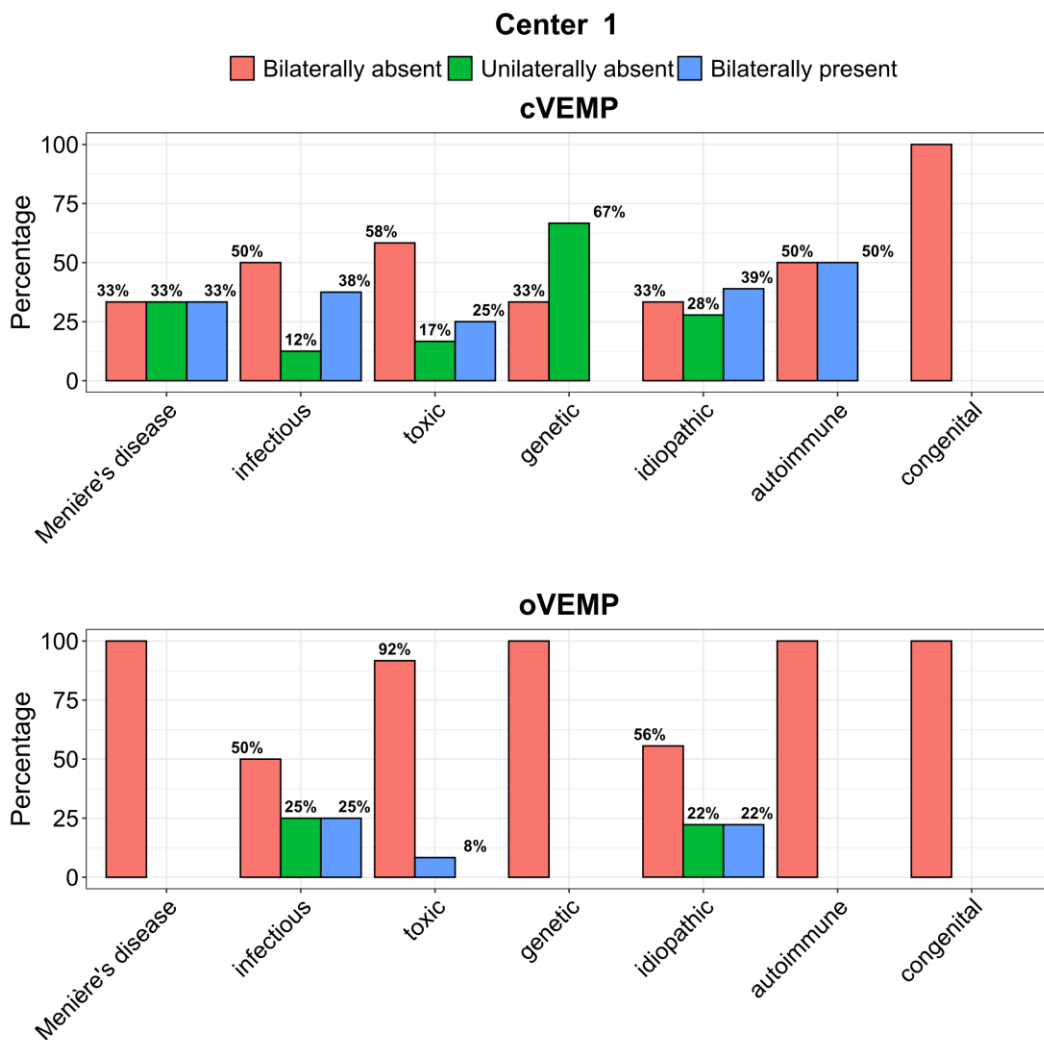
Figure 4. The prevalence of patients in center 1 having bilaterally absent (red), unilaterally absent (green) or bilaterally present (blue) cVEMP and oVEMP responses.
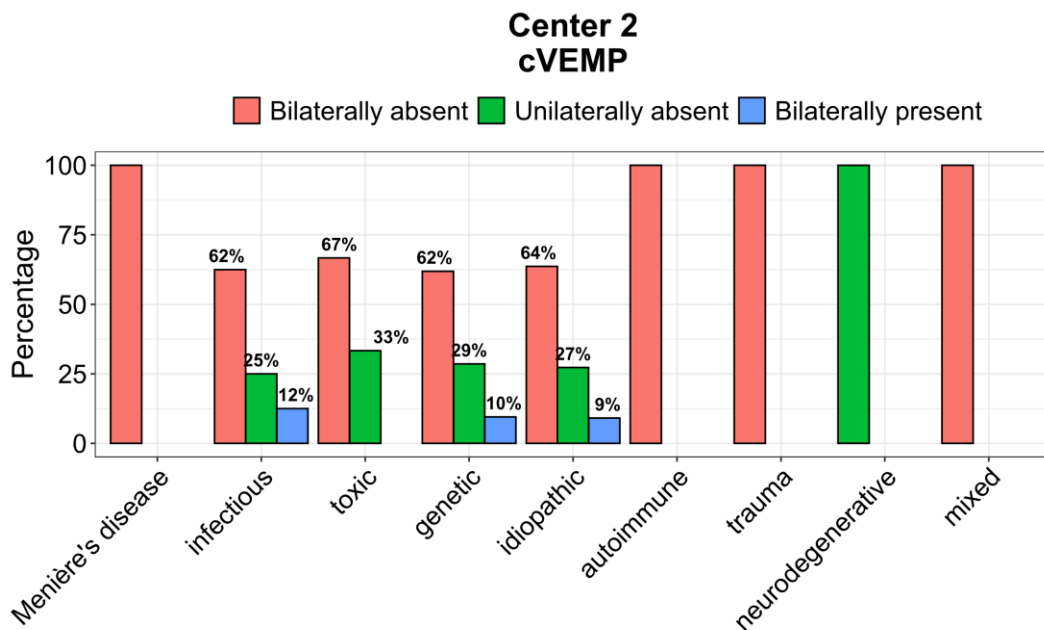
Figure 5. The prevalence of patients in center 2 having bilaterally absent (red), unilaterally absent (green) or bilaterally present (blue) cVEMP responses.

Table 5. Overview of all median test results with interquartile range (q1-q3) and Mann-Withney U test statistics (W and p-value) for cluster 1 (n=30) and cluster 2 (n=15). Significant p-values are shown in bold font. (vHIT = video Head Impulse Test)

Cluster		1	2	W	*p*-value
Caloric test	(q1-q3)	0,00 (0,00-0,00)	5,00 (3,00-7,00)	395	**<0.001**
Torsion swing test	(q1-q3)	0,05 (0,02-0,11)	0,15 (0,09-0,27)	370.5	**<0.001**
Horizontal vHIT	(q1-q3)	0,30 (0,13-0,36)	0,56 (0,44-0,62)	416	**<0.001**

Anterior vHIT	(q1-q3)	0,34 (0,23-0,46)	0,65 (0,54-0,70)	430	**<0.001**
Posterior vHIT	(q1-q3)	0,29 (0,15-0,45)	0,56 (0,44-0,63)	366.5	**<0.001**

Table 6. Overview of bilaterally absent, unilaterally absent and bilaterally present cervical Vestibular Evoked Myogenic Potential (cVEMP) and ocular Vestibular Evoked Myogenic Potential (oVEMP) responses in cluster 1 (n=30) and cluster 2 (n=15) with Fisher's Exact Test statistics. Significant p-values are shown in bold font.

		cVEMP (n)	oVEMP (n)
Cluster 1	Bilaterally absent	14	24
	Unilaterally absent	10	4
	Bilaterally present	6	2
Cluster 2	Bilaterally absent	6	10
	Unilaterally absent	1	1
	Bilaterally present	8	4
Fisher's Exact Test	*P* value	0.044	0.212
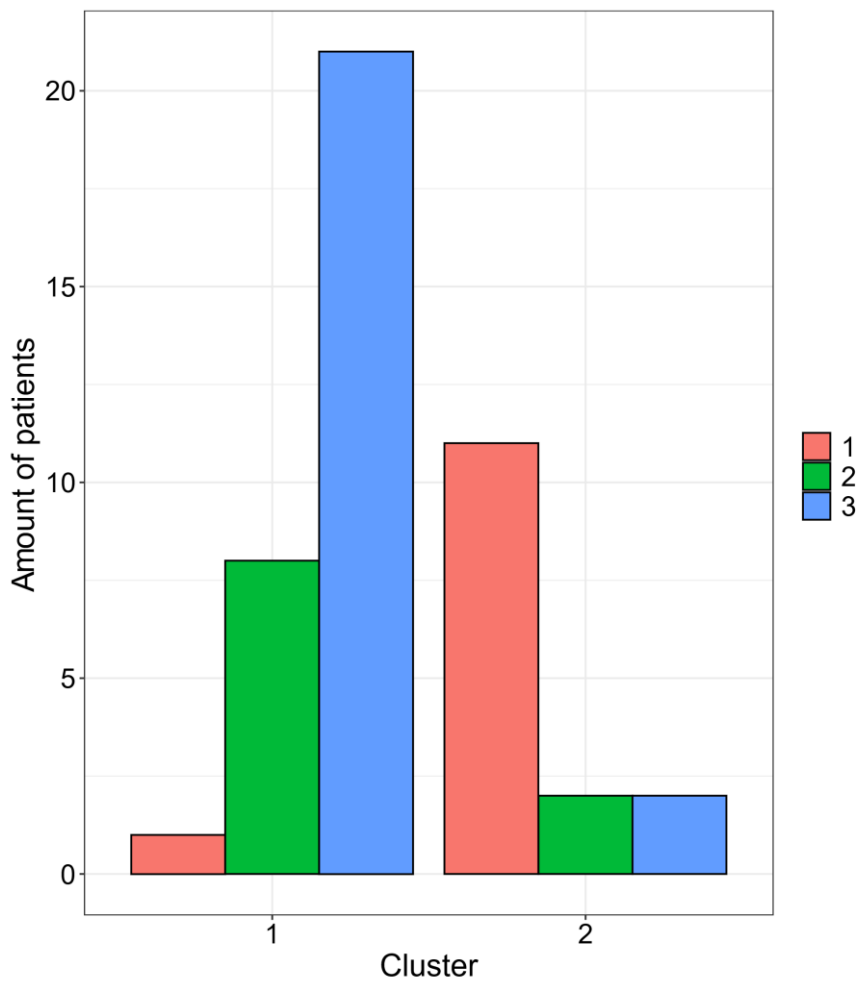
Figure 6. The prevalence of patients meeting one (red), two (green) or three (blue) Bárány criteria per cluster (cluster 1, n=30 and cluster 2, n=15).
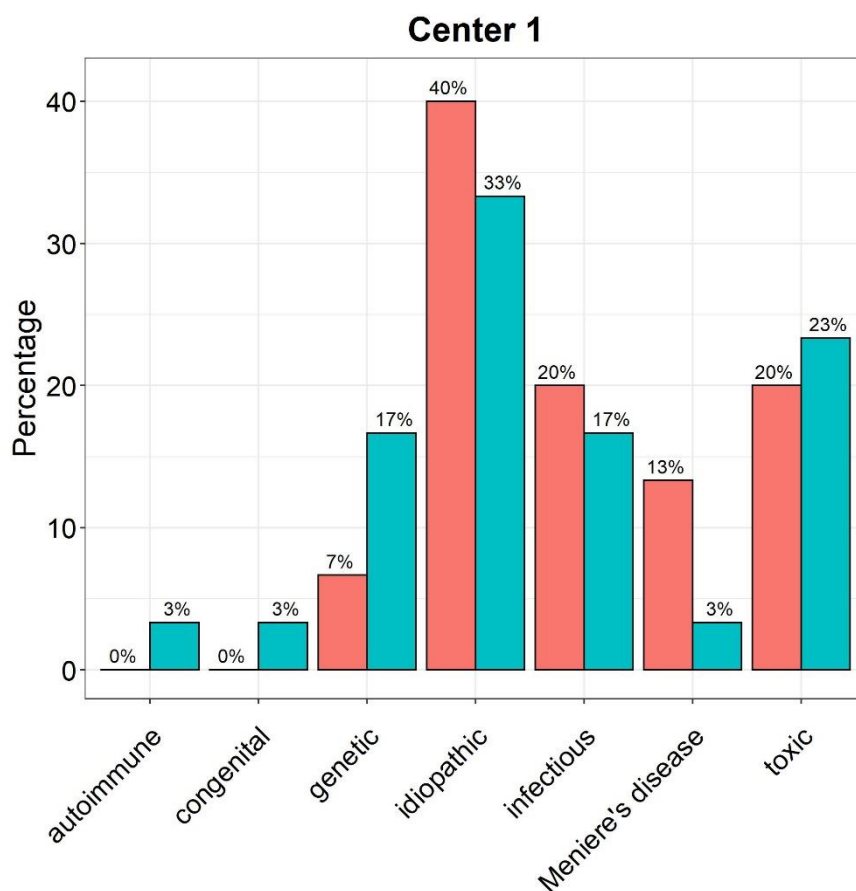
Figure 7. The prevalence (%) of different etiologies in cluster 1 (blue, n=30) and cluster 2 (red, n=15).

Table 7. Frequency distribution of different etiologies between cluster 1 (n=30) and cluster 2 (n=15) with Fisher's Exact Test statistics.

	Cluster 1 (n)	Cluster 2 (n)
Menière's disease	1	2
Infectious disorders	5	3
Ototoxicity	7	3
Genetic disorders	5	1
Idiopathic	10	6
Autoimmune	1	0
Congenital	1	0
Fisher's Exact Test *p*-value		0.854

Appendix 2. Conductivity of the 0.9% NaCl saline solution

The conductivity of saline solution (σ_{saline}) can be estimated from its ionic compound by the Ohm's law for electrolytes:

$$j = zne(u_+ + u_-)E \tag{1}$$

where z is the ion charge, n – concentration, e is electron charge, u_+ and u_- are the motility of positive and negative ions respectively, E is the electric field strength. In its way, the motility can be found via

$$u = \frac{ze}{6\pi\eta r} \tag{2}$$

where z is the ion charge, e is electron charge, η is the liquid dynamic viscosity, and r is the ion radius. Apparently, comparing Ohm's law for electrolytes (1) with Ohm's law in differential form:

$$j = \sigma E \tag{3}$$

it is easy to see that the conductivity can be calculated as:

$$\sigma = zne(u_+ + u_-) \tag{4}$$

Concentrations of Na^+ and Cl^- ions can be found using the molar concentration formula:

$$C_M = \frac{m_{NaCl}}{M_{NaCl} \cdot V} \tag{5}$$

where m_{NaCl} is mass of dissolved NaCl, M_{NaCl} is the molar mass of NaCl molecule, V is the solution volume.

For 0.9% NaCl solution there are 9 g of salt per 1 liter of water. The obtained value of C_M for NaCl molecule is also true for each ion comprising it, since dissolution happens in equal halves. The necessary parameters for calculating the electrical conductivity of 0.9% NaCl solution can be found in the table 2.

Table 2. Constants for calculation of saline conductivity.

Parameter	Value	Unit of measurement
z	1	1
r_{Na^+}	$0.98 \cdot 10^{-10}$	m
r_{Cl^-}	$1.06 \cdot 10^{-10}$	m
η_{water}	$1 \cdot 10^{-3}$	$Pa \cdot s$
m_{NaCl}	9	g
M_{NaCl}	58.44	g/mol
V	1	l
n_{Na}	154	$\frac{mmol}{l} (\frac{mol}{m^3})$
n_{Cl}	154	$\frac{mmol}{l} (\frac{mol}{m^3})$

As the result $\sigma_{saline} = 2.216 \, S/m$.

Appendix 3. Frequency composition of a typical biphasic cathodic-first square pulse used in implants

EXPERIMENTAL

The signal was recorded by DRIB VI research setup in UM at a sampling frequency $F_s = 20kHz$, which corresponds to 50 us sampling time (Figure 1). The assumption is that the electrical pulse rise time is about 1 usec.

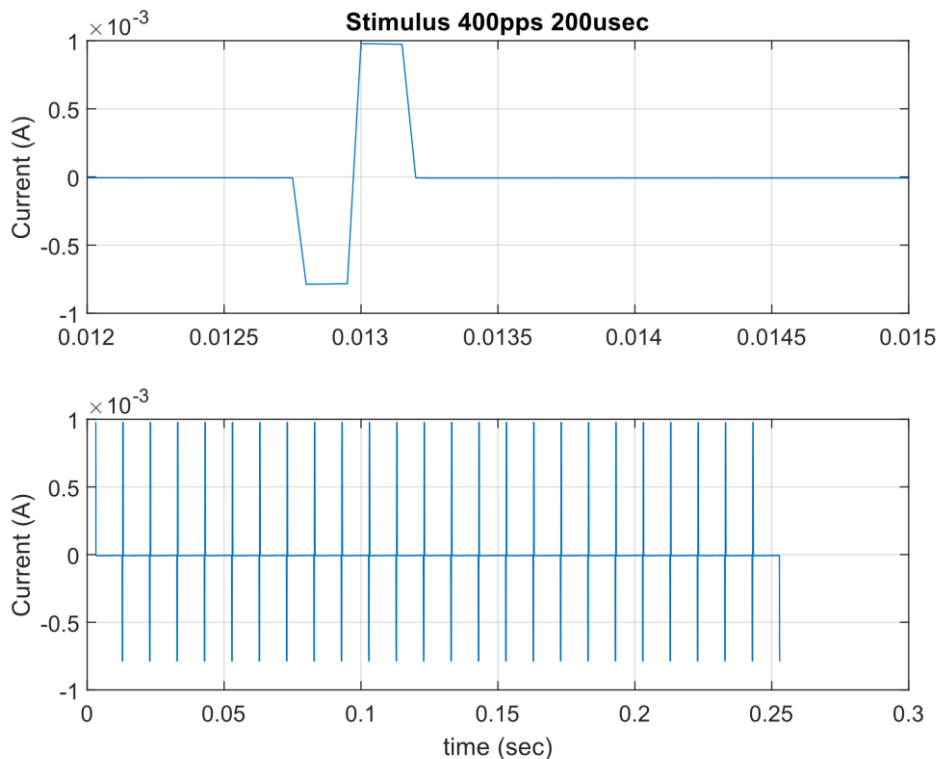Figure 1. VI stimulation signal. Amplitude 1 mA, phase 200 us, repetition rate 400pps.

According to the Nyquist sampling theorem the highest frequency that can be registered is a half of a given sampling rate. Therefore, the signal spectrum is present between 0 Hz and 10 kHz (Figure 2).

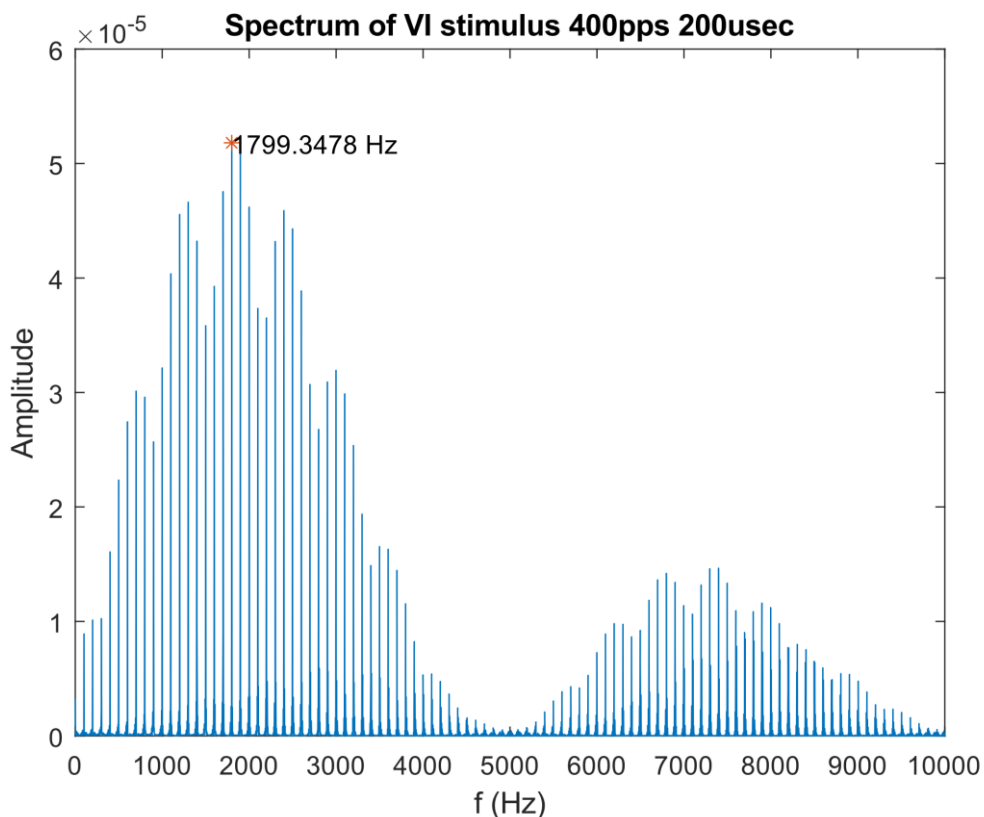Appendix 3. Frequency composition of a typical biphasic cathodic-first square pulse used in implants

Figure 2. Fourier spectrum of the recorded signal: absolute magnitude vs frequency. The maximum amplitude frequency is 1799.34 Hz.

The energy of the signal was calculated as a square of the amplitude. The cumulative sum was then calculated over the frequency (Figure 3). 95% of the signal energy is contained below 7.4 kHz. Therefore, is it crucial to investigate the electrical properties of the inner ear in a relatively low frequency range below 10 kHz.
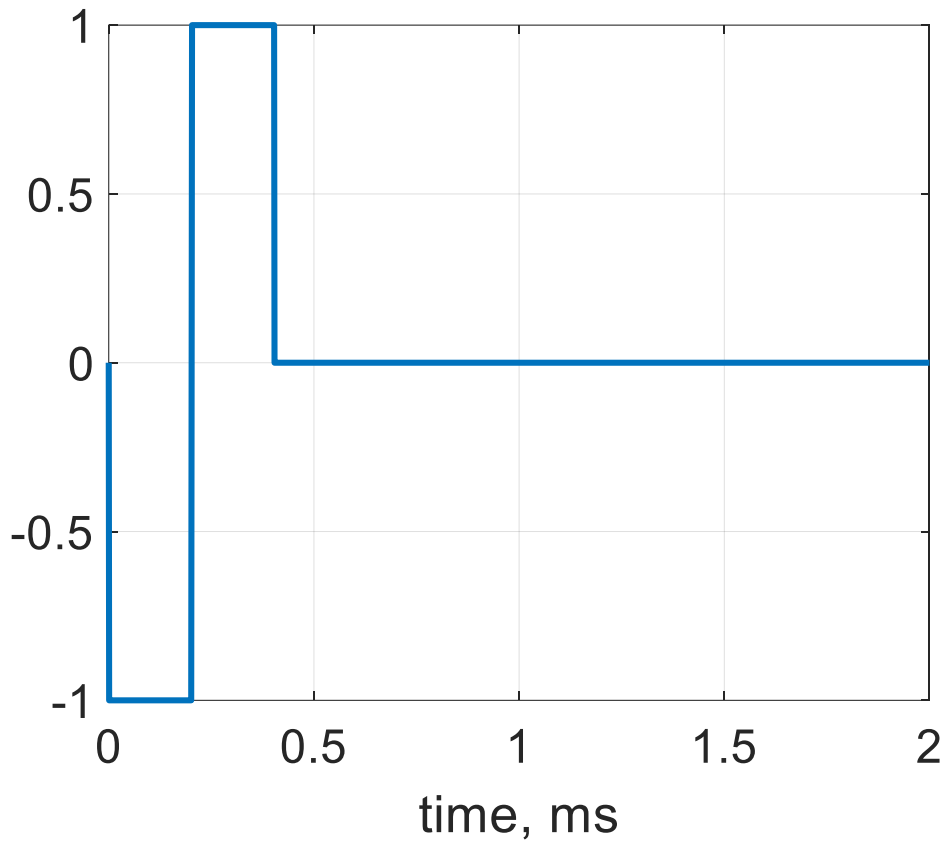
CPS of rect pulse 200usec 400pps
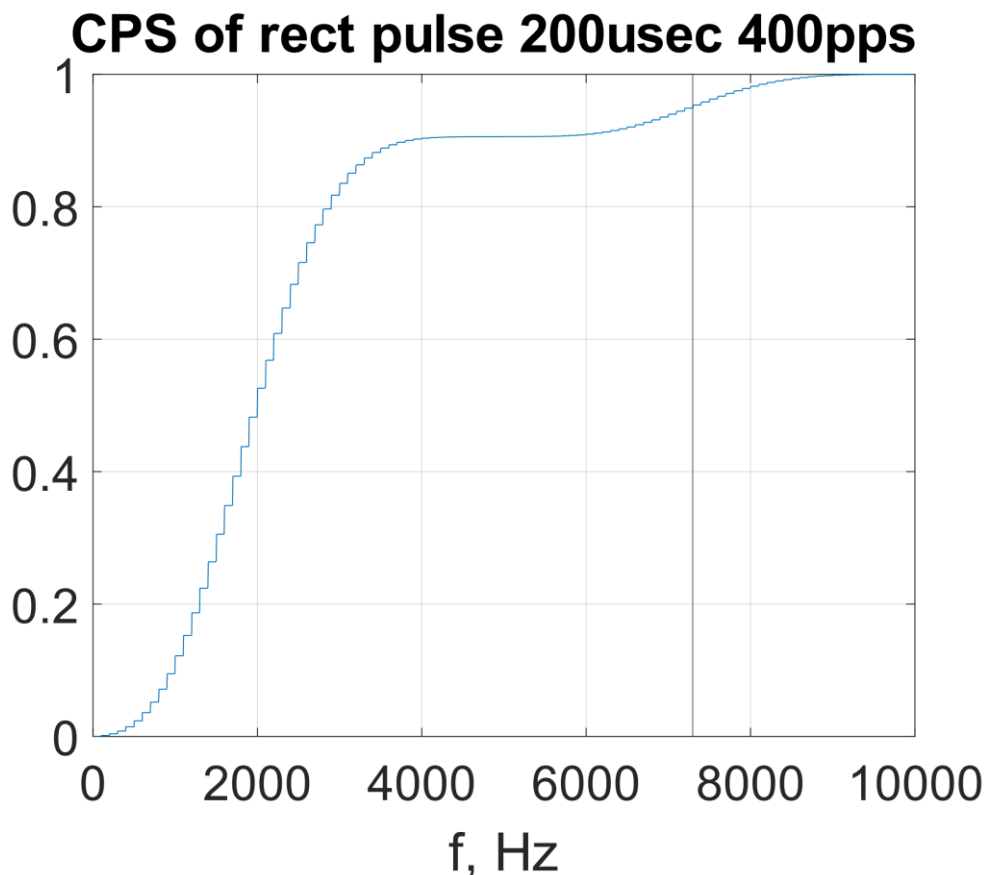
Figure 3. Cumulative power spectrum (CPS) of the recorded signal. Vertical line indicates the frequency containing 95% of the signal energy, which is approximately located at 7.3 kHz.

THEORETICAL APPROACH

The rectangular pulse with the 200us phase and total duration of 2.1 ms (which roughly corresponds to 400 pps) was formed in Matlab as a piecewise (analytical) function (Figure 4). The rise and decay were set at 1 us tangent of a slope. The pulse was digitalized at a sampling frequency $F_s = 1\ MHz$. Since pulse amplitude does not play any role in spectrum analysis, it was set to be equal to 1.

Figure 4. The rectangular biphasic (200us per phase) negative-first pulse plotted at the sampling frequency of 1MHz and resulting in 2001 data point.
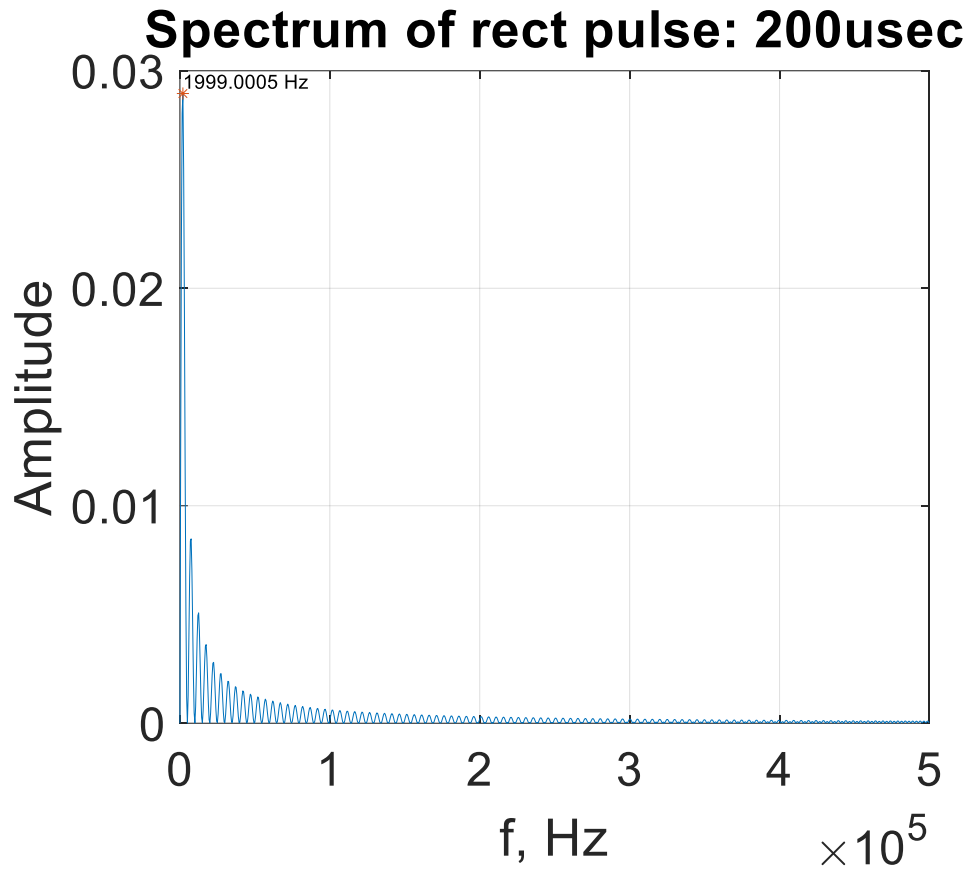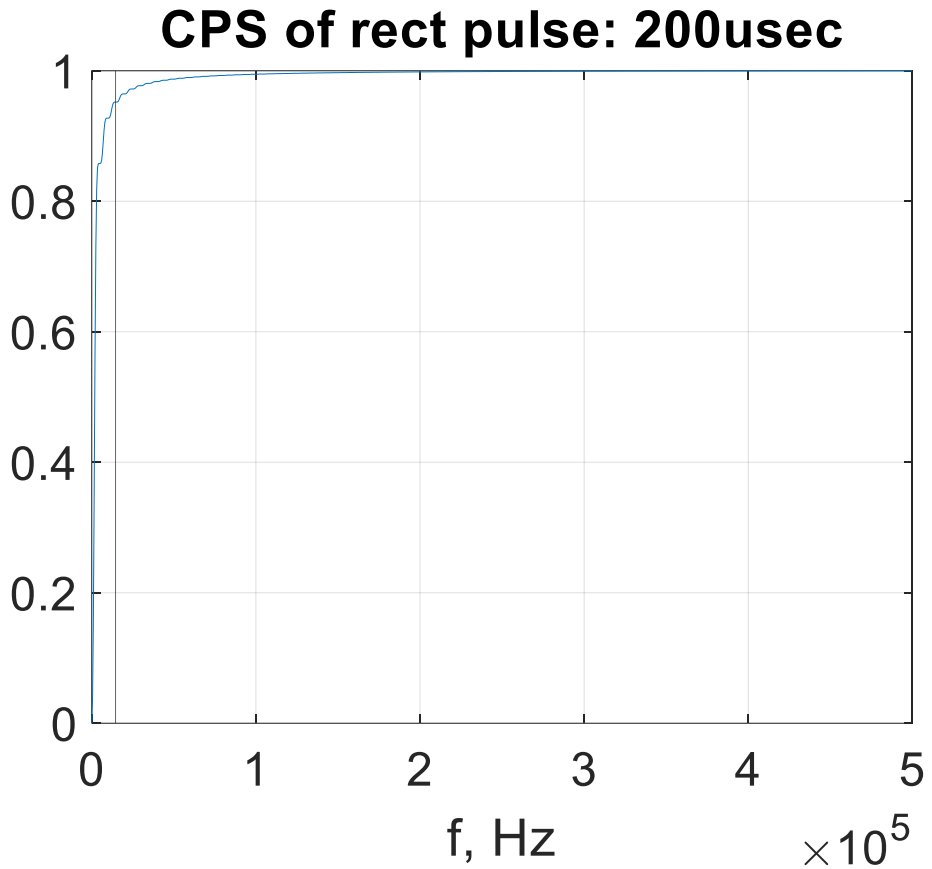
Spectrum of rect pulse: 200usec

*Figure 5. Fourier spectrum of the theoretical signal: absolute magnitude vs frequency.
The maximum amplitude frequency is 1999.34 Hz.*

Appendix 3. Frequency composition of a typical biphasic cathodic-first square pulse used in implants

CPS of rect pulse: 200usec

Figure 6. Cumulative power spectrum (CPS) of the theoretical signal. Vertical line indicates the frequency containing 95% of the signal energy which is approximately located at 14.5 kHz.

The longer phase duration will result in shifting the first (and the biggest) peak in Fourier spectrum in a range of lower frequencies.

Abbreviations

All abbreviations are mentioned separately in their chapters.
Mostly used abbreviations are (in alphabetical order):

ASCC	Anterior semicircular canal
BVP	Bilateral vestibulopathy
CT	Computed tomography
cVEMP	Cervical vestibular evoked myogenic potential
EDL	Electrical double layer
EOG	Electro-oculography
FEM	Finite element model
HIT	Head impulse test
LSCC	Lateral semicircular canal
NRMSE	Normalized root mean square error
oVEMP	Ocular vestibular evoked myogenic potential
PSCC	Posterior semicircular canal
VHIT	Video head impulse test
VI	Vestibular implant
VOG	Video-oculography
VOR	Vestibulo-ocular reflex
VN	Vestibular nerve